EDITORIAL STAFF

EDITORIAL BOARD

European Reviews of Chemical Research

2015

Is. 2

Статьи, поступившие в редакцию, рецензируются. За достоверность сведений, изложенных в статьях, ответственность несут авторы публикаций.
Мнение редакции может не совпадать с мнением авторов материалов.

2015

№ 2

CONTENTS

UDC 631.531.027: 635.63

The Evaluation of the Mathematical Model of Interaction of Electrochemically Activated Water Solutions (Anolyte and Catholyte) with Water

[1*] Ignat Ignatov
[2] Oleg Mosin
[3] Georgi Gluhchev
[4] Stoil Karadzhov
[5] Georgi Miloshev
[6] Nikolay Ivanov

[1] The Scientific Research Center of Medical Biophysics (SRC MB), Bulgaria
Professor, D. Sc., director of SRC MB
1111, Sofia, N. Kopernik street, 32
*E-mail: mbioph@dir.bg
[2] Moscow State University of Applied Biotechnology, Russian Federation
Senior research Fellow of Biotechnology Department, Ph. D.
103316, Moscow, Talalihina ulitza, 33
E-mail: mosin-oleg@yandex.ru
[3] Institute of Information and Communication Technologies
Bulgarian Academy of Sciences, Bulgaria
Assoc. Professor, Ph. D.
1113, Sofia, Acad. G. Bonchev Street, 2
E-mail: gluhchev@iinf.bas.bg
[4] Bulgarian Association of Activated Water, Bulgaria
Professor, D. Sc.
1619, Sofia, Kutuzov blvd., 39
[5] Institute of Molecular Biology, Bulgarian Academy of Science, Bulgaria
Assoc. Professor, Ph. D.
1113, Sofia, Acad. G. Bonchev Street, 21
[6] Institute of Information and Communication Technologies
Bulgarian Academy of Sciences, Bulgaria
Assis. Professor, Dipl. Eng.
1113, Sofia, Acad. G. Bonchev Street, 2

Abstract
This paper deals with the evaluation of the basis of the mathematical model of interaction of electrochemically activated water solutions (catholyte/anolyte), obtained in the diaphragm electrolysis cell, with water and sodium chloride and the basic physical-chemical processes underlying the electrolysis of water as well. In order to provide additional data about the distribution of H_2O molecules according to the energies of hydrogen bonds in the electrochemically activated water solutions of the catholyte and the anolyte, the non-equilibrium energy spectrum

(NES) and differential non-equilibrium energy spectrum (DNES) of the anolyte and the catholyte were measured as a result of which were established the basis for evaluation of the mathematical model explaining the behavior of the anolyte and the catholyte regarding the distribution of H_2O molecules to the energies of hydrogen bonds. The local maximum for catholyte in the NES-spectrum was at -0,1285 eV, for anolyte – at -0,1227 eV and for the control sample of deionized water – at -0,1245 eV. The calculations of $\Delta E_{H...O}$ for catholyte with using the DNES method compiles (-0,004±0,0011 eV) and for anolyte (+1,8±0,0011 eV). The average energy of hydrogen bonds between H_2O molecules was measured by the DNES method to be compiled at -0,1067±0,0011 eV.

Keywords: electrochemical treatment of water, electrolysis, anolyte, catholyte, NES, DNES.

Introduction

The phenomenon of electrochemical activation of water (EAW) is a set of electrochemical and electrical processes occur in water in the electric double layer (EDL) type of electrodes (anode and cathode) with non-equilibrium electric charge transfer through EDL by electrons under the intensive dispersion in water the gaseous products of electrochemical reactions [1]. In 1985 EAW was officially recognized as a new class of physical and chemical phenomena.

As a result of the treatment of water by a constant electric current at electric potentials equal to or greater than the decomposition potential of water (1,25 V), water goes into a metastable state, accompanied by electrochemical processes and characterized by the abnormal activity levels of electrons, the redox potential, and other physical-chemical parameters (pH, E_h, ORP) [2].

During the EAW occur four main processes:

1) Electrolytical decomposition of water by electrolysis on account of redox reactions on the electrodes due to the external electric field;

2) Electrophoresis – the movement in the electric field of a positively charged particles and ions toward the cathode and negatively charged particles and ions toward the anode;

3) Electroflotation – the gas formation and flocculation of aggregates consisting of fine-dispersed gas bubbles (H_2 at the cathode and O_2 at the anode) and suspended solids in water;

4) Electrocoagulation – the formation of colloidal aggregates of particles of deposited disperse phase through a process of anode dissolution of the metal and the formation of metal cations Al^{3+}, Fe^{2+}, Fe^3 under the influence of electric field.

The electrochemical processes, which occur at the passage of the direct electric current through the water volume, are accompanied as a result of redox reactions leading to coagulation of colloids, flocculation of suspended solids and subsequent flotation. The advantages of electrochemical water treatment is that it allows to correct the pH value and redox potential E_h, on which depends the possibility of occurrence of various chemical processes in water; increases the enzymatic activity of activated sludge in aeration tanks; reduces the resistivity and improves coagulation and sedimentation of organic sediments from water.

The purpose of this research was the evaluation of the basis of the mathematical model of interaction of electrochemically activated water solutions – the anolyte and catholyte.

Material and Methods

The experiments were conducted with the diaphragm electrolysis apparatus "Wasserionisierer Hybrid PWI 2100" (Drink In Clear Co., Germany), equipped with four titanium plate electrodes coated with platinum.

Technical data: dimensions – 380×230×230 mm; weight – 3,8 kg; the voltage of the electric power supply – 220 V, the frequency of the electric current – 50 Hz, the power of the electric current 0,2–0,7 A; the power consumption – 200 Watts; pH range – 3,5 - 10,5; inlet water temperature 5–30 °C; the time of electro processing – 30–40 min. The volumes of the electrochemically activated water solutions: anolyte – 0,3 l; catholyte – 0,9 l.

The elementary electrolysis cell was formed by two electrodes – a positively charged anode and a negatively charged cathode connected to different poles to a DC source. Interelectrode space was filled with water, which is an electrolyte capable of conducting the electrical current, or with 0,3% solution of chemically pure NaCl in distilled H_2O, as schematically shown in Figure 1 below.

The anolyte had pH = 3,2 and ORP = +1070 mV; the active components – HClO, Cl_2, HCl, HO_2*;

The catholyte had pH = 9,0 and ORP = -300...-500 mV); the active components – O_2, HO_2^-, HO_2^*, H_2O_2, H^+, OH^-.
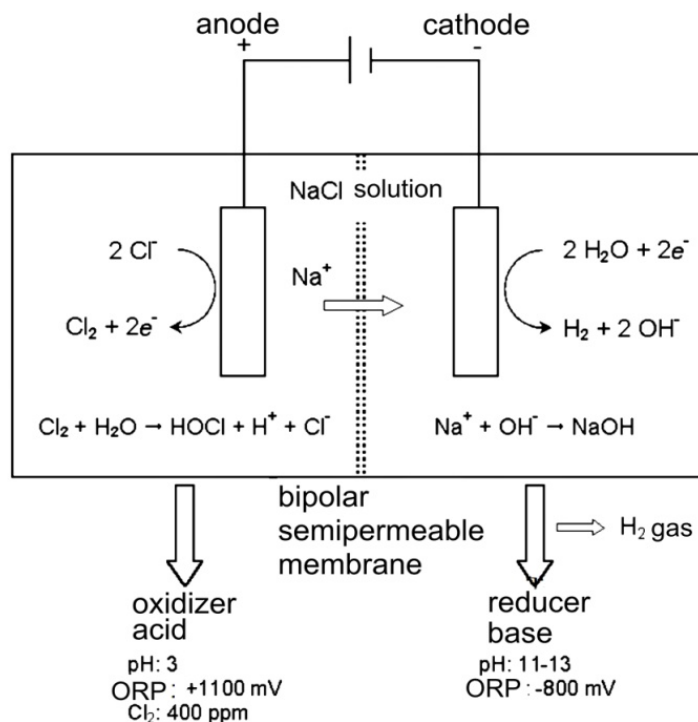
Figure 1. The diaphragm electrolysis apparatus for preparation of acid (anolyte) and alkali (catholyte) solutions via the electrochemical activation of sodium chloride

NES, and DNES methods were used for the estimation of energy of hydrogen bonds of the anolyte, the catholyte and deionized water in order to make a supposition about the spectrum characteristics. The device measured the angle of evaporation of water drops ranged from 72^0 to 0^0. As the main estimation criterion was used the average energy ($\Delta E_{H...O}$) of hydrogen O...H-bonds among H_2O molecules in water's samples. NES, and DNES spectra of water were measured in the range of energy of hydrogen bonds at 0,08–0,387 eV or λ = 8,9–13,8 μm with using a specially designed computer program. Statistical processing of experimental data was performed using *t*-criterion of Student (at p < 0,05).

Results and Discussion
Electrolysis of water
The main stage of electrochemical treatment of water is the electrolysis of water or aqueous solutions with low mineralization as aqueous solutions of 0,5–1,0% NaCl [3], which occurs in the electrolysis cell, consisting of the cathode and the anode separated by a special semipermeable membrane (diaphragm) which separates water to alkaline fraction – the catholyte and acidic fraction – the anolyte (Figure 1). When the passing over the electric current through water, the flow of electrons from cathode as well as the removal of electrons from water at the anode, is accompanied by series of redox reactions on the surface of the cathode and anode [4]. As the result, new elements are formed, the system of intermolecular interactions, as well as the composition of water and the water structure are changed [5, 6].
The typical apparatus for electrochemical treatment of water comprises water preparation/treatment unit (1), the electrolyzer (2), and the processing unit after the electrochemical treatment of water (3) (Figure 2).
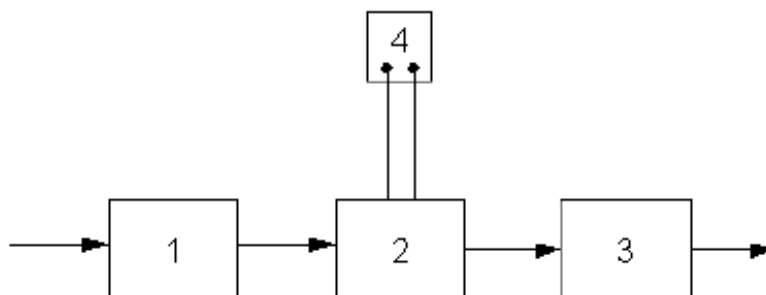
Figure 2. The apparatus for electrochemical water treatment: 1 – water preparation/treatment unit; 2 – electrolyzer; 3 – the block of post-treatment; 4 – rectifier of electric current.
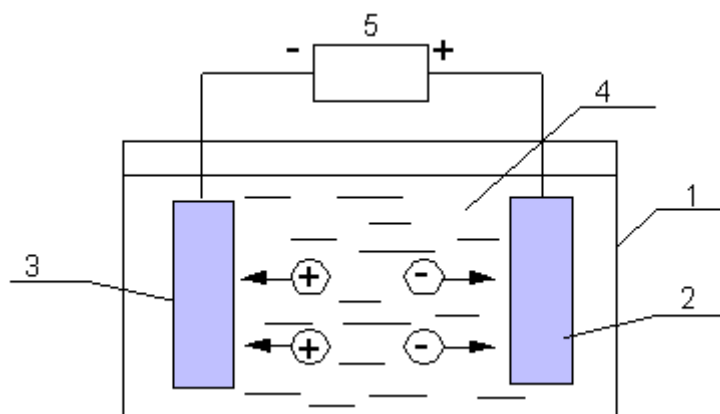
Figure 3. Scheme of the electrolysis cell: 1 – the case; 2 – anode; 3 – cathode; 4 – interelectrode space; 5 – DC power source.

The main element of the apparatus is electrolyzer consisting of one or more electrolysis cells (Figure 3). The typical electrolysis cell is formed by two electrodes – a positively charged anode and a negatively charged cathode connected to different poles to a DC source. Interelectrode space is filled with water, which is an electrolyte capable of conducting electrical current, or with 0,5–0,1% solution of NaCl. As a result it occurs the transferring of electric charges through the water – electrophoresis, i.e. migration of the polar particle charge carriers – ions for the electrode having an opposite sign. Wherein the negatively charged anions are moved toward the anode, the positively charged cations are moved toward the cathode. At electrodes the charged ions lose the charge and become depolarized, turning into the decay products. In addition to these charged ions, in the electrophoresis participate the polar particles with different particle sizes, including solid particles (emulsified particles, gas bubbles, etc.), but the main role in the transfer of electrochemical charges plays the ions possessed by the greatest mobility.

The products of electrode reactions are the neutralized aqueous admixtures, gaseous hydrogen and oxygen generated during the electrolytic destruction of H_2O molecules, metal cations (Al^{3+}, Fe^{2+}, Fe^{3+}) in the case of metal anodes made of aluminum and steel, and the molecular chlorine. Wherein at the cathode is generated the gaseous hydrogen, and at the anode – oxygen. Water also contains a certain amount of hydronium ions (H_3O^+) depolarizing at the cathode with formation of the atomic hydrogen ($H\cdot$):

$$H_3O^+ + e^- \rightarrow H\cdot + H_2O, \tag{1}$$

In an alkaline environment there occurs the disruption of H_2O molecules, accompanied by formation of the atomic hydrogen ($H\cdot$) and hydroxide ion (OH^-):

$$H_2O + e^- \rightarrow H\cdot + OH^-, \tag{2}$$

The reactive hydrogen atoms are adsorbed on the surfaces of the cathode, and after recombination are formed the molecular hydrogen H_2, released in the gaseous form:

$$H\cdot + H\cdot \rightarrow H_2, \tag{3}$$

At the same time at the anode is released the atomic oxygen. In an acidic environment, this process is accompanied by the destruction of H_2O molecules:

$$2H_2O - 4e^- \rightarrow O_2 + 4H^+, \tag{4}$$

In an alkaline environment, the source of oxygen source is OH^- ions, moving under the electrophoresis from the cathode to the anode:

$$4OH^- \rightarrow O_2 + 2H_2O + 4e^-, \qquad (5)$$

The normal redox potentials of these reactions compiles +1,23 V and +0,403 V, respectively, but the process takes place in certain conditions of electric overload.

The cathodes are made of metals that require high electrical voltage (lead, cadmium), allow to generate the reactive free radicals as Cl^*, O^*, OH^*, HO_2^*, which react chemically with other radicals and ions.

In bulk oxidative processes a special role plays products of electrolysis of water – oxygen (O_2), hydrogen peroxide (H_2O) and hydrochlorine acid ($HClO$). During the electrolysis, an extremely reactive compound formed – H_2O_2, the formation of which occurs due to hydroxyl radicals (OH^*), which are the products of the discharge of hydroxyl ions (OH^-) at the anode:

$$2OH^- \rightarrow 2OH^* \rightarrow H_2O_2 + 2e^-, \qquad (6)$$

where OH^* – the hydroxyl radical.

The chlorine-anion is transformed to Cl_2:

$$2Cl^- \rightarrow Cl_2 + 2e^-, \qquad (7)$$

Gaseous Cl_2 forms highly active oxidants: Cl_2O; ClO_2; ClO^-; $HClO$; Cl^*; HO_2^*. The parameters of pH, the redox potential, ORP and the electrical conductivity of the anolyte/catholyte depend on different factors including the ratio of water volumes in the two electric chambers, the material of electrodes, NaCl concentration, the temperature, electric voltage and processing time [7, 8].

The electrolysis cell can be regarded as a generator of the above mentioned products, some of them, entering into the chemical interaction with each other and water impurities in the interelectrode space, providing additional chemical treatment of water (electrophoresis, electroflotation, electrocoagulation) [9]. These secondary processes do not occur on the electrode surface, but in the bulk water. Therefore, in contrast to the electrode processes they are indicated as the volume processes. They generally are initiated with increasing the temperature of water during the electrolysis process and with increasing the pH value.

There are distinguished the cathodic and anodic oxidation. When the cathodic oxidation the organic molecules absorbed on cathodes, accepting free electrons and reduced. The reduction process usually takes place in one step:

$$R + H^+ + e^- \rightarrow RH, \qquad (8)$$

where R – the organic compound; RH – the hydrated form of the compound.

In other cases, the cathodic reduction takes place in two stages: at the first stage (9) the organic molecule is converted into an anion, in the second (10) – the hydrated anion interacts with the proton of H_2O water:

$$R + e^- \rightarrow R^-, \qquad (9)$$
$$R^- + H^+ \rightarrow RH, \qquad (10)$$

The cathodes made of materials that require high electrical voltage (lead, cadmium), allow for large amounts of electricity to generate the reactive free radicals – particles having on the outer orbits of atoms or molecules free unpaired electrons (Cl^*, O^*, OH^*, HO_2^*). The latter circumstance makes the free radicals the reactivity, i.e. to react chemically with other radicals and ions.

At the anodic oxidation the organic molecules, adsorbed on the anode, give up electrons to simultaneous or prior hydration:

$$RH \rightarrow R + H^+ + e^-, \qquad (11)$$

The anodic oxidation of organic compounds often results in the formation of free radicals, which further transformations is defined by their reactivity. Anodic oxidation processes are multistage and proceed with the formation of intermediate products. Anodic oxidation lowers the chemical resistance of organic compounds and facilitates their subsequent destruction in volume processes.

The rate of the anodic oxidation depends on the temperature and the pH value. Often in the process of oxidation of organic compounds are formed intermediates, which differ from the original compounds by the resistance to further transformations and indicators of toxicity.

The source of active chlorine and its oxygen-containing compounds are chlorides generated in the electrolyser, and NaCl, which is added into the electrochemically treated water before the electrolysis. As a result of the anodic oxidation of Cl^- anions is generated the gaseous Cl_2.

Depending on the pH value Cl_2. is either hydrolyzed to form hypochlorous acid (HOCl), or forms hypochlorite ions (ClO⁻). The equilibrium of the reaction depends on the pH value; at pH = 4–5 all chlorine is present in the form of HClO, and at pH = 7 – half in the form of ClO⁻ ion and half – in the form of HClO (Figue 4).
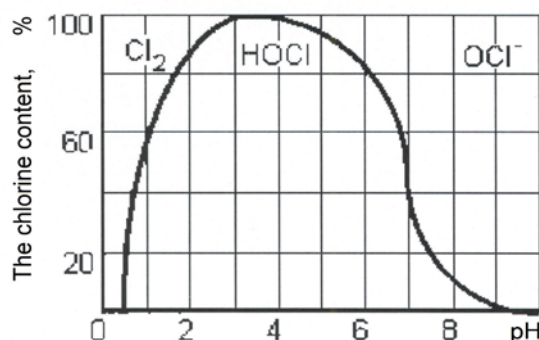
Figure 4. Content (%) of various forms of chlorine (Cl_2, HOCl, OCl⁻) in the electrochemically activated water depending on the pH value

The mechanism of interaction between the hypochlorite ions (ClO⁻) with the oxidizing agent described by the following equation:

$$ClO^- + A \rightarrow C + Cl, \tag{12}$$

where A – the oxidizing substances; C – the oxidation product.

The electrochemical oxidation of organic compounds by hypochlorite ions (ClO⁻) is accompanied by an increase of the redox potential E_h, indicating the predominance of oxidative processes. The E_h value growth depends on the ratio of active chlorine concentration in the interelectrode space to the content of organic impurities in water. As the purification and reducing the amount of impurities, the ratio increases, which leads to an increase of E_h, but after some time the rate stabilizes.

The amount of substance reacted at the electrodes by passing a constant electric current through the Faraday's law, is directly proportional to the current strength and the time of the electrochemical treatment:

$$G = AI_{cur}t, \tag{13}$$

where A – the electrochemical equivalent of an element (g/A·h); I_{cur} – the amperage (A); t – the processing time (h).

The electrochemical equivalent of an element is defined by the formula:

$$A = M/26,8z, \tag{14}$$

where M – the atomic mass of the element (g); z – its valence.

The values of the electrochemical equivalents of some elements are shown in Table. 1.

Table 1: Electrochemical equivalents of some elements

Element	The electrochemical equivalent of an element, g/A·h
H_2	0,0376
O_2	0,289
Fe (II)	1,042
Fe (III)	0,695
Al (III)	0,336
Cr (III)	0,647
Cr (VI)	0,324
Cu (II)	1,186
Zn (II)	1,22
Cl_2	1,324
Ca (II)	0,748

The actual amount of a substance, generated during the electrolysis is less than the theoretical, calculated from the formula (13) as part of the electric power is expended on heating the electrodes and water. Therefore, at calculations take into account the current efficiency $\eta < 1$, the value of which is determined experimentally.

The electrode processes are accompanied by an exchange of charged particles and ions between the electrodes and the electrolyte – water. For this the equilibrium must be established to provide an electric potential minimum value, which depends on the sort of the redox reaction and the water temperature measured at +25 ^{0}C (Table 2).

Table 2: The electrode potentials of some elements

Electrode reaction	Electric voltage [V]	Electrode reaction	Electric voltage [V]
$Al \rightarrow Al^{3+} + 3e^-$	-1,66	$Cu \rightarrow Cu^{2+} + e^-$	+0,345
$Zn \rightarrow Zn^{2+} + 2e^-$	-0,763	$4OH^- \rightarrow 2H_2O + O_2 + 4e^-$	+0,401
$Fe \rightarrow Fe^{2+} + 2e^-$	-0,44	$2H_2O \rightarrow O_2 + 4H^+ + 4e^-$	+1,23
$Cd \rightarrow Cd^{2+} + 2e^-$	-0,403	$2Cl^- \rightarrow Cl_2 + 2e^-$	+1,36
$H_2 \rightarrow 2H^+ + 2e^-$	0,0001	$Cl^- + H_2O \rightarrow HClO + H^+ + 2e^-$	+1,49

The electrical voltage generated in the electrode cell, should be sufficient to cause oxidation-reduction reactions at the electrodes. The voltage depends on the ionic composition of water, the presence of impurities in water, such as detergents, the electric current density (its power per unit area of the electrode), the electrode material, and others. Other things being equal the task of selecting the electrode material is to undergo the oxidation-reduction reactions at the electrodes, the voltage required to be minimized since it reduces the cost of electricity.

Some redox reactions are competing – they occur simultaneously and mutually inhibit each others. Their flow can be regulated by changing the electric voltage in the electrolytic cell. Thus, the normal electrical potential of the reaction of formation of molecular oxygen is +0,401 V or +1,23 V; when the voltage increases to +1,36 V (the normal potential of the reaction of formation of molecular chlorine) at the anode will be allocated only oxygen, and at the further increase in capacity – both oxygen and chlorine, and the evolution of chlorine will occur with insufficient intensity. At the voltage value +5,0 V the oxygen evolution will be almost ceased, and the electrolytic cell will only generate chlorine.

The physical-chemical properties of the catholyte and the anolyte

As a result of the cathode (catholyte) treatment water becomes alkaline: its ORP decreases, the surface tension is reduced, decreasing the amount of dissolved oxygen in water, increases the concentration of hydrogen, hydroxyl ions (OH$^-$), decreases the conductivity of water, changes the structure of hydration shells of ions [10]. By external characteristics the catholyte – is a soft, light, with an alkaline taste liquid, sometimes with white sediment; its pH = 10–11, ORP = -200...-800 mV.

On physical and chemical parameters the catholyte has the significantly enhanced electron-donating properties, and getting into the physiological fluids of an organism can enhance the electron-background for a few tens of millivolts [11]. The catholyte reportedly has antioxidant, immunestimulating, detoxifying properties, normalizing ORP, metabolic processes (increases the ATP synthesis, modification of enzyme activity), stimulates the regeneration of tissues, increases the DNA synthesis and stimulates the growth and division of cells by increasing the mass transfer of ions and molecules across the cell membrane, improves trophic processes in tissues and blood circulation [12]. It was also reported that catholyte with the redox potential at -700...-100 mV favorizes the development of anaerobs, whereas the anolyte with the redox potential at +200...+750 mV supports the growth of aerobs [13]. The antibacterial effect of the catholite is differentiated: the bactericidal effect is appeared relative to *Enterobacteriaceae*, resistant to it are enterococci and the group of streptococci B, and against Gram-negative microorganisms – only the bacteriostatic effect [14].

The electrochemically activated solutions of the catholite, depending on the strength of the transmitted electric current may be of several types:

C – alkaline catholyte (pH > 9,0; ORP = -700...-820 mV), the active components – NaOH, O_2, HO_2^-, HO_2^*, OH^-, OH^*, HO_2^-, O_2;

CN – neutral catholyte (pH = 9,o; ORP = -300...-500 mV), the active components – O_2, HO_2^-, HO_2^*, H_2O_2, H^+, OH^-.

As a result of the anode (anolyte) treatment water becomes acid reaction, the ORP increases slightly, the surface tension is slightly reduced, the conductivity increases, the amount of the dissolved oxygen and chlorine in water also increases, whereas the amount of hydrogen decreases [15]. The anolyte is a brownish, acid, with a characteristic odor and taste the liquid with a pH = 4–5 and ORP = +500...+1100 mV. The specific anolyte toxicity when being administered in the stomach and applying to the skin refers to the class 4 of harmful substances according to the Russian Standard GOST 12.1.007-76, with the minimal toxicity within this class. When being inhaled the anolyte with oxidants content of 0,02% and total mineralization 0,25–0,35% does not irritate the respiratory system and mucous membranes of the eyes. When introduced into the organism, the anolyte has no immunotoxic action and increased chromosomal aberrations in the bone marrow cells and other tissues, and it has no cytogenetic activity. When being heated to +50 ^{0}C the bactericidal activity of the anolyte is increased by 30–100% [16].

The electrochemically activated solutions of the anolyte are divided into four main types:

A – acidic anolyte (pH < 5,0; ORP = +800...+1200 mV), the active components – HClO, Cl_2, HCl, HO_2^*;

AN – neutral anolyte (pH = 6,0; ORP = +600...+900 mV), the active components – HClO, O_3, HO^-, HO_2^*;

ANK – neutral anolyte (pH = 7,7; ORP = +250...+800 mV), the active components – HClO, ClO^-, HO_2^-, H_2O_2, O_2, Cl^-, HO^*;

ANKD – neutral anolyte (pH = 7,3; ORP = +700...+1100 mV), the active components – HClO, $HClO_2$, ClO^-, ClO_2^*, HO_2^*, H_2O_2, O_2, O_3, Cl^-, HO^-, O^*.

The anolyte has antibacterial, antiviral, antifungal, anti-allergic, anti-inflammatory, antiedematous and antipruritic effect, may be cytotoxic and antimetabolite action without harming the human tissue cells [17]. The biocide elements in the anolyte are not toxic to somatic cells, as represented by oxidants, such as those ones produced by the cells of higher organisms.

Studies on the virucidal effect of the anolyte are rare and insufficient, basically on the possibilities of applying the anolyte in the implementation of effective control of viral diseases in humans and animals and especially on particularly dangerous viral infections, as staphylococcal Enterotoxin-A [18] and the classical swine fever (CSF) virus, caused by enveloped viruses belonging to the genus *Pestivirus* [19]. According to J.A. Sands [20] and U.S. Springthorpe [21], the effective disinfection of viruses whose infectivity is associated with the elements of the casing may be achieved by disinfectants dissolving fats, surfactants, disinfectants or fatty acids, organic solvents (ether and chloroform), detergents, proteases, and common disinfectants. It is believed that 2% solution of NaCl is most suitable for the disinfection of spaces contaminated with them. It is thought that to achieve the effective electrochemical disinfection it is necessary to irreversibly damage the RNA [22].

The research [23] carried out with of *E. coli* using as a desinfectant the anolyte with ORP equal or greater than +1100 mV and pH = 5,5, obtained via electrolysis of diluted NaCl solution demonstrated that within 5 min of influence all cells were inflated and burst. Also, it was occurred a full destruction of proteins, DNA and RNA. Supposedly the anolyte enters the cells provoking structural and functional damages on the cell's membrane and cell's wall.

Similar research was performed by S.V. Kumar et al. [24] to evaluate the inactivation efficacy of the anolyte at pH = 2,7 and ORP = +1100 mV on *E. coli O157:H7, Salmonela enteritidis* and *Lusteria monocytogenes*. As it was demonstrated on five strains of *E. coli E06* (milk), E08 (meat), E10 (meat), E16 (meat) and E22 (calf feces), all patogens were significantly reduced (7,0 log CFU/ml) or fully destroied (8,0 log CFU/ml) after 2 to 10 min inactivation by the anolyte within the temperature range from +4 ^{0}C to +23 ^{0}C. Supposedly, the low pH value of the anolyte makes sensitive the outer cell's membrane, thus facilitating HClO to enter into the cell and further destroy it. Unexpectedly, the stronger biocidal effect of the catholyte was observed when a strain of *E. coli DH5* was treated by the anolyte and catholyte, respectively.

The virucidal action of the anolyte was studied by us on cell culture and suspensions of the CSF virus [25]. After inoculating them with cell cultures, the viral presence (the presence of viral antigen) was measured using the immunoperoxidase technique. It was found that anolyte did not affect the growth of the cell culture PK-15; viral growth during the infection of a cell monolayer with a cell culture virus was affected in the greatest degree by the anolyte in 1:1 dilution and less in other dilutions; whereas the viral growth at the infection of a cell suspension with the CSF virus was affected by the anolyte in dilution 1:1 in the greatest degree, and less by other dilutions; viral growth at the infection with a virus in suspension of the cell monolayer was affected by the anolyte in all dilutions. However, it should be noted that the pharmacological studies of electrochemically activated solutions of water and their virucidal effects and toxicity have not yet been completely evaluated.

The evaluation of the mathematical model of interaction of the catholyte and the anolyte with water

The peculiarities of the chemical structure of H_2O molecules and weak bonds stipulated by electrostatic forces and donor-acceptor interaction between hydrogen and oxygen atoms in H_2O molecules create favorable conditions for formation of directed intermolecular hydrogen bonds (O–H...O) with neighboring H_2O molecules, binding them into complex intermolecular associates which composition represented by general formula $(H_2O)_n$, where n can vary from 3 to 50 units [26]. The hydrogen bond – is a form of association between the electronegative oxygen O-atom and hydrogen H-atom, covalently bound to another electronegative oxygen O-atom, is of vital importance in the chemistry of intermolecular interactions, based on weak electrostatic forces and donor-acceptor interactions with charge-transfer. It results from interaction between electron-deficient H-atom of one H_2O molecule (hydrogen donor) and unshared electron pair of an electronegative O-atom (hydrogen acceptor) on the neighboring H_2O molecule; the structure of hydrogen bonding, therefore may be defined as $O...^{.}H^{\delta+}-O^{\delta-}$. As the result, the electron of the H-atom due to its relatively weak bond with the proton easily shifts to the electronegative O-atom. The O-atom with increased electron density becomes partly negatively charged – δ^-, while the H-atom on the opposite side of the molecule becomes positively charged – δ^+ that leads to the polarization of $O^{\delta-}-H^{\delta+}$ covalent bond. In this process the proton becomes almost bared, and due to the electrostatic attraction forces are provided good conditions for convergence of O...O or O...H atoms, leading to the chemical exchange of a proton in the reaction O–H...O ↔ O...H–O. Although this interaction is essentially compensated by mutual repulsion of the molecules' nuclei and electrons, the effect of the electrostatic forces and donor-acceptor interactions for H_2O molecule compiles 5–10 kcal per 1 mole of substance. It is explained by negligible small atomic radius of hydrogen and shortage of inner electron shells, which enables the neighboring H_2O molecule to approach the hydrogen atom of another molecule at very close distance without experiencing any strong electrostatic repulsion.

The H_2O molecule has four sites of hydrogen bonding – two uncompensated positive charges at hydrogen atoms and two negative charges at the oxygen atom. Their mutual disposition is characterized by direction from the centre of regular tetrahedron (nucleus of oxygen atom) towards its vertexes. This allows to one H_2O molecule in condensed state to form up to 4 classical hydrogen bonds, two of which are donor bonds and the other two – acceptor ones (taking into consideration bifurkate ("two-forked") hydrogen bond – 5) [27].

A hydrogen bond according to Bernal–Fowler rules [28] is characterized by the following parameters:

a) an oxygen atom of each H_2O molecule is bound with four neighboring hydrogen atoms: by covalent bonding with two own hydrogen atoms, and by hydrogen bonding – with two neighboring hydrogen atoms (as in the crystalline structure of ice); each hydrogen atom in its turn is bound with oxygen atom of neighbour H_2O molecule;

b) on the line of oxygen atom – there can be disposed only one proton H^+;

c) the proton, which takes part in hydrogen bonding situated between two oxygen atoms, therefore has two equilibrium positions: it can be located near its oxygen atom at approximate distance of 1,0 Å, and near the neighboring oxygen atom at the distance of 1,7 Å as well, hence both a usual dimmer HO–H...OH_2 and an ion pair HO...H–OH_2 may be formed during hydrogen

bonding, i.e. the hydrogen bond is part electrostatic (~90%) and part (~10%) covalent [29]. The state of "a proton near the neighboring oxygen" is typical for the interphase boundary, i.e. near water-solid body or water–gas surfaces.

d) the hydrogen bonding of a triad O–H...O possess direction of the shorter O–H ($\rightarrow$) covalent bond; the donor hydrogen bond tends to point directly at the acceptor electron pair (this direction means that the hydrogen atom being donated to the oxygen atom acceptor on another H_2O molecule).

The most remarkable peculiarity of hydrogen bond consists in its relatively low strength; it is 5–10 times weaker than chemical covalent bond [30]. In respect of energy the hydrogen bond has an intermediate position between covalent bonds and intermolecular van der Waals forces, based on dipole-dipole interactions, holding the neutral molecules together in gasses or liquefied or solidified gasses. Hydrogen bonding produces interatomic distances shorter than the sum of van der Waals radii, and usually involves a limited number of interaction partners. These characteristics become more substantial when acceptors bind H-atoms from more electronegative donors. Hydrogen bonds hold H_2O molecules on 15% closer than if water was a simple liquid with van der Waals interactions. The hydrogen bond energy compiles 5–10 kcal/mole, while the energy of O–H covalent bonds in H_2O molecule – 109 kcal/mole [31]. The values of the average energy ($\Delta E_{H...O}$) of hydrogen H...O-bonds between H_2O molecules make up -0,1067±0,0011 eV [32]. With fluctuations of water temperature the average energy of hydrogen H...O-bonds in of water molecule associates changes. That is why hydrogen bonds in liquid state are relatively weak and unstable: it is thought that they can easily form and disappear as the result of temperature fluctuations.

Another key feature of hydrogen bond consists in its cooperativity coupling. Hydrogen bonding leads to the formation of the next hydrogen bond and redistribution of electrons, which in its turn promotes the formation of the following hydrogen bond, which length increasing with distance. Cooperative hydrogen bonding increases the O–H bond length, at the same time causing a reduction in the H...O and O...O distances [33]. The protons held by individual H_2O molecules may switch partners in an ordered manner within hydrogen networks [34]. As the result, aqueous solutions may undergo autoprotolysis, i.e. the H^+ proton is released from H_2O molecule and then transferred and accepted by the neighboring H_2O molecule resulting in formation of hydronium ions as H_3O^+, $H_5O_2^+$, $H_7O_3^+$, $H_9O_4^+$, etc. This leads to the fact, that water should be considered as associated liquid composed from a set of individual H_2O molecules, linked together by hydrogen bonds and weak intermolecular van der Waals forces. The simplest example of such associate can be a dimmer of water:

$$(H_2O)_2 = H_2O \cdots HOH$$

The energy of the hydrogen bonding in the water dimmer makes up 0,2 eV (~5 kcal/mol) that is larger than the energy of thermal motion of the molecules at the temperature of 300 K. Hydrogen bonds are easily disintegrated and re-formed through an interval of time, which makes water structure quite unstable and changeable [35]. This process leads to structural inhomogeneity of water characterizing it as an associated heterogeneous two-phase liquid with short-range ordering, i.e. with regularity in mutual positioning of atoms and molecules, which reoccurs only at distances comparable to distances between initial atoms, i.e. the first H_2O layer. A liquid is a dynamic system: its atoms, ions or molecules, keeping short-range order in mutual disposition, participate in thermal motion, the character of which is much more complicated than that of crystals. For example H_2O molecules in liquid state under normal conditions (1 atm, +22 ^0C) are quiet mobile and can oscillate around their rotation axes, as well as to perform the random and directed shifts. This enabled for some individual molecules due to cooperative interactions to "jump up" from one place to another in an elementary volume of water. Random motion of molecules in liquids causes continuous changes in the distances between them. The statistical character of ordered arrangement of molecules in liquids results in fluctuations – continuously occurring deviations not only from average density, but from average orientation as well, because molecules in liquids are capable to form groups, in which a particular orientation prevails. Thus, the smaller these deviations are, the more frequently they occur in liquids.
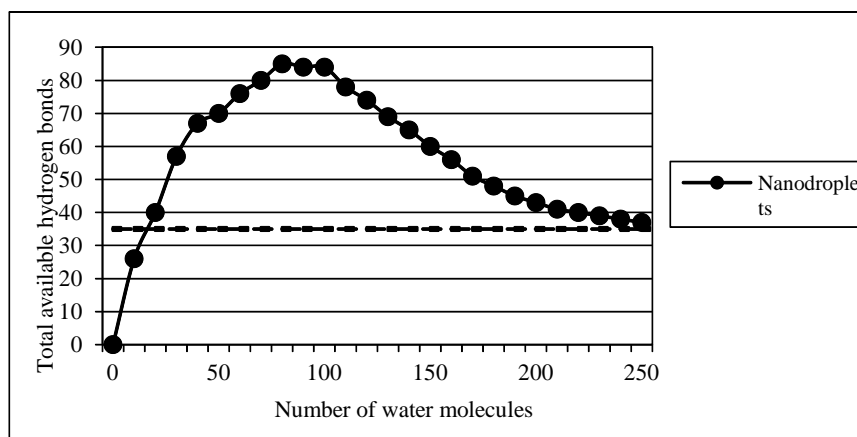
Figure 5. The total number of hydrogen bonds depending on the number
of H_2O molecules in clusters.

Hydrogen bonds are easily disintegrated and re-formed through an interval of time, which makes water structure quite unstable and changeable. External influences can provoke changes in the water structure that will reflect on the number of hydrohen bonds, i.e. on the size of clusters. In 2005 R. Saykally [36] calculated the possible number of hydrogen bonds and the stability of water clusters depending on the number of H_2O molecules (Figure 5). The possible number of available hydrogen bonds (90) depending on the number of H_2O molecules (250) in clusters was also estimated [37]. O. Loboda and O.V. Goncharuk provided data about the existence of icosahedral water clusters consisting of 280 H_2O molecules with average size up to 3 nm [38].

It was noticed that under the influence of electric field the hydrogen bonds become highly polarized and get disrupted, therefore the cluster size is diminished to up to a few H_2O molecules, but not more than 20.

Another convenient method for obtaining useful information about the structural changes in water and the average energy of hydrogen bonds is the measuring of the energy spectrum of the water state (ESWS). It was established experimentally that at evaporation of water droplet the contact angle θ decreases discretely to zero, whereas the diameter of the droplet changes insignificantly [39]. By measuring this angle within a regular time intervals a functional dependence $f(\theta)$ can be determined, which is designated by the spectrum of the water state. For practical purposes by registering the ESWS it is possible to obtain information about the averaged energy of hydrogen bonds in an aqueous sample. For this purpose the model of W. Luck is used, which consider water as an associated liquid, consisted of O−H...O−H groups [40]. The major part of these groups is designated by the energy of hydrogen bonds (-E), while the others are free ($E = 0$). The energy distribution function $f(E)$ is measured in electron-volts (eV^{-1}) and may be varied under the influence of various external factors on water as temperature and pressure.

For calculation of the function $f(E)$ experimental dependence between the water surface tension measured by the wetting angle (θ) and the energy of hydrogen bonds (E) is established:

$$f(E) = bf(\theta) \,/\, [1 − (1 + bE)^2]^{1/2}, \tag{15}$$

where $b = 14{,}33$ eV^{-1}; $\theta = arcos(1 − bE)$

The energy of hydrogen bonds (E) measured in electron-volts (eV) is designated by the spectrum of energy distribution. This spectrum is characterized by non-equilibrium process of water droplets evaporation, thus the term "non-equilibrium energy spectrum of water" (NES) is applied.

The difference $\Delta f(E) = f$ (samples of water) − f (control sample of water)
− is designated the "differential non-equilibrium energy spectrum of water" (DNES).

The DNES-spectrum measured in milielectron volts (0,001 eV) is a measure of structural changes in the bulk water as a result of external factors. Figure 5 shows the characteristic NES-spectrum of deionized water made from 25 independence measurements done in a period of one year.
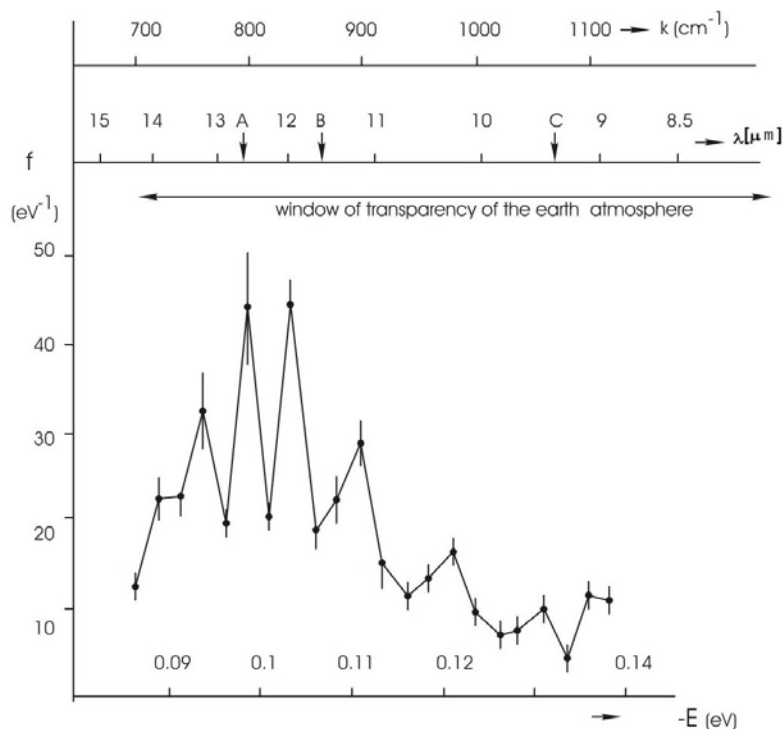
Figure 5. NES-spectrum of deionized water (chemical purity – 99,99%; pH – 6,5–7,5; total mineralization – 200 mg/l; electric conductivity – 10 μS/cm). The horizontal axis shows the energy of the H...O hydrogen bonds in the associates – E (eV). The vertical axis – energy distribution function – f (eV^{-1}). k – the vibration frequency of the H−O−H atoms (cm^{-1}); λ – wavelength (μm).

We studied the characteristics of NES and DNES-spectra of catholyte and anolyte solutions and distribution of local maximums in them. Also the average energy ($\Delta E_{H...O}$) of hydrogen H...O-bonds among individual molecules H_2O was calculated for the catholyte and the anolyte by NES- and DNES-methods. Local maximums of catholyte and anolyte solutions in NES- and DNES-spectra are shown in Table 3. The local maximum for the catholyte in the NES-spectrum was detected at -0,1285 eV, for anolyte – at -0,1227 eV, and for the control sample of deionized water – at -0,1245 eV. The calculations of $\Delta E_{H...O}$ for catholyte with using the DNES method compiles (-0,004±0,0011 eV) and for anolyte (+1,8±0,0011 eV).

The evaluation of the possible number of hydrogen bonds as percent of H_2O molecules with different values of distribution of energies for electrochemicaly activated catholyte and anolyte solutions is presented in Table 4. These distributions are basically connected with the restructuring of H_2O molecules having the same energies. These data serves as the mathematical model explaining the behavior of the anolyte and the catholyte regarding the distribution of H_2O molecules to the energies of hydrogen bonds in samples of electrochemically activated water solutions of the catholyte and the anolyte. These data testifies that not only the number of H_2O molecules with different energies of hydrogen bonds changes, but also the number of hydrogen bonds, the redistribution of H_2O molecules and the character of hydrogen bonding changes as well. This phenomenon may be explained by the fact that under the influence of electric field the hydrogen bonds between H_2O molecules become polarized and get disrupted, therefore the cluster size may be changed to up to a few H_2O molecules. However, these are our preliminary judgments, based on the character of NES and DNES-spectra and distribution of local maximums and minimums in spectra that will be continued in future studies.

Table 3: Local maximums of catholyte and anolyte solutions in NES- and DNES-spectra

-E(eV) x-axis	Catholyte	Anolyte y-axis (eV^{-1})	Control sample y-axis (eV^{-1})	DNES Catholyte	DNES Anolyte	-E(eV) x-axis	Catholyte y-axis (eV^{-1})	Anolyte y-axis (eV^{-1})	Control sample y-axis (eV^{-1})	DNES Catholyte y-axis (eV^{-1})
0,0937	0	0	0	0	0	0,1187	0	66,7	66,7	-66,7
0,0962	0	0	0	0	0	0,1212	66,7	0	0	66,7
0,0987	0	0	0	0	0	0,1237	0	0	0	0
0,1012	66,7	66,7	33,3	33,4	33,4	0,1262	0	0	66,7	-66,7
0,1037	0	0	33,3	-33,3	-33,3	0,1287	0	0	66,7	-66,7
0,1062	0	0	0	0	0	0,1312	33,3	100	33,3	0
0,1087	0	0	0	0	0	0,1337	33,3	33,3	33,3	0
0,1112	0	0	0	0	0	0,1362	0	0	0	0
0,1137	0	66,7	66,7	-66,7	0	0,1387	200	66,7	66,7	133,3
0,1162	0	0	0	0	0	–	–	–	–	–

Table 4: Energy distribution of catholyte and anolyte solutions in electrochemicaly activated solutions of sodium chloride

-E(eV) x-axis	Catholyte y-axis, % ($-E_{value}$)/ ($-E_{total\ value}$)	Anolyte y-axis, % ($-E_{value}$)/ ($-E_{total\ value}$)	-E(eV) x-axis, % ($-E_{value}$)/ ($-E_{total\ value}$)	Catholyte y-axis, % ($-E_{value}$)/ ($-E_{total\ value}$)	Anolyte y-axis, % ($-E_{value}$)/ ($-E_{total\ value}$)
0,0937	0	0	0,1187	0	16,7
0,0962	0	0	0,1212	16,7	0
0,0987	0	0	0,1237	0	0
0,1012	16,7	16,7	0,1262	0	0
0,1037	0	0	0,1287	0	0
0,1062	0	0	0,1312	8,4	24,8
0,1087	0	0	0,1337	8,4	8,4
0,1112	0	0	0,1362	0	0
0,1137	0	16,7	0,1387	49,8	16,7
0,1162	0	0	–	–	–

Conclusions

The electrochemical water treatment has several advantages compared to alternative chemical methods for disinfection of water. These advantages are the efficiency, stability, controllability and convenient automatic control of the electrolysis processes, as well as simplicity of the construction scheme. The devices for the electrochemical water treatment are compact, have a high level of reliability, easy operation and demand, and may be fully automated. In multi-stage schemes to improve water quality and its disinfection the electrochemical treatment can conveniently be combined with other water treatment methods. We have applied NES and DNES-methods for studying the physical-chemical properties of the catholyte and anolyte the evaluation of the possible number of hydrogen bonds as percent of H_2O molecules with different values of distribution of energies. These distributions suggest that not only the number of H_2O molecules with different energies of hydrogen bonds changes, but also the number of hydrogen bonds, the redistribution of H_2O molecules and the character of hydrogen bonding changes as well. These data serves as the mathematical model explaining the behavior of the anolyte and the catholyte regarding the distribution of H_2O molecules to the energies of hydrogen bonds.

References:

1. Bahir V.M., Liakumovich A.G., Kirpichnikov P.A., Spector L.E., Mamajanov U.D. The physical nature of the phenomena of activation substances // *Izv. UzSSR. Ser. Tehn. Sciences.* 1983. Vol. 1. P. 60–64.

2. Kirpichnikov P.A., Bahir V.M., Hamer P.U. On the nature of electrochemical activation of media // *Dokl. USSR Academy of Sciences.* 1986. Vol. 286. № 3. P. 663–666.

3. Morita C., Sano K., Morimatsu S., Kiura H., Goto T., Kohno T. Disinfection potential of electrolyzed solutions containing sodium chloride at low concentrations // *Journal of Virological Methods.* 2000. Vol. 85(2). P. 163–174.

4. Petrushanko I.Ju., Lobyshev V.I. Non-equilibrium state of electrochemically activated water and its biological activity // *Biofizika.* 2001. Vol. 46. № 3. P. 389–401.

5. Mosin O.V. Electrochemical treatment of water // *Santechnics Heating Air Conditioning. C.O.K. Moscow: Media Technology.* 2012. № 12. P. 20–26.

6. Dykstra C.E. External electric field effects on the water trimmer // *Chemical Physics Letters.* 1999. Vol. (2)299. P. 132–136.

7. Bahir V.M. *Electrochemical activation.* – Moscow: All Russian Scientific Research and Experimental Institute of Medical Engineering (VNIIIMT). 1992. Vol. 2. P. 632–657.

8. Hsu S.Y. Effects of flow rate, temperature and salt concentration on chemical and physical properties of electrolyzed oxidizing water // *Journal of Food Engineering.* 2005. Vol. 66. P. 171–176.

9. Bahir V.M., Zadorozhnii Y.G., Leonov B.I., Panicheva S.A., Prilutsky V.I. *Electrochemical activation: water purification and production of useful solutions.* – Moscow: VNIIIMT. 2001. Vol. 1. P. 100–176.

10. Toropkov V.V., Altschul E.B., Toropkova E.V. Toxicological characterization of catholyte / in: *3d International Symposium "Electrochemical Activation".* – Moscow-Leningrad. 2001. Vol. 1. P. 57–62.

11. Leonov B.I., Prilutsky V.I., Bahir V.M. *Physico-chemical aspects of the biological effect of electrochemically activated water.* – Moscow: VNIIIMT. 1999. Vol. 1. P. 224–240.

12. Petrushanko I.Ju., Lobyshev V.I. Physico-chemical properties of aqueous solutions, prepared in a membrane electrolyzer // *Biofizika.* 2004. T. 49(1). P. 22–31.

13. Kirkpatrick R.D. *The Mechanism of antimicrobial action of electro-chemically activated (ECA) water and its healthcare applications.* – Doctoral Thesis, University of Pretoria. 2009.

14. Leonov B.I., Bahir V.M., Vtorenko V.I. Electrochemical activation in the practice of medicine / in: *2nd International Symposium "Electrochemical Activation".* Proc. rep. and brief reports. – Moscow. 1999. Vol. 1. P. 15–23.

15. Toropkov V.V., Altshul E.B., Peresypkin O.I. Therapeutic efficacy of anolyte and ANC on the mucous membranes of the oral cavity / in: *2nd International Symposium "Electrochemical Activation".* – Moscow. 1999. Vol. 1. P. 93–95.

16. Prilutsky V.I., Bakhir V.M. *Electrochemically activated water: Anomalous properties, mechanism of biological action.* – Moscow: VNIIIMT, 1997. Vol. 1. 124 p. [in Russian].

17. Babtsova N.F., Komarov I.F. Experience of using STELS in the surgical department / in: *2nd International Symposium. Electrochemical activation.* Proc. and brief reports. 1999. Vol. 1. P. 131–132.

18. Suzuki T., Itakura J., Watanabe M., Ohta M., Sato Y., Yamata Y. Inactivation of staphylococcal *Enterotoxin-A* with an electrolyzed anodic solution // *Journal of Agricultural and Food Chemistry.* 2002. Vol. 50. P. 230–234.

19. Karadzov S., Atanasov A., Ivanova E., Mosin O.V., Ignatov I. Mathematical models of electrochemical aqueous sodium chloride solutions (anolyte and catolyte) as types of water. Study of the effects of anolyte on the virus of classical swine fever virus // *Journal of Health, Medicine and Nursing.* 2014. Vol. 5. P. 30–55.

20. Sands J.A., Landin P., Auperin D. Enveloped virus inactivation by fatty acid derivates // *Antimicrob. Agents Chem.* 1979. Vol. 15. P. 134–136.

21. Springthorpe U.S., Sattar S.A. Chemical disinfection of virus-contaminated surfaces // *Crit. Rev. Environ. Control.* 1990. Vol. 20. P. 169–229.

22. Stoner G.E., Cahen G.L. Jr., Sachyani M., Gileadi E. The mechanism of low frequency a.c. electrochemical disinfection // *Bioelectrochemistry and Bioenergetics.* 1982. Vol. 9(3). P. 229–24.

23. Zinkevich V., Beech I.B., Tapper R., Bogdarina I. The effect of super-oxidized water on *Escherihia coli* // *Journal of Hospital Infection.* 2000. Vol. 46. P. 153–156.

24. Kumar S.V., Ezeike G.O., Hung Y.C., Doyle M.P. Efficacy of electrolyzed oxidizing water for inactivating *Escherihia coli O157:H7, Salmonela enteritidis*, and *Lusteria monocytogenes* // *Applied and Environmental Microbiology.* 1999. Vol. 23. P. 4276–4279.

25. Atanasov A., Karadzhov S., Ivanova E., Mosin O.V., Ignatov I. Study of the effects of electrochemical aqueous sodium chloride solution (anolite) on the virus of classical swine fever virus. Mathematical models of anolyte and catolyte as types of water // *Journal of Medicine, Physiology and Biophysics.* 2014. Vol. 4. P. 1–26.

26. Ignatov I., Mosin O.V. Structural mathematical models describing water clusters // *Journal of Mathematical Theory and Modeling.* 2013. Vol. 3. № 11. P. 72–87.

27. Pasichnyk I., Everaers R., Maggs A.C. Simulating van der Waals-interactions in water/hydrocarbon-based complex fluids // *J. Phys. Chem. B.* 2008. Vol. 112. № 6. P. 1761–1764.

28. Bernal J.D., Fowler R.H. A theory of Water and Ionic Solutions, with particular reference to hydrogen and hydroxyl ions // *J. Chem. Phys.* 1933. Vol. 1. P. 515–548.

29. Mosin O.V., Ignatov I. Structure of water and physical reality // *Soznanije i physicheskaja realnost*, 10(1), 32–48 [in Russian].

30. Pimentel G.C., McClellan A.L. *The Hydrogen Bond /* L. Pouling, Ed. – New York: Reinhold Publishing Co., 1960. 126 p.

31. Ignatov I., Mosin O.V. Mathematical models describing the nanostructure of water and nanoclusters // *Nanoingenering, Izdatel'stvo Mashinostroenie, Moscow.* 2013. №. 8. P. 32–46 [in Russian].

32. Ignatov I., Mosin O.V. Structural models of water describing the cyclic clusters // *Micro- and Nanosystem Technique.* 2014. № 3. P. 47–56.

33. Petkov V., Ren Y., Suchomel M. Molecular arrangement in water: random but not quite // *J. Phys. Condens. Matter.* 2012. V. 24. P. 155102.

34. Bartha F., Kapuy O., Kozmutza C., Van Alsenoy C. Analysis of weakly bound structures: hydrogen bond and the electron density in a water dimmer // *J. Mol. Struct. (Theochem).* 2003. Vol. 666. P. 117–122.

35. Ignatov I., Mosin O. Structural Mathematical Models of Water Clusters Regarding the Energy of Hydrogen Bonding // *Nanotechnology Research and Practice.* 2015. Vol.(5). P. 37–56.

36. Saykally R. Unified Description of Temperature-Dependent Hydrogen Bond Rearrangements in Liquid Water // *PNAS.* 2005. V. 102. № 40. P. 14171–14174.

37. Sykes M. Simulations of RNA Base Pairs in a Nanodroplet Reveal Solvation-Dependent Stability // *PNAS.* 2007. V. 104. № 30. P. 12336–12340.

38. Loboda O., Goncharuk V. Theoretical study on icosahedral water clusters // *Chemical Physics Letters.* 2010. V. 484. № 4–6. P. 144–147.

39. Ignatov I., Mosin O.V. Methods for measurements of water spectrum. Differential non-equilibrium energy spectrum method (DNES) // *Journal of Health, Medicine and Nursing.* 2014. Vol. 6. P. 50–72.

40. Luck W., Schiöberg D., Ulrich S. Infared investigation of water Structure in desalination membranes // *J. Chem. Soc. Faraday Trans.* 1980. Vol. 2. № 76. P. 136–147.
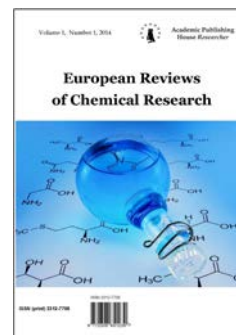
UDC 579.871.08

Deuterated Methylotrophic Biomass as a Substrate for Microbiological Synthesis of ²H-Labeled Purine Ribonucleoside Inosine by Chemoheterotrophic Bacterium *Bacillus Subtilis B-3157*

[1*] Oleg Mosin
[2] Ignat Ignatov

[1] Moscow State University of Applied Biotechnology, Russian Federation
Senior research Fellow of Biotechnology Department, Ph. D. (Chemistry)
103316, Moscow, Talalihina ulitza, 33
*E-mail: mosin-oleg@yandex.ru
[2] Scientific Research Center of Medical Biophysics (SRC MB), Bulgaria
Professor, D. Sc., director of SRC MB
1111, Sofia, N. Kopernik street, 32
E-mail: mbioph@dir.bg

Abstract

We propose to use the hydrolyzed deuterated biomass of the facultative methylotrophic bacterium *Brevibacterium methylicum B-5662* as a source of ²H-labeled growth substrates for microbiological synthesis of ²H-labeled purine ribonucleoside inosine, excreted into the liquid microbial culture (LC) by a Gram-positive chemoheterotrophic bacterium *Bacillus subtilis B-3157*. The bacterium was grown on heavy water (HW) medium with 2% (v/v) hydrolysate of deuterated biomass of the methylotrophic bacterium *Brevibacterium methylicum B-5662* obtained on minimal salt media M9 supplemented with 2% (v/v) [²H]methanol and increasing gradient of ^2H_2O concentration from 0; 24,5; 49,0; 73,5 up to 98% (v/v) ^2H_2O. Isolation of ²H-labeled inosine from LC was performed by adsorption/desorption on activated carbon with following extraction by 0,3 *M* ammonium−formate buffer (*pH* = 8,9), crystallization in 80% (v/v) EtOH, and ion exchange chromatography (IEC) on a column with AG50WX 4 cation exchange resin equilibrated with 0,3 *M* ammonium−formate buffer and 0,045 *M* NH_4Cl. The investigation of deuterium incorporation into the inosine molecule by FAB method demonstrated incorporation of 5 deuterium atoms into the molecule (the total level of deuterium enrichment − 65,5 atom% ²H) with 3 deuterium atoms being included into the ribose and 2 deuterium atoms – into the hypoxanthine residue of the molecule.

Keywords: ²H-labeled inosine, biosynthesis, metabolism, heavy water, *Bacillus subtilis*, FAB-mass-spectrometry.

Introduction

Natural nucleosides labeled with deuterium (²H) are of considerable scientific and practical interest for various biochemical and diagnostic purposes [1], structure-function studies [2], and research into cell metabolism [3]. Their usage is determined by the absence of radiation danger and the possibility of localizing the deuterium label in a molecule by ¹H-NMR [4], IR spectroscopy [5]

and mass spectrometry [6] methods. The latter seems more preferable due to high sensitivity of the method and possibility to study the distribution of deuterium label *de novo*. The recent advance in technical and computing capabilities of these analytical methods has allowed a considerable increase the efficiency of carrying out biological studies with ^{2}H-labeled molecules *de novo*, as well as to carry out the analysis of the structure and function of nucleosides and their analogs at the molecular level [7]. In particular, ^{2}H-labeled ribonucleosides and their analogs are used in template-directed syntheses of deuterated RNA macromolecules for studying their spatial structure and conformational changes [8]. Perdeuteration and selective deuteration techniquemay be useful approaches for simplification of NMR spectra and for other structural studies of large biomolecules. Driven by the progress in multinuclear multidimensional NMR spectroscopy, deuteration of nucleic acids has especially found wide applications in the NMR studies of these macromolecules in solution. Deuterated ribonucleosides may be of further interest for NMR spectroscopy studies. Another usage of these deuterated molecules has been in atom transfer and kinetic isotope effect experiments.

An important factor in studies with ^{2}H-labeled nucleosides and their analogs is their availability. ^{2}H-labeled nucleosides can be synthesized with using chemical, enzymatic, and microbiological methods [9, 10]. Chemical synthesis is frequently multistage; requires expensive reagents and ^{2}H-labeled substrates, and eventually results to a racemic mixture of D- and L-enantiomers, requiring special methods for their separation [11]. Finer chemical synthesis of [^{2}H]nucleosides combine both chemical and enzymatic approaches [12].

Microbiology proposes an alternative method for synthesis of [^{2}H]nucleosides, applicable for various scientific and applied purposes; the main characteristics of the method are high outputs of final products, efficient deuterium incorporation into synthesized molecules, and preservation of the natural L-configuration of ^{2}H-labeled molecules [13]. A traditional approach for biosynthesis of ^{2}H-labeled natural compounds consists in growing of strains-producers on growth media containing maximal concentrations of ^{2}H$_2$O and ^{2}H-labeled substrates [14]. However, the main obstacle seriously implementing this method is a deficiency in ^{2}H-labeled growth substrates with high deuterium content. First and foremost, this stems from a limited availability and high costs of highly purified deuterium itself, isolated from natural sources. The natural abundance of deuterium makes up 0,0015 atom%; however, despite a low deuterium content in specimens, recently developed methods for its enrichment and purification allow to produce ^{2}H-labeled substrates with high isotopic purity.

Starting from first experiments on the growth of biological objects in heavy water, the approach involving hydrolysates of deuterated bacterial and micro algal biomass as growth substrates for growth of other bacterial strains-producers have been developed in this country [15]. However, these experiments discovered a bacteriostatic effect of ^{2}H$_2$O consisted in inhibition of vitally important cell functions in ^{2}H$_2$O; this effect on micro algal cells is caused by 70% (v/v) ^{2}H$_2$O and on protozoan and bacterial cells – 80–90% (v/v) ^{2}H$_2$O [16]. Attempts to use biological organisms of various taxonomic species, including bacteria, micro algae, and yeasts [17] for growth in ^{2}H$_2$O have not been widely used because of complexity of biosynthesis, consisted in need of complex growth media, applying intricate technological schemes, etc. That is why a number of applied items regarding the biosynthesis of natural ^{2}H-labeled compounds in ^{2}H$_2$O remain to be unstudied.

More promising seem the technological schemes involving as a source of ^{2}H-labeled growth substrates the biomass of methylotrophic bacteria, assimilating methanol *via* the ribulose-5-monophosphate (RMP) and serine pathways of carbon assimilation [18]. The assimilation rate of methylotrophic biomass by prokaryotic and eukaryotic cells makes up 85–98% (w/w), and their productivity calculated on the level of methanol bioconversion into cell components reaches 50–60% (w/w) [19]. As we have earlier reported, methylotrophic bacteria are convenient objects able to grow on minimal salt media containing 2–4% (v/v) [^{2}H]methanol, whereon other bacteria are unable to reproduce, and may easily be adapted to maximal ^{2}H$_2$O concentrations, that is the most important for the biosynthesis of ^{2}H-labeled natural compounds [20].

The aim of this research was studying the possibility of using hydrolysates of deutero-biomass of the facultative methylotrophic bacterium *Brevibacterium methylicum B-5662* as a source of ^{2}H-labeled growth substrates for microbiological synthesis of ^{2}H-labeled purine ribonucleoside inosine by a Gram-positive chemoheterotrophic bacterium *Bacillus subtilis B-3157*.

Material and methods
Bacterial strain

The object of the research was a strain of inosine producer, spore-forming aerobic Gram-positive chemoheterotrophic bacterium *B. subtilis B-3157*, polyauxotrophic for histidine, tyrosine, adenine, and uracil (demand, 10 mg/l), obtained from Institute of Genetics and Selection of Industrial Microorganisms (Russia). The initial strain was adapted to deuterium by plating individual colonies onto 2% (w/v) agarose with stepwise increasing gradient of ^2H_2O concentration and subsequent selection of individual cell colonies stable to the action of ^2H_2O.

Chemicals

Growth media were prepared using ^2H_2O (99,9 atom% ^2H), ^2HCl (95,5 atom% ^2H), and [^2H]methanol (97,5 atom% ^2H), purchased from JSC "Izotop" (St. Petersburg, Russia). Inorganic salts, D- and L-glucose ("Reanal", Hungary) were preliminary crystallized in ^2H_2O. ^2H_2O was distilled over $KMnO_4$ with subsequent control of the isotope purity by ^1H-NMR spectroscopy on a Brucker WM-250 ("Brucker Daltonics" Germany) with a working frequency 70 MHz (internal standard – Me_4Si). According to ^1H-NMR, the level of isotopic purity of the growth medium was by 8–10 atom% lower than the isotope purity of the initial ^2H_2O.

Biosynthesis of [^2H]inosine

Biosynthetic [^2H]inosine was produced with an output 3,9 g/l in heavy water (HW) medium (89–90 atom% ^2H) using 2% (w/v) hydrolysate of deuterated biomass of the methanol assimilating strain of the facultative Gram-positive methylotrophic bacterium *Brevibacterium methylicum B-5662* as a source of ^2H-labeled growth substrates. The strain was obtained by multistage adaptation on a solid (2% (w/v) agarose) minimal salt M9 medium, containing 3 g/l KH_2PO_4, 6 g/l Na_2HPO_4, 0,5 g/l NaCl, 1 g/l NH_4Cl and 2% (v/v) [^2H]methanol with a stepwise increasing gradient of ^2H_2O concentration (0; 24,5; 73,5, and 98% (v/v) ^2H_2O). Raw methylotrophic biomass (output, 200 g/l) was suspended in 100 ml of 0,5 *N* ^2HCl (in ^2H_2O) and autoclaved for 30–40 min at 0,8 atm. The suspension was neutralized with 0,2 *N* KOH (in ^2H_2O) to *pH* = 7,0 and used as a source of growth substrates while growing the inosine producer strain. For this purpose, an inoculum (5–6 % (w/v)) was added into HW medium with 99,8 atom% ^2H_2O containing 12% (w/v) glucose, 2% (w/v) hydrolysate of deuterated biomass of *B. methylicum B-5662*, 2% (w/v) NH_4NO_3, 1% (w/v) $MgSO_4 \cdot 7H_2O$, 2% (w/v) $CaCO_3$, 0,01% (w/v) adenine, and 0,01% (w/v) uracil. As a control was used equivalent protonated medium containing 2% (w/v) yeast protein–vitamin concentrate (PVC).

Growth conditions

The bacterium was grown in 500 ml Erlenmeyer flasks (containing 100 ml of the growth medium) for 3–4 days at t = 32 °C under intensive aeration on a Biorad orbital shaker ("Biorad Labs", Hungary). The bacterial growth was controlled on the ability to form individual colonies on the surface of solid (2% (w/v) agarose) media with the same ^2H_2O-content, as well as on the optical density of the cell suspension measured on a Beckman DU-6 spectrophotometer ("Beckman Coulter", USA) at λ = 540 nm in a quartz cuvette with an optical pathway length 10 mm.

Analytical determination of [^2H]inosine

Inosine was analytically determined in 10 μl of liquid culture (LC) samples on Silufol UV-254 chromatographic plates (150×150 mm) ("Kavalier", Czech Republic) using a standard set of ribonucleosides "Beckman-Spinco" (USA) in the solvent system: *n*-butanol–acetic acid–water (2:1:1, % (v/v)). Spots were eluted with 0,1 *N* HCl. The UV absorbance of eluates was recorded on a Beckman DU-6 spectrophotometer ("Beckman Coulter", USA) using a standard calibration plot. The level of bioconversion of the carbon substrate was assessed using glucose oxidase (EC 1.1.3.4).

Isolation of [^2H]inosine from LC

Samples of LC were separated on a T-26 centrifuge ("Carl Zeiss", Germany) at 2000 g for 10 min, concentrated at 10 mm Hg in a RVO-6 rotor evaporator ("Microtechna", Hungary) to half of their initial volume, and supplemented with acetone (3×5 ml). The mixture was kept for ~10 h at

4°C, and the precipitate was separated by centrifugation at 1200 g for 5 min. The supernatant was supplemented with 20 g of activated carbon and kept for 24 h at 4 °C. The water fraction was separated by filtration; the solid phase was supplemented with 20 ml 50% (v/v) EtOH solution in 25% (v/v) ammonia (1:1, (v/v)) and heated at 60°C with a reflux water condenser. After 2–3 h, the mixture was filtered and evaporated at 10 mm Hg. The product was extracted with 0,3 M ammonium–formate buffer (pH = 8,9), washed with acetone (2×10 ml), and dried over anhydrous CaCl$_2$. Inosine was crystallized from 80% (v/v) ethanol ($[\alpha]_D^{20}$ = +1,61^0; output, 3,1 g/l (80%)). Inosine was finally purified by ion exchange chromatography using a calibrated column (150×10 mm) with AG50WX 4 cation exchange resin ("Pharmacia", USA). The column was equilibrated with 0,3 M ammonium–formate buffer (pH = 8,9) containing 0,045 M NH$_4$Cl and eluted with the same buffer under isocratic conditions (chromatographic purity, 92%). The eluate was dried in vacuum and stored in sealed ampoules at -14°C in frost camera. [^{2}H]inosine: yield – 3,1 g/l (80%); T_m = 68–70 °C; $[\alpha]_D^{20}$ = 1,61 (ethanol); R_f = 0,5; pK_a = 1,2 (phosphate buffer with pH = 6,87). UV-spectrum (0.1 N HCl): λ_{max} = 249 nm; ε_{249} = 7100 M^{-1}·cm^{-1}. FAB mass spectrum (glycerol matrix, Cs$^+$; accelerating voltage, 5 kV; ion current – 0,6–0,8 mA): [M + H]$^+$ m/z (I, %) 273, 20% (4 atoms ^{2}H); 274, 38 % (5 atoms ^{2}H); 275, 28% (6 atoms ^{2}H); 276, 14% (7 atoms ^{2}H); [A + H]$^+$ 136, 46%; [B + H]$^+$ 138, 55%; [B – HCN]$^+$ 111, 49%; [B – HCN]$^+$ 84, 43%.

Protein hydrolysis

Dry biomass (10 g) was treated with a chloroform–methanol–acetone mixture (2:1:1, % (v/v)), evaporated in vacuum, and supplemented with 5 ml of 6 N ^{2}HCl (in ^{2}H$_2$O). The ampules were kept at 110 °C for ~24 h. Then the reaction mixture was suspended in hot ^{2}H$_2$O and filtered. The hydrolysate was evaporated at 10 mm Hg. Residual ^{2}HCl was removed in an exsiccator over solid NaOH. For preparation of ^{2}H-labeled growth substrates 200 mg of raw deuteron-biomass was suspended in 200 ml of 0,5 M ^{2}HCl (in ^{2}H$_2$O) and autoclaved at 60 ^{0}C for ~1,5 h. The reaction mixture was neutralized with 0,5 M NaOH (in ^{2}H$_2$O) till pH = 6,5–6,7, and evaporated at 10 mm Hg. The dry residue was used for preparation of growth media.

Hydrolysis of intracellular policarbohydrates

Dry biomass (50 mg) was placed into a 250 ml round bottomed flask, supplemented with 50 ml distilled ^{2}H$_2$O and 1,6 ml 25% (v/v) H$_2$SO$_4$ (in ^{2}H$_2$O), and boiled in a reflux water evaporator for ~90 min. After cooling, the reaction mixture was suspended in one volume of hot distilled ^{2}H$_2$O and neutralized with 1 N Ba(OH)$_2$ (in ^{2}H$_2$O) to pH = 7,0. BaSO$_4$ was separated by centrifugation (1500 g, 5 min); the supernatant was decanted and evaporated at 10 mm Hg.

Amino acid analysis

The amino acids of the hydrolyzed biomass were analyzed on Biotronic LC-5001 (230×3,2 mm) column ("Eppendorf–Nethleler–Hinz", Germany) with UR-30 sulfonated styrene resin ("Beckman–Spinco", USA) as a stationary phase; the mobile phase – 0,2 N sodium–citrate buffer (pH = 2,5); the granule diameter – 25 μm; working pressure – 50–60 atm; the eluent input rate – 18,5 ml/h; the ninhydrin input rate – 9,25 ml/h; detection at λ = 570 and λ = 440 nm (for proline).

Analysis of carbohydrates

Carbohydrates were analyzed on Knauer Smartline chromatograph ("Knauer", Germany) equipped with a Gilson pump ("Gilson Inc.", USA) and a Waters K 401 refractometer ("Waters Associates", Germany) using Ultrasorb CN column (250×10 mm) as a stationary phase; the mobile phase, acetonitrile–water (75:25, % (v/v); the granule diameter – 10 μm; the input rate – 0,6 ml/min.

UV spectroscopy

The UV spectra were registered with Beckman DU-6 programmed spectrophotometer ("Beckman Coulter", USA) at λ = 220–280 nm.

FAB mass spectrometry

FAB mass spectra were recorded on VG-70 SEQ chromatograph ("Fisons VG Analytical", USA) equipped with a cesium source on a glycerol matrix with accelerating voltage 5 kV and ion current 0,6–0,8 mA.

Results and Discussion
Preparation of Deutero-Biomass of B. methylicum

For this study was used a mutant strain of the Gram-positive chemoheterotrophic bacterium *B. subtilis B-3157*, polyauxotrophic for histidine, tyrosine, adenine, and uracil (preliminary adapted to deuterium by selection of individual colonies on growth media with increased ^2H_2O content). Due to impaired metabolic pathways involved in the regulation of the biosynthesis of purine ribonucleosides, this strain under standard growth conditions (PVC medium, late exponential growth, 32 °C) synthesizes 17–20 g of inosine per 1 liter of LC [21].

The maximal yield of inosine was attained on a protonated medium with 12% (w/v) glucose as a source of carbon and energy and 2% (w/v) yeast PVC as a source of growth factors and amine nitrogen. In our experiments it was necessary to replace the protonated growth substrates with their deuterated analogs, as well as to use ^2H_2O of high isotopic purity. For this purpose, we used autoclaved biomass of the Gram-positive facultative methylotrophic bacterium *B. methylicum B-5662*, capable to assimilate methanol *via* RuMP pathway of carbon assimilation. Owing to a 50–60% rate of methanol bioconversion (conversion efficiency – 15,5–17,3 gram dry biomass per 1 gram of assimilated substrate) and stable growth on deuterated minimal medium M9 with 98% (v/v) ^2H_2O and 2% (v/v) [^2H]methanol, this strain is the most convenient source for producing the deuterated biomass; moreover, the cost of bioconversion is mainly determined by the cost of ^2H_2O and [^2H]methanol [22].

Adaptation of *B. methylicum B-5662* was necessary to improve the growth characteristics of this strain and attain high output of microbial biomass on the maximally deuterated M9 medium. For this purpose, we used a stepwise increasing gradient of ^2H_2O-concentration in M9 growth media (from 24,5; 49,0; 73,5 up to 98% (v/v) ^2H_2O) in the presence of 2% (v/v) methanol and its ^2H-labeled analog ([^2H]methanol), because we assumed that gradual cell adaptation to ^2H_2O would have a favorable effect on the growth parameters of the strain.

Table 1: Isotopic components of growth media M9 and characteristics of bacterial growth of *B. methylicum B-5662**

Experiment number	Media components, % (v/v)				Lag-period (h)	Yield of biomass, gram from 1 l of LC	Generation time (h)
	H_2O	^2H_2O	Methanol	[^2H]methanol			
1	98,0	0	2	0	20±1,40	200,2±3,20	2,2±0,20
2	98,0	0	0	2	30±1,44	184,6±2,78	2,4±0,23
3	73,5	24,5	2	0	32±0,91	181,2±1,89	2,4±0,25
4	73,5	24,5	0	2	34±0,89	171,8±1,81	2,6±0,23
5	49,0	49,0	2	0	40±0,90	140,2±1,96	3,0±0,32
6	49,0	49,0	0	2	44±1,38	121,3±1,83	3,2±0,36
7	24,5	73,5	2	0	45±1,.41	112,8±1,19	3,5±0,27
8	24,5	73,5	0	2	49±0,91	94,4±1,74	3,8±0,25
9	0	98,0	2	0	58±1,94	65,8±1,13	4,4±0,70
10	0	98,0	0	2	60±2,01	60,2±1,44	4,9±0,72
10'	0	98,0	0	2	40±0,88	174,0±1,83	2,8±0,30

Notes: * The data in Expts. 1–10 are submitted for *B. methylicum* at growing on growth media with 2% (v/v) methanol/[^2H]methanol and specified amounts (%, v/v) ^2H_2O. The data in Expt. 10' are submitted for adapted for maximum content of deuterium in growth medium bacterium *B. methylicum* at the growing on growth media with 2% (v/v) of [^2H]methanol and 98% (v/v) of ^2H_2O. As the control used experiment where used ordinary protonated water and methanol.

To study the effect of the degree of the carbon source deuteration on the growth parameters of the strain, in experiments 1, 3, 5, 7, and 9 was used protonated methanol, and [^{2}H]methanol in experiments 2, 4, 6, 8, and 10 (Table 1). The results demonstrated that the replacement of protonated methanol with its deuterated analog within the same concentration of ^{2}H$_2$O in the growth media slightly decreased the growth characteristics (Table 1, experiments 2, 4, 6, 8, and 10). Therefore, in further experiments were used M9 media with ^{2}H$_2$O and [^{2}H]methanol. When the initial strain of *B. methylicum* was cultivated on protonated M9 medium with water and methanol, the duration of lag-phase and cell generation time were 20 and 2,2 h, respectively, with an output of biomass 200 gram per 1 liter of LC (Table 1, experiment 1). In the intermediate experiments (2– 10), these parameters varied proportionally to the ^{2}H$_2$O concentration (Table 1). The observed effect consisted in the increase in the lag-phase period and cell generation time with a simultaneous decrease in microbial biomass outputs on media with increasing ^{2}H$_2$O-content. The most remarkable values of this parameters were detected in experiment 10, in which was used the maximally deuterated medium with 98% (v/v) ^{2}H$_2$O and 2% (v/v) [^{2}H]methanol; the lag-phase and cell generation time in these conditions were increased in 3- and 2,2-fold times, respectively, as compared to the control conditions (water and methanol; Table 1, experiment 1), and the biomass output decreased in 3,1-fold. The adaptation to deuterium (experiment 10', Table 1) permitted to improve essentially the growth characteristics of *B. methylicum B-5662* on maximally deuterated growth medium. The output of biomass produced by the adapted bacterium decreased by 13% as compared to the control with an increase in the generation time to 2,8 h and the lag phase to 40 h (experiment 10', Table 1).
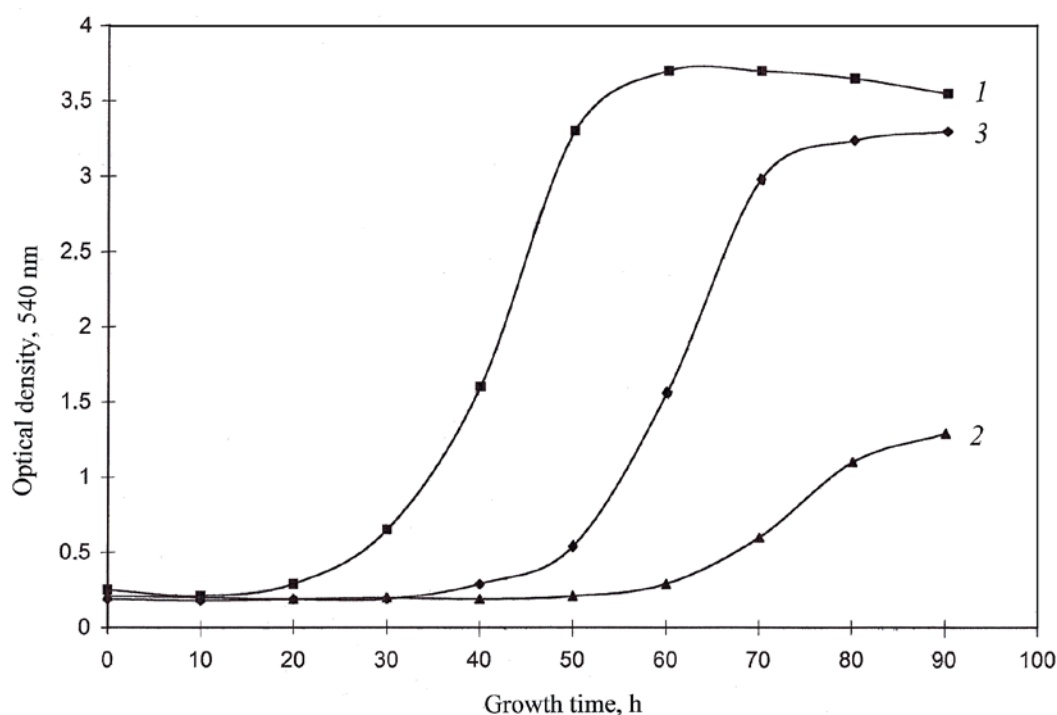
Figure 1. Growth dynamics of *B. methylicum B-5662* (1, 2, 3) on media M9 with various isotopic content: *1* – non-adapted bacterium on protonated medium M9 (Table 1, experiment 1); *2* – non-adapted bacterium on maximally deuterated medium M9 (Table 1, experiment 10); *3* – adapted to ^{2}H$_2$O bacterium on maximally deuterated medium M9 (Table 1, experiment 10')

The adaptation was monitored by recording the growth dynamics of the initial bacterium (Figure 1, curve *1*, control, protonated M9 medium) and adapted to deuterium *B. methylicum B-5662* (Figure 1, curve *3*) on the maximally deuterated M9 medium with 98% (v/v) ^{2}H$_2$O and 2% (v/v) [^{2}H]methanol. Unlike the adapted bacterium (Figure 1, curve *3*), the growth dynamics of the initial bacterium (Figure 1, curve *1*) on the maximally deuterated medium were inhibited by deuterium. Being transferred to the protonated medium, the adapted bacterium returned to

normal growth after a certain lag-phase period that was characteristic for other adapted bacterial strains. The effect of growth reversion in protonated/deuterated media demonstrates that adaptation to ^2H_2O is a phenotypic phenomenon, although it cannot be excluded that a certain genotype determined the manifestation of the same phenotypic attribute in media with high deuterium content. In general, the improved growth characteristics of the adapted bacterium significantly simplify the scheme for the production of deuterated biomass, the optimal conditions for which are satisfied the following: maximally deuterated M9 medium with 98% (v/v) ^2H_2O and 2% (v/v) [^2H]methanol, incubation period 3–4 days, and temperature 35 °C.

The data on the yield of biomass of initial and adapted *B. methylicum*, magnitude of lag-period and generation time on the protonated and the maximumally deuterated M9 medium are shown in Figure 2. The degree of cell survive on maximum deuterated medium was approx. 40%. The yield of biomass for adapted methylotroph (*c*) was decreased approx. on 13% in comparison with control conditions (*a*) at an increase in the time of generation up to 2,8 h and the lag-period up to 40 h (Figure 2). As is shown from these data, as compared with the adapted strain, the growth characteristics of initial strain on maximally deuterated medium were inhibited by deuterium.

Figure 2. Yield of microbial biomass of *B. methylicum B-5662*, the magnitude of lag-period and generation time in various experimental conditions: initial strain on protonated M9 medium (control) with water and methanol (*a*); initial strain on maximally deuterated M9 medium (b); adapted to deuterium strain on maximally deuterated M9 medium (c): 1 – yield of biomass, % from the control; 2 – duration of lag-period, h; 3 – generation time, h.

Biosynthesis of [²H]Inosine

The strategy for the biosynthesis of [^2H]inosine using biomass of *B. methylicum B-5662* as growth substrates was developed taking into account the ability of methylotrophic bacteria to synthesize large amounts of protein (output, 50% (w/w) of dry weight), 15–17% (w/w) of polysaccharides, 10–12% (w/w) of lipids (mainly, phospholipids), and 18% (w/w) of ash [23]. To provide high outputs of these compounds and minimize the isotopic exchange (^1H–^2H) in amino acid residues of protein molecules, the biomass was hydrolyzed by autoclaving in 0,5 *N* ^2HCl (in ^2H_2O).

Since the inosine-producing strain of *B. subtilis B-3157* is a polyauxotroph requiring tyrosine and histidine for its growth, we studied the qualitative and quantitative content of amino acids in the hydrolyzed methylotrophic biomass produced in the maximally deuterated medium M9 with 98% (v/v) ^2H_2O and 2% (v/v) [^2H]methanol, and the levels of their deuterium enrichment (Table 2). The methylotrophic hydrolysate contains 15 identified amino acids (except for proline detected at λ = 440 nm) with tyrosine and histidine content per 1 gram of dry methylotrophic hydrolysate 1,82% and 3,72% (w/w), thereby satisfying the auxotrophic requirements of the inosine

producer strain for these amino acids. The content of other amino acids in the hydrolysate is also comparable with the needs of the strain in sources of carbon and amine nitrogen (Table 2).

Table 2: Amino acid composition of hydrolyzed biomass of the facultative methylotrophic bacterium *B. methylicum B-5662* obtained on maximally deuterated M9 medium with 98% (v/v) ^2H_2O and 2% (v/v) [^2H]methanol and levels of deuterium enrichment*

Amino acid	Yield, % (w/w) dry weight per 1 gram of biomass		Number of deuterium atoms incorporated into the carbon backbone of a molecule**	Level of deuterium enrichment of molecules, % of the total number of hydrogen atoms***
	Protonated sample (control)	Sample from deuterated M9 medium		
Glycine	8,03	9,69	2	90,0±1,86
Alanine	12,95	13,98	4	97,5±1,96
Valine	3,54	3,74	4	50,0±1,60
Leucine	8,62	7,33	5	49,0±1,52
Isoleucine	4,14	3,64	5	49,0±1,50
Phenylalanine	3,88	3,94	8	95,0±1,85
Tyrosine	1,56	1,83	7	92,8±1,80
Serine	4,18	4,90	3	86,6±1,56
Threonine	4,81	5,51	–	–
Methionine	4,94	2,25	–	–
Asparagine	7,88	9,59	2	66,6±1,62
Glutamic acid	11,68	10,38	4	70,0±1,64
Lysine	4,34	3,98	5	58,9±1,60
Arginine	4,63	5,28	–	–
Histidine	3,43	3,73	–	–

Notes: * The data were obtained for methyl esters of N-5-dimethylamino(naphthalene)-1-sulfonyl (dansyl) chloride amino acid derivatives.
** At calculation the level of deuterium enrichment, the protons (deuterons) at COOH- and NH$_2$-groups of amino acid molecules were not taken into account because of the dissociation in H_2O/^2H_2O.
*** A dash denotes the absence of data.

The indicator determining the high efficiency of deuterium incorporation into the synthesized product is high levels of deuterium enrichment of amino acid molecules, varied from 49 atom% ^2H for leucine/isoleucine to 97,5 atom% ^2H for alanine (Table 2). This allowed using the hydrolysate of deuterated biomass of *B. methylicum* as a source of growth substrates for growing the inosine-producing strain *B. subtilis*.

The growth and biosynthetic characteristics of inosine-producing strain *B. subtilis B-3157* were studied on protonated yeast PVC medium with H_2O and 2% (w/v) yeast PVC and on HW medium with 89% (v/v) ^2H_2O and 2% (w/w) of hydrolysate of deuterated biomass of *B. methylicum* (Figure 2). Experiments demonstrated a certain correlation between the changes of growth dynamics of *B. subtilis B-3157* (Figure 3, curves *1, 1'*), output of inosine (Figure 2, curves *2, 2'*), and glucose assimilation (Figure 2, curves *3, 3'*). The maximal output of inosine (17 g/l) was observed on protonated PVC medium at a glucose assimilation rate 10 g/l (Figure 3, curve *2*). The output of inosine in the HW medium decreased in 4,4-fold, reaching 3,9 g/l (Figure 3, curve *2'*), and the level of glucose assimilation – 4-fold, as testified by the remaining 40 g/l non-assimilated glucose in LC (Figure 3, curve *3'*). The experimental data demonstrate that glucose is less efficiently assimilated during growth in the HW medium as compared to the control conditions in H_2O.
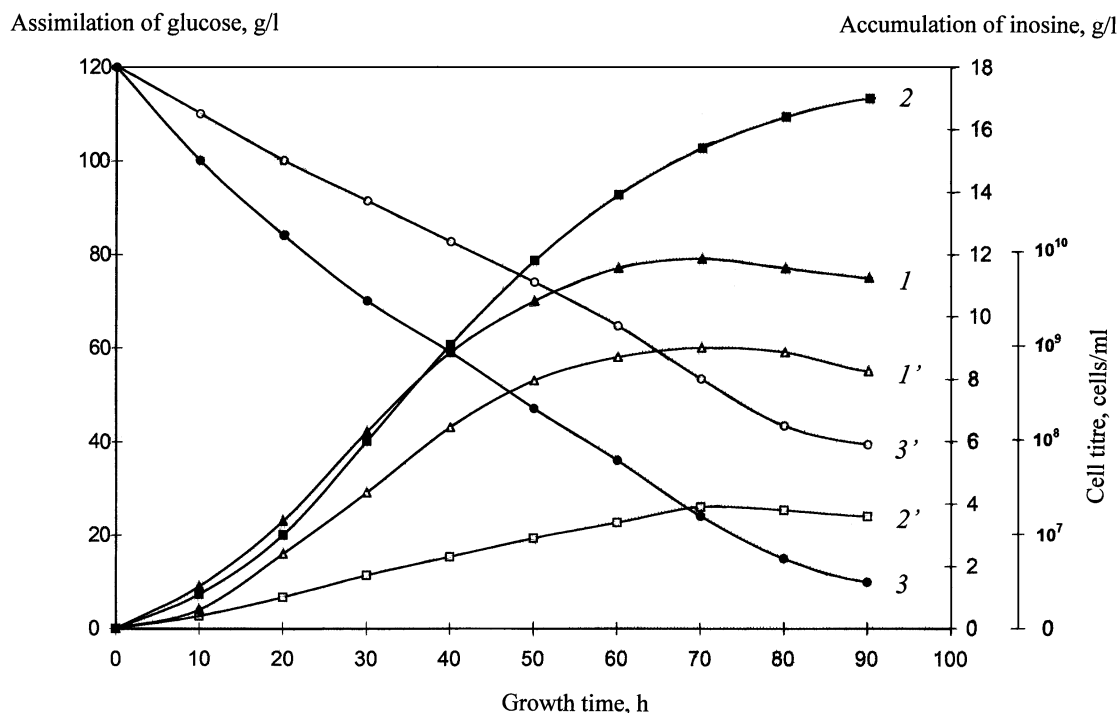
Figure 3. Growth dynamics of *B. subtilis B-3157* (*1, 1'*) (cells/ml), inosine accumulation in LC (*2, 2'*) (g/l), and glucose assimilation (*3, 3'*) (g/l) under different experimental conditions: (*1–3*) – protonated yeast PVC medium; (*1'–3'*) – HW medium with 2% (w/v) hydrolysate of deuterated biomass of *B. methylicum B-5662*.

This result demanded the examination of the content of glucose and other intracellular carbohydrates in the biomass of the inosine-producer strain of *B. subtilis B-3157*, which was performed by reverse phase HPLC on an Ultrasorb CN column (10 μm, 10×250 mm) with a mixture of acetonitrile–water (75:25, % (v/v)) as a mobile phase (Table 3). The fraction of intracellular carbohydrates in Table 3 (numbered according to the sequence of their elution from the column) comprises monosaccharides (glucose, fructose, rhamnose, and arabinose), disaccharides (maltose and sucrose), and four unidentified carbohydrates with retention times of 3,08 (15,63% (w/w)), 4,26 (7,46% (w/w)), 7,23 (11,72% (w/w)), and 9,14 (7,95% (w/w) min (not shown). As was expected, the output of glucose in the deuterated hydrolysate was 21,4% (w/w) of dry weight, that is, higher than the outputs of fructose (6,82% (w/w)), rhamnose (3,47% (w/w)), arabinose (3,69% (w/w)), and maltose (11,62% (w/w)) (Table 3). Their outputs in microbial biomass did not differ considerably related to the control in H_2O except for sucrose, which is undetectable in the deuterated sample. The levels of deuterium enrichment in carbohydrates varied from 90,7 atom% ^2H for arabinose to 80,6 atom% ^2H for glucose.

Table 3: Qualitative and quantitative compositions of intracellular carbohydrates isolated from
B. subtilis B-3157 after growing on HW-medium and levels of the deuterium enrichment*

Carbohydrate	Content in biomass, % (w/w) of 1 g of dry biomass		Level of deuterium enrichment of molecules, %**
	Protonated sample (control)	**Sample from the HW medium**	
Glucose	20,01	21,40	80,6±1,86
Fructose	6,12	6,82	85,5±1,92
Rhamnose	2,91	3,47	90,3±2,12
Arabinose	3,26	3,69	90,7±3,10
Maltose	15,30	11,62	–
Sucrose	8,62	ND**	–

Notes: * The data were obtained by IR-spectroscopy.
** ND – not detected.
*** A dash denotes the absence of data.

Isolation of [²H]Inosine from LC

The use of a combination of physical-chemical methods for isolating [²H]inosine from LC was determined by the need for preparing inosine of a high chromatographic purity (no less than 95%). Since LC along with inosine contains inorganic salts, proteins, and polysaccharides, as well as accompanying secondary nucleic metabolites (adenosine and guanosine) and non-reacted substrates (glucose and amino acids), LC was fractionated in a stepwise manner for isolating of [²H]inosine. The high sensitivity of inosine to acids and alkali and its instability during isolation required applying diluted acid and alkaline solutions with low concentration, as well as carrying out the isolation procedure at low temperature, thus avoiding long heating of the reaction mixture. The fractionation of LC consisted in low-temperature precipitation of high molecular weight impurities with organic solvents (acetone and methanol), adsorption/desorption on the surface of activated carbon, extraction of the end product, crystallization, and ion exchange chromatography. The proteins and polysaccharides were removed from LC by precipitation with acetone at 4 °C with subsequent adsorption/desorbtion of total ribonucleosides on activated carbon. The desorbed ribonucleosides were extracted from the reacted solid phase by eluting with EtOH-NH$_3$-solution at 60 °C; inosine – by extracting with 0,3 *M* ammonium–formate buffer (*pH* = 8,9) and subsequent crystallization in 80% (v/v) ethanol. The final purification consisted in column ion exchange chromatography on AG50WX 4 cation exchange resin equilibrated with 0.3 M ammonium–formate buffer containing 0,045 *M* NH$_4$Cl with collection of fractions at R_f = 0,5. The curves *1–3* in Figure 4 show UV-absorption spectra of inosine isolated from the LC of *B. subtilis B-3157* at various stages of isolation procedure. The presence of major absorbance band I, corresponding to natural inosine (λ_{max} = 249 nm, ε_{249} = 7100 M^{-1} cm^{-1}), and the absence of secondary metabolites II and III in the analyzed sample (Figure 4, curve *3*), demonstrates the homogeneity of isolated product and the efficiency of the isolation method.
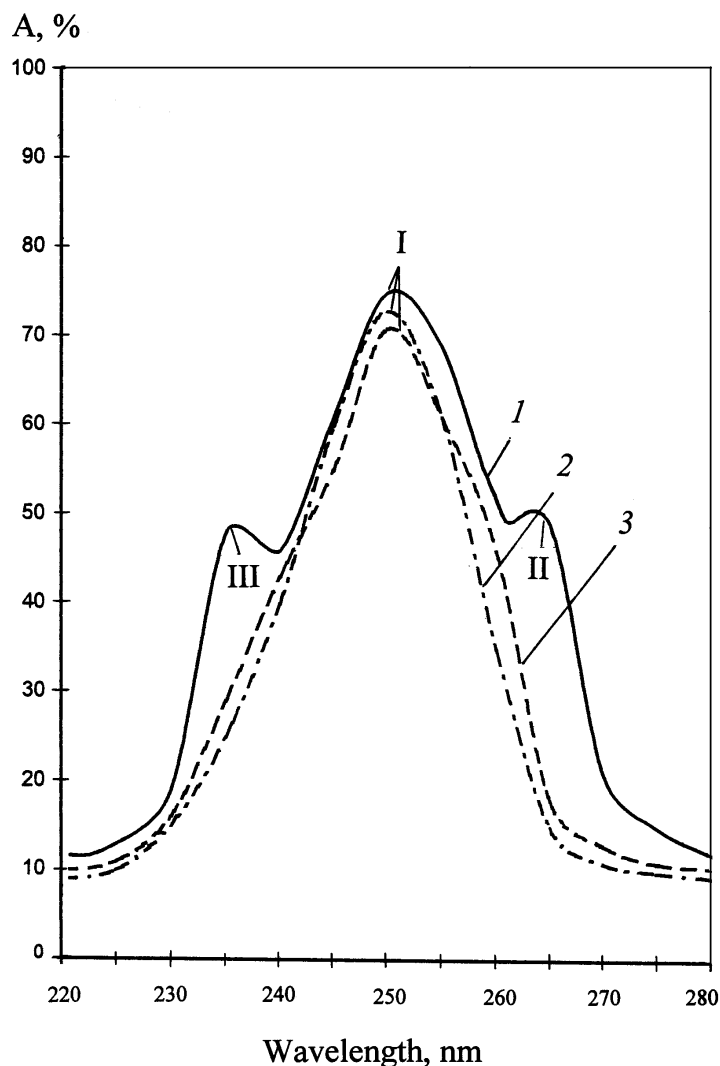
Figure 4. UV-absorption spectra of inosine (0,1 M HCl): (*1*) – initial LC after the growth of
B. subtilis B-3157 on HW medium; (*2*) – natural inosine; (*3*) – inosine extracted from the LC of
B. subtilis B-3157. Natural inosine (*2*) was used as a control: (I) – inosine,
(II, III) – secondary metabolites.

The Studying of the Level of Deuterium Enrichment of [²H]Inosine

The level of deuterium enrichment of the [²H]inosine molecule was determined by FAB mass spectrometry, the high sensitivity of which allows to detect 10^{-8} to 10^{-10} moles of a substance in a sample [24]. The formation of a molecular ion peak for inosine in FAB mass spectrometry was accompanied by the migration of H⁺. Biosynthetically ²H-labeled inosine, which FAB mass-spectrum represented in Figure 5*b* regarding the control (natural protonated inosine, Figure 5*a*), represented a mixture of isotope-substituted molecules with different numbers of hydrogen atoms replaced by deuterium. Correspondingly, the molecular ion peak of inosine [M + H]⁺, was polymorphically splintered into individual clusters with admixtures of molecules with statistical set of mass numbers m/z and different contributions to the total level of deuterium enrichment of the molecule. It was calculated according to the most intensive molecular ion peak (the peak with the largest contribution to the level of deuterium enrichment) recorded by a mass spectrometer under the same experimental conditions. These conditions are satisfied the most intensive molecular ion peak [M + H]⁺ at m/z 274 with 38% (instead of [M + H]⁺ at m/z 269 with 42% under the control conditions; Figure 5*a*). That result corresponds to five deuterium atoms incorporated into the inosine molecule, obtained after growing of *B. subtilis B-3157* on HW-medium (Figure 5b). The molecular ion peak of inosine also contained less intensive peaks with admixtures of molecules

containing four (*m/z* 273, 20%), five (*m/z* 274, 38%), six (*m/z* 275, 28%), and seven (*m/z* 276, 14%) deuterium atoms (Table 4).

Table 4: Values of peaks [M+H]⁺ in the FAB mass spectra and levels of deuterium enrichment of biosynthetic inosine isolated from HW-medium

Value of peak [M+H]⁺	Contribution to the level of deuterium enrichment, mol.%	The number of deuterium atoms	Level of deuterium enrichment of molecules, % of the total number of hydrogen atoms*
273	20	4	20,0±0,60
274	38	5	62,5±1,80
275	28	6	72,5±1,96
276	14	7	87,5±2,98

Notes: *At calculation of the level of deuterium enrichment, the protons(deuterons) at the hydroxyl (OH⁻) and imidazole protons at NH⁺ heteroatoms were not taken into account because of keto−enol tautomerism in $H_2O/^2H_2O$.

Taking into account the contribution of the molecular ion peaks [M]⁺, the total level of deuterium enrichment (TLDE) of the inosine molecule calculated using the below equation was 65,5% of the total number of hydrogen atoms in the carbon backbone of the molecule:

$$TLDE = \frac{[M]^+_{r1} \cdot C_2 + [M]^+_{r2} \cdot C_2 + \ldots + [M]^+_{rn} \cdot C_n}{\sum C_n} \,, \tag{1}$$

where $[M]^+_r$ – the values of the molecular ion peak of inosine; C_n – the contribution of the molecular ion peaks to TLDE (mol %).
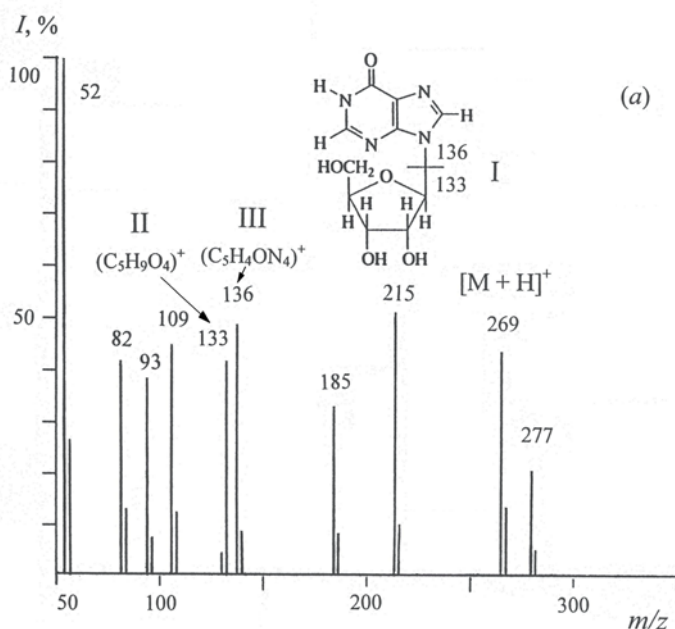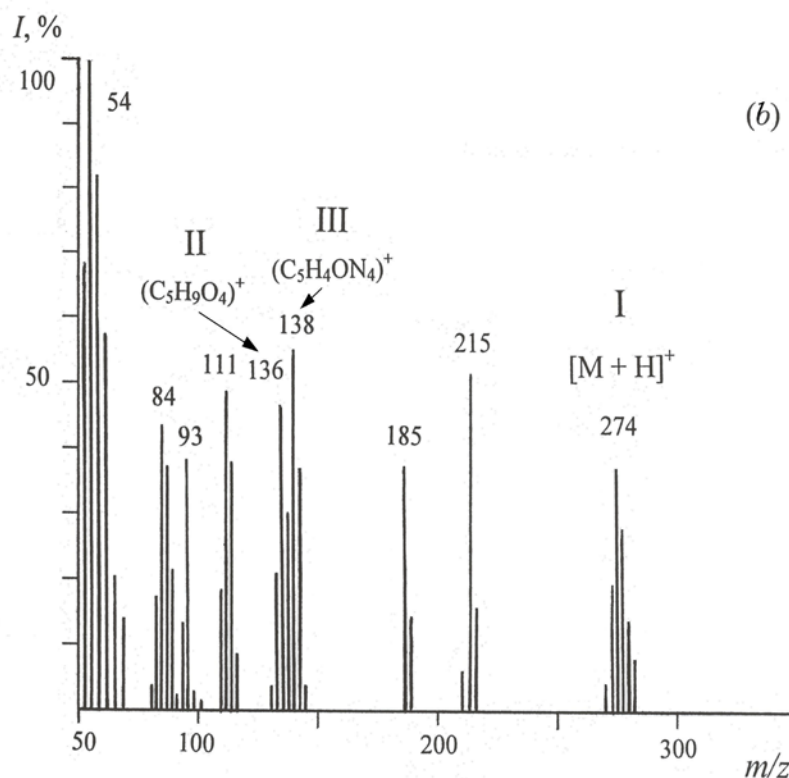
Figure 5. FAB mass spectra of inosine (glycerol as a matrix) under different experimental conditions: (*a*) − natural inosine; (*b*) − [²H]inosine isolated from HW medium (ionization conditions: cesium source; accelerating voltage, 5 kV; ion current, 0,6−0,8 mA): *I* − relative intensity of peaks (%); (I) − inosine; (II) − ribose fragment; (III) − hypoxanthine fragment.

The fragmentation of the inosine molecule, shown in Figure 6, gives more precise information on the deuterium distribution in the molecule. The FAB fragmentation pathways of the inosine molecule (I) lead to formation of ribose $(C_5H_9O_4)^+$ fragment (II) at m/z 133 and hypoxanthine $(C_5H_4ON_4)^+$ fragment (III) at m/z 136 (their fragmentation is accompanied by the migration of H^+), which in turn, later disintegrated into several low-molecular-weight splinter fragments at m/z 109, 108, 82, 81, and 54 due to HCN and CO elimination from hypoxanthine (Figure 6). Consequently, the presence of two "heavy" fragments of ribose II $(C_5H_9O_4)^+$ at m/z 136 (46%) (instead of m/z 133 (41%) in the control) and hypoxanthine III $(C_5H_4ON_4)^+$ at m/z 138 (55%) (instead of m/z 136 (48%) in the control), as well as the peaks of low molecular weight splinter fragments formed from FAB-decomposition of hypoxanthine fragment at m/z 111 (49%) (instead of m/z 109 (45%) in the control) and m/z 84 (43%) (instead of 82 (41%) in the control) suggests that three deuterium atoms are incorporated into the ribose residue, and two other deuterium atoms − into the hypoxanthine residue of the inosine molecule (Figure 5). Such selective character of the deuterium inclusion into the inosine molecule on specific locations of the molecule was confirmed by the presence of deuterium in the smaller fission fragments.

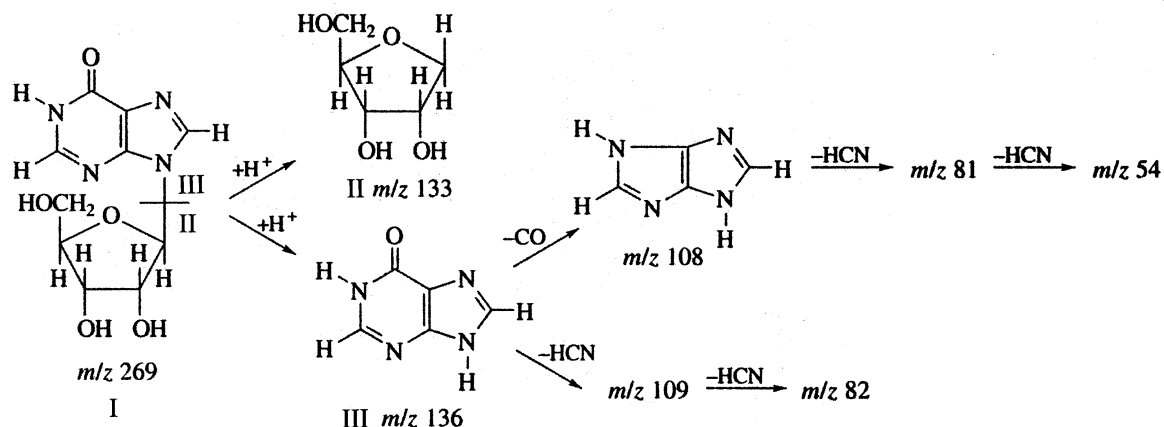*Figure 6.* The fragmentation pathways of the inosine molecule leading to formation of smaller fragments by the FAB-method

When analyzing the level of deuterium enrichment of the inosine molecule we took into account the fact that the character of deuterium incorporation into the molecule is determined by the pathways of carbon assimilation. The carbon source was glucose as a main substrate and a mixture of deuterated amino acids from deuterated hydrolizate of methylotrophic bacterium *B. methylicum B-5662* as a source of deuterated substrated and amine nitrogen. Since the protons (deuterons) at positions of the ribose residue in the inosine molecule could have been originated from glucose, the character of deuterium inclusion into the ribose residue is mainly determined by hexose-5-monophosphate (HMP) shunt [25], associated with the assimilation of glucose and other carbohydrates. HMP shunt is a complex of 12 reversible enzymatic reactions resulting in the oxidation of glucose to CO_2 to form reduced NADPH, and H^+, and synthesis of phosphorylated sugars containing from 3 to 7 carbon atoms. Since glucose in our experiments was used in a protonated form, its contribution to the level of deuterium enrichment of the ribose residue was neglected. However, as the investigation of deuterium incorporation into the molecule by FAB method showed that deuterium was incorporated into the ribose residue of the inosine molecule owing to the preservation in this bacterium the minor pathways of *de novo* glucose biosynthesis in ^2H_2O-medium. It became possible that the cell uses its own resources for intracellular biosynthesis of glucose from intracellular precursors.

It should be noted that numerous isotopic $^1H-^2H$ exchange processes could also have led to specific incorporation of deuterium atoms at certain positions in the inosine molecule. Such accessible positions in the inosine molecule are hydroxyl (OH^-)- and imidazole protons at NH^+ heteroatoms, which can be easily exchanged on deuterium in ^2H_2O *via* keto–enol tautomerism. Three non-exchangeable deuterium atoms in the ribose residue of inosine are synthesized *de novo* and could have been originated from HMP shunt reactions, while two other deuterium atoms at C2,C8-positions in the hypoxanthine residue could be synthesized *de novo* at the expense of [^2H]amino acids, primarily glutamine and glycine (Figure 7), that originated from deuterated hydrolysate of methylotrophic bacterium *B. methylicum* obtained on 98% of ^2H_2O medium. In particular, the glycoside proton at β-N9-glycosidic bond could be replaced with deuterium *via* the reaction of CO_2 elimination at the stage of ribulose-5-monophosphate formation from 3-keto-6-phosphogluconic acid with subsequent proton (deuteron) attachment at the C1-position of ribulose-5-monophosphate (Figure 8). Two other protons at C2(C3) and C4 positions in ribose residue could be replaced with deuterium *via* further enzimatic isomerization of ribulose-5-monophosphate into ribose-5-monophosphate. In general, our studies confirmed this scheme [27]. However, it should be noted that the level of deuterium enrichment of inosine molecule is determined by isotopic purity of ^2H_2O and deuterated substrates and, therefore, for the total administration of the deuterium label into the inosine molecule instead of protonated glucoce it must be used its deuterated analogue. Deuterated glucose may be isolated in gram-scale quntities from deuterated biomass of the methylotrophic bacterium *B. methylicum*.

Figure 7. Scheme of biosynthesis of IMP by microbial cell (adapted from Bohinski, 1983 [26])

Conclusion

We have demonstrated the possibility of using the hydrolyzate of deuteron-biomass of the facultative methylotrophic bacterium *B. methylicum B-5662* as a substrate for microbiological synthesis of ^{2}H-labeled inosine by the bacterium *Bacillus subtilis B-3157*. ^{2}H-labeled inosine was isolated from HW-medium by adsorption/desorption on activated carbon, extraction by 0,3 M ammonium–formate buffer (pH = 8,9), crystallization in 80% (v/v) EtOH, and IEC on AG50WX 4 cation exchange resin equilibrated with 0,3 M ammonium–formate buffer and 0,045 *M* NH4Cl with output 3,9 g/l. The total level of deuterium enrichment of the inosine molecule was 5 deuterium atoms (65,5 atom% ^{2}H). From total 5 deuterium atoms in the inosine molecule, 3 deuterium atoms were localized in the ribose residue, while 2 deuterium atoms – in the hypoxanthine residue of the molecule. Deuterium was incorporated into the ribose residue of the inosine molecule owing to the preservation in this bacterium the minor pathways of *de novo*

glucose biosynthesis in ^2H_2O-medium. Three non-exchangeable deuterium atoms in the ribose residue of inosine were synthesized *de novo* and originated from HMP shunt reactions, while two other deuterium atoms at C2,C8-positions in the hypoxanthine residue could be synthesized *de novo* from [^2H]amino acids, that originated from deuterated hydrolysate of *B. methylicum B-5662* obtained on 98% of ^2H_2O medium. To attain higher deuterium enrichment level of the final product, it is necessary to thoroughly control the isotope composition of the growth medium and exclude any possible sources of additional protons, in particular, to use [^2H]glucose, which may be isolated from deuterated biomass of the methylotrophic bacterium *B. methylicum B-5662*.

References:

1. H. Andres. Synthesis and applications of isotopically labeled compounds / U. Pleiss and R. Voges (Eds.). – New York: John Wiley & Sons, 2001. 728 p.

2. Kundu M.T. Synthetic studies to improve the deuterium labelling in nucleosides for facilitating structural studies of large RNAs by high-field NMR spectroscopy / M.T. Kundu, A. Trifonova, Z. Dinya, A. Foldes, J. Chattopadhyaya // Nucleosides, Nucleotides and Nucleic Acids. 2001. V. 20, № 4–7. P. 1333–1337.

3. Kushner D.J. Pharmacological uses and perspectives of heavy water and deuterated compounds / D.J. Kushner, A. Baker, T.G. Dunstall // Can. J. Physiol. Pharmacol. 1999. V. 77, № 2. P. 79–88.

4. Crespi H.L. Fully deuterated microorganisms: tools in magnetic resonance and neutron scattering / H.L. Crespi // in: *Synthesis and applications of isotopically labeled compounds.* **P**roc. 2nd Intern. Sympos. / Eds. T. Baillie, J.R. Jones. Amsterdam: Elsevier, 1989. 332 p.

5. Caire G. Measurement of deuterium oxide by infrared spectroscopy and isotope ratio mass spectrometry for quantifying daily milk intake in breastfed infants and maternal body fat / G. Caire, C.A.M. de la Barca, A.V. Bolanos, M.E. Valencia, A.W. Coward, G. Salazar, E. Casanueva // Food Nutr. Bull. 2002. V. 23, № 3. P. 38–41.

6. Mosin O.V. Mass spectrometric evaluation of the incorporation of ^2H and ^{13}C into amino acids of bacteria / O.V. Mosin, D.A. Skladnev, T.A. Egorova, V.I. Shvets // Bioorganic Chemistry. 1996. V. 22, № 10-11. P. 856-869.

7. Lukin M. Structure and stability of DNA containing an aristolactam II-dA lesion: implications for the NER recognition of bulky adducts / M. Lukin, C. de los Santos // Nucleosid., Nucleotid. Nucleic Acids. 2010. V. 29, № 7. P. 562–573.

8. Chirakul P. Preparation of base-deuterated 2'-deoxyadenosine nucleosides and their site-specific incorporation into DNA / P. Chirakul, J.R. Litzer, S.T. Sigurdsson // Nucleosid., Nucleotid. Nucleic Acids. 2001. V. 20, № 12. P. 1903–1913.

9. Chen B. A general synthesis of specifically deuterated nucleotides for studies of DNA and RNA / B. Chen, E.R. Jamieson, T.D. Tullius // Bioorg. & Med. Chem. Lett. 2002. V. 12. P. 3093–3096.

10. Jung M.E. Efficient synthesis of specifically deuterated nucleosides: preparation of 4′-deuteriothymidine / M.E. Jung, Y. Xu // Cheminform Abstract. 1998. V. 29, № 16. P. 235–238.

11. Daub G.H. Synthesis with stable isotopes // Stable isotopes. Proc. 3d Intern. Conference / Ed. E. R. Klein. – New York: Acad. Press, 1979. P. 3–10.

12. Huang X. An efficient and economic site-specific deuteration strategy for NMR studies of homologous oligonucleotide repeat sequences / X. Huang, P. Yu, E. LeProust, X. Gao // Nucleic Acids Res. 2006. V. 25, № 23. P. 4758–4763.

13. Miroshnikov A.I. A new strategy for the synthesis of nucleosides: one-pot enzymatic transformation of D-pentoses into nucleosides / *A.I.* Miroshnikov, R.S. Esipov, T.I. Muravyova, I.D. Konstantinova, I.V. Fateev, I.A. Mikhailopulo // Open Conf. Proc. J. 2010. V. 1. P. 98–102.

14. Mosin O.V. Biosynthesis of ^2H-labeled phenylalanine by a new methylotrophic mutant *Brevibacterium methylicum* / O.V. Mosin, D.A. Skladnev, V.I. Shvets // Biosci, Biotechnol., Biochem. 1999. V. 62, № 2. P. 225–229.

15. Den'ko E.I. Influence of heavy water (D$_2$O) on animal, plant and microorganism's cells / E.I. Den'ko // Usp. Sovrem. Biol. 1970. V. 70, № 4. P. 41–49.

16. Vertes A. Physiological effect of heavy water. Elements and isotopes: formation, transformation, distribution / A. Vertes, Ed. – Vienna: Dordrecht: Kluwer Acad. Publ., 2003. 112 p.

17. Mosin O.V. Isotope effects of deuterium in bacterial and microalgae cells at growth on heavy water (D$_2$O) / O.V. Mosin, I. Ignatov // Voda: Khimiya I Ecologiya. 2012. V. 3. P. 83–94.

18. Mosin O.V. Microbial synthesis of ^{2}H-labelled L-phenylalanine with different levels of isotopic enrichment by a facultive methylotrophic bacterium Brevibacterium methylicum with RuMP assimilation of carbon / O.V. Mosin, V.I. Shvets, D.A. Skladnev, I. Ignatov // Biochemistry (Moscow) Supplement Series B: Biomedical Chemistry. 2013. V. 7, № 3. P. 249–260.

19. Trotsenko Y.A. The ribulose monophosphate (Quayle) cycle: News and views // Microbial growth on C1 compounds. Proc. 8th Intern. Sympos. / Eds. M.E. Lindstrom, F.R. Tabita. Boston: Kluwer Acad. Publ., 1995. P. 24–26.

20. Mosin O.V. Microbiological synthesis of [^{2}H]inosine with high degree of isotopic enrichment by Gram-positive chemoheterotrophic bacterium *Bacillus subtilis* / O.V. Mosin, V.I. Shvez, D.A. Skladnev, I. Ignatov // Applied Biochemistry and Microbiology. 2013. V. 49. № 3. P. 255–266.

21. Mosin O.V. Biosynthesis of ^{2}H-labelled inosine by bacterium *Bacillus subtilis* / O.V. Mosin, D.A. Skladnev, V.I. Shvets // Izv. RAN. Ser. Biologicheskaja. 1999. V. 4. P. 396–402.

22. Mosin O.V. Studying of microbial synthesis of deuterium labeled L-phenylalanine by methylotrophic bacterium *Brevibacterium methylicum* on media with different content of heavy water / O.V. Mosin, V.I. Shvets, D.A. Skladnev, I. Ignatov // Russian Journal of Biopharmaceuticals. 2012. V. 4. P. 11–22.

23. Mosin O.V. Microbiological synthesis of ^{2}H-labeled phenylalanine, alanine, valine, and leucine/isoleucine with different degrees of deuterium enrichment by the Gram-positive facultative methylotrophic bacterium *Brevibacterium methylicum* // O.V. Mosin, I. Ignatov // International Journal of BioMedicine. 2013. V. 3. № 2. P. 132–138.

24. Caprioli R.M. Continuous flow fast atom bombardment mass spectrometry / R.M. Caprioli, Ed. – New York: Wiley, 1990. 125 p.

25. Stryer L. Biochemistry / L. Strayer, Ed., translated from English. – M: Mir, 1985. pp. 95-105.

26. Bohinski R.C. Modern concepts in biochemistry / R.C. Bohinski, Ed. – Boston, London, Sydney, Toronto, Massachusetts: Allyn & Bacon Inc., 1983. 378 p.

27. Ignatov I. Possible processes for origin of life and living matter with modeling of physiological processes of bacterium *Bacillus subtilis* in heavy water as model system / I. Ignatov, O.V. Mosin // Journal of Natural Sciences Research. 2013. V. 3, № 9. P. 65–76.
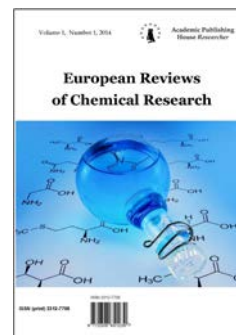
UDC 541.49; 543.544-414

Determination of Trace Amount of Cd (II) by using a Chromogenic reagent Diacetylmonoxime-3-amino-4-hydroxy benzoyl hydrazone (DMAHBH) with UV-Visible Spectrophotometry

[1] B.N. Nagalaxmi
[2] C. Viswanatha
[3] K. Ramakrishna Reddy
[4] K.B. Chandrasekhar
[5] N. Donappa

[1] Maharani Lakshmi Ammanni College for Women, Bangalore-12, India
Department of Chemistry
Associate Professor
[2] Arba Minch University, Post Box No 21, Ethiopia
Department of Chemistry
Assistant Professor
E-mail: chamanchula.viswanatha@amu.edu.et
[3] Engineering College, Nandayal, Kurnool, A.P., India
Department of Chemistry, RGM
Assistant Professor
[4] Oil Technological Research Institute (OTRI), JNTU-A Anantapur, A.P., India
Professor of Chemistry
[5] Maharani Lakshmi Ammanni College for Women, Bangalore-12, India
Department of Chemistry
Professor, HOD

Abstract

Diacetylmonoxime-3-amino-4-hydroxy benzoyl hydrazone (DMAHBH) is used as a novel chromogenic organic reagent for the determination of Cadmium (II) with spectrophotometer. The novel chromogenic organic reagent – diacetylmonoxime-3-amino-4-hydroxy benzoyl hydrazone (DMAHBH) gave yellow colored water soluble complex with Cd (II) in buffer (pH = 8.0–9.0) medium. The color complex shows maximum absorbance at λ = 378 nm. The system obeyed Beer's law in the concentration range of 0.5035–5.0535 μg/ml. The optimum Cadmium (II) concentration range for accurate determination as evaluated from Ringbom plot was 0.5035–5.0535 μg/ml. The molar absorptivity and Sandell's sensitivity were $2.94 \cdot 10^4$ $l \cdot mol^{-1} \cdot cm^{-1}$ and 0.0036 μg/cm^2 respectively. Cadmium (II) forms M:L (I:I) color complex with DMAHBH and stability constant of the complex was found to be $8.58 \cdot 10^7$. Soil samples were analyzed for the determination of Cadmium (II) present, using the proposed method. This developed method was applied for the determination of Cadmium (II) in soil and cigarette samples and good analytical results.

Keywords: chromogenic organic reagent, derivative spectrophotometry, Cadmium (II), soil, cigarette tobacco samples.

Introduction

Cadmium occurs in nature in association with zinc in minerals. Growing plants acquire and concentrate Cd(II) within the same biochemical setup. The outbreak of Cadmium (II) poisoning occurred in Japan in the form of itai itai or ouch ouch disease. Many people suffered from this disease, in which their bones became fragile. At high levels cadmium causes kidney problems, anemia and bone marrow disorders [1]. Cadmium is a lustrous, silver-white, ductile and highly malleable metal. It is soluble in acids but not in alkalis. About three-fourth of cadmium is used in Ni–Cd batteries and the remaining one fourth is used mainly pigments, coating and plating and as stabilizers for plastics [2–3]. Cadmium has been used particularly to electroplate steel and as a barrier to control nuclear fission. Naturally a very large amount of cadmium is released into the environment. About half of this cadmium is released into rivers through weathering of rocks and some cadmium is released into air through forest fires and volcanoes. The rest of the cadmium is released through human activities, such as manufacturing processes, etc. Human intake of cadmium takes place mainly through diet like liver, mushrooms, shellfish, mussels, cocoa powder and dried seaweed [4]. One of the main resources for cadmium accumulating in the human body is the extensive use of tobacco. Trace amounts of cadmium are important in industry [5], as a toxicant [6], and biological nonessential [7], as an environmental pollutant [8], and an occupational hazard [9]. It is an extremely toxic metal, and the effects of acute cadmium poisoning are manifested in a variety of different symptoms including high blood pressure, kidney damage and destruction of red blood cells [10]. The reported cadmium content in the environment is 70–110 µg/l in sea water and 2–960 µg/l in fresh water [11]. For the determination of cadmium in trace amount levels, there are several frequently adopted methods using analytical techniques, such as AAS, ICP–AES, ICP–MS, X-ray fluorescence spectroscopy, spectrophotometry, spectrofluorometry and so on. Among these, the spectrophotometric method is preferred, because it is cheaper and easy to handle, and comparable in sensitivity and accuracy, besides having good precision. There are many organic complexing reagents [12–21] which are used for spectrophotometric determination of Cadmium (II). Yet they suffer from disadvantages such as low sensitivity, incomplete extraction and interferences from a large number of foreign ions (Table 1). Recently, there has been a rapid growth in the popularity of sulfur bearing ligands such as thiosemicarbazones in analytical/inorganic chemistry for determination of metal ions [22]. The metal chelate of these sulfur and nitrogen containing reagents find wide range of applications in medicine and agriculture [23]. A survey of literature reveals that only a few thiosemicarbazones are employed for direct spectrophotometric determination of Cd(II), but not extractive spectrophotometric determination. Hence the authors introduced a new chromogenic reagent – diacetylmonoxime-3-amino-4-hydroxy benzoyl hydrazone (DMAHBH) for the determination of trace amount of Cd (II) in soil and tobacco samples.

Experimental

Spectrophotometric measurements were made using a Shimadzu 160 microcomputer based UV–Visible spectrophotometer (Shimadzu Corp., Japan) equipped with 1.0 cm quartz cuvette and an ELICO LI-120 digital pH meter. All reagents used were of analytical reagent (AR) grade unless otherwise stated. All solutions were prepared with distilled water.

Reagent:
Synthesis of diacetylmonoxime-3-amino-4-hydroxy benzoyl hydrazone (DMAHBH)

DMAHBH was prepared by refluxing a mixture of diacetyl monoxime (1.0111 g, 0.01 mole) and 3-amino-4-hydroxybenzhydrazide (1.6717 g, 0.01 mole) in ethanol (15 ml) for 5 hours. On cooling the reaction mixture, a light yellowish crystalline product was separated out. The crystalline hydrazone was collected by filtration and washed several times with 20% of ethanol in water and dried in vacuum. The product was re crystallised with ethanol. Yield, 79%; m.p., 220 °C. The chemical structure DMAHBH is shown in Fig. 1.
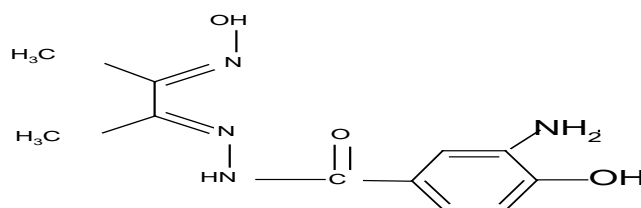
Figure 1: Structure of DMAHBH

Analytical properties of DMAHBH

The reactions of some important metal ions were tested at different pH values. The characteristics of the most important complexes are summarized in Table 1. The samples were prepared in 10 ml standard volumetric flasks by adding 3 ml of buffer (pH=1.0–11), 0.5 ml of metal ion ($1 \cdot 10^{-3}$ M) and 0.5 ml of DMAHBH ($1 \cdot 10^{-2}$ M) solutions. The solution mixture was diluted up to the mark with distilled water. The absorbance was measured in 300–800 nm range against reagent blank.

The data obtained from appropriate spectra which were derived in the presence of 10-fold molar excess of the reagent to metal ion. The pH values, which facilitate the formation of different complexes were also included.

Table 1: Characteristics of DMAHBH complexes in solution

Metal ion	λ_{max} (nm)	pH range	Surfactant used	Colour of the complex
Os(VIII)	390	4.0	–	bright yellow
Zr(IV)	388	4.0	–	yellow
Cu(II)	412	9.0	–	bright yellow
Pb(II)	387	3.0–10.0	TritionX-100	yellow
Cd(II)	378	8.0–9.0	TritionX-100	yellow

Recommended procedure:
Determination of Cadmium (II) (zero order)

An aliquot of the solution containing 0.5035–5.0503 μg/ml of Cadmium (II), 3 ml of buffer solution pH 1.0 to 10.0 and 0.5 ml ($1 \cdot 10^{-2}$ M) of DMAHBH reagent were taken in a 10 ml standard volumetric flask and the resulting solution was diluted up to the mark with distilled water. The absorbance of the solution was recorded at λ=378 nm in a 1.0 cm quartz quevette. The corresponding reagent blank is prepared in the same way, but without Cadmium(II) metal solution. The absorption spectra of DMAHBH and its Cd(II) complex under the optimum conditions are shown in Figure 2. The [Cd(II)–DMAHBH] complex shows the maximum absorbance at λ=378 nm, whereas the reagent blank does not absorb appreciably.
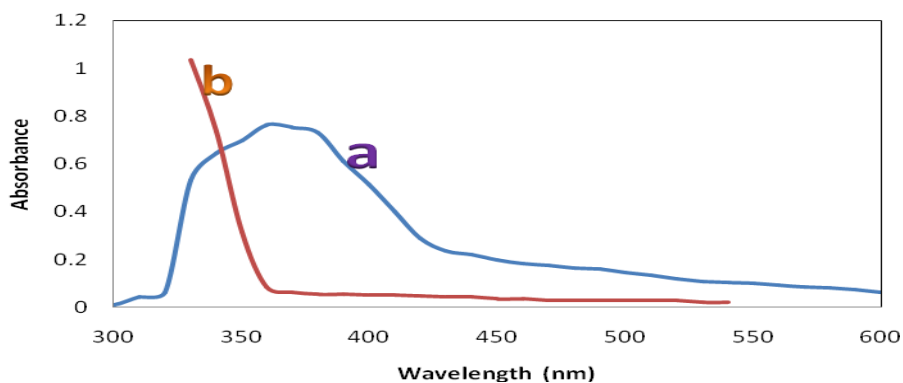
Figure 2: Absorption spectra: (a) – [Cd(II)–DMAHBH] complex Vs. reagent blank;
(b) – DMAHBH Vs. buffer blank

Effect of pH on the absorbance of the [Cd(II)–DMAHBH] complex

The study of the effect of pH on the colour intensity of the reaction mixture showed that the maximum colour was obtained in the pH range within 8.0–9.0 Analytical studies were therefore, carried out at pH 8.0 (Fig. 3).
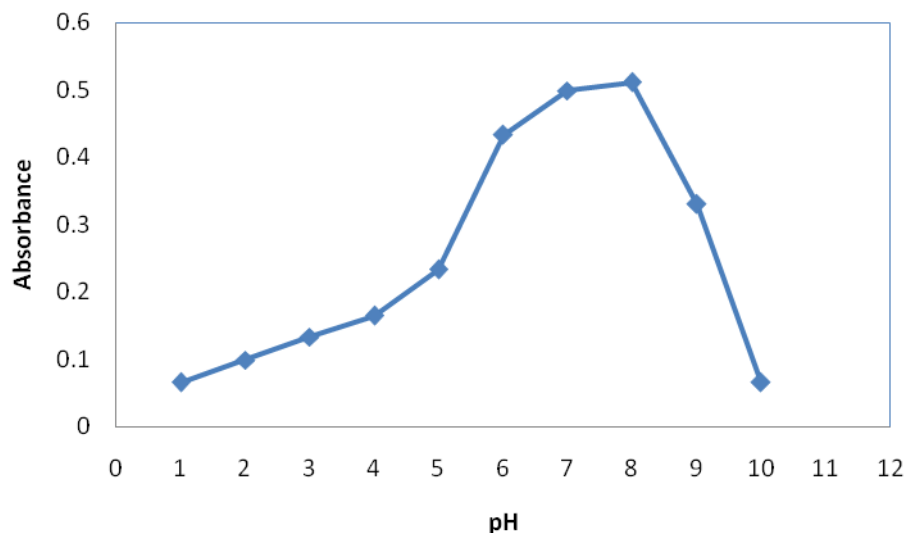

Figure 3: The dependence of absorbance of the [Cd(II)–DMAHBH]
complex on the pH value

Applicability of Beer's law

For the possible determination of Cadmium (II) at micro levels, the absorbance of the solutions containing different amounts of metal ion was measured. Calibration plot drawn between absorbance and amount of Cadmium (II) presented in Figure 4 showed that Beer's law was obeyed in the concentration range 0.5035–5.0535 $\mu g \cdot ml^{-1}$ of Cadmium (II). The molar absorptivity and Sandall's sensitivity were $2.94 \cdot 10^4$ $l \cdot mol^{-1} \cdot cm^{-1}$ and 0.0036 $\mu g/cm^2$ respectively. The correlation coefficient of the calibration curve for experimental data was 0.996.

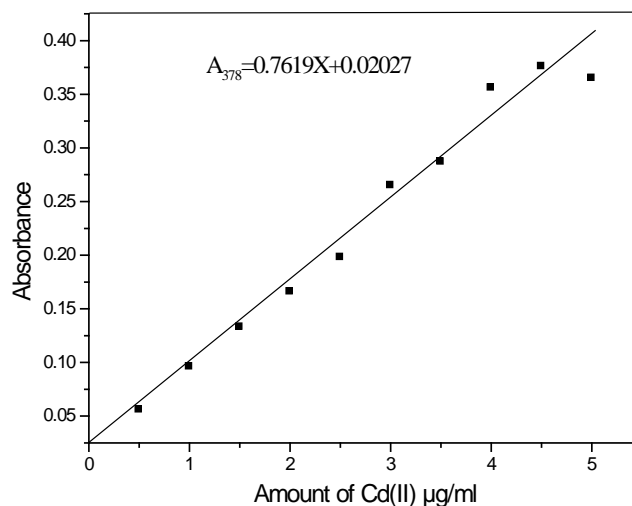**Figure 4:** Absorbance Vs Amount of Cd(II) (µg/ml):
[DMAHBH] = $1 \cdot 10^{-2}$ µg/ml
pH = 8.0
Wavelength = 378 nm

Results and discussion
Determination of Cadmium (II) using *DMAHBH*

Diacetylmonoxime-3-amino-4-hydroxy benzoyl hydrazone (DMAHBH) reagent is a blend of a carbonyl compound and hydrazide. The reagent solution is stable for more than 24 hours in the presence of buffer medium. The ligand presumably coordinates the metal ions to give a neutral water soluble complex.

Cadmium (II) reacts with DMAHBH in basic medium to give yellow coloured water-soluble [Cd(II)–DMAHBH] complex. The colour reaction between Cadmium (II) and DMAHBH was instantaneous even at room temperature in the pH range 8.0 to 10.0 . The absorbance of the yellow coloured complex remains constant for three hours. The maximum colour intensity is observed at pH 8.0. A 10-fold molar excess of reagent is adequate for full colour development. The order of addition of buffer solution, metal ion and the reagent has no adverse effect on the absorbance. The complex formation reaction between Cadmium (II) and DMAHBH has been studied in detail based on the composition of the [Cd(II)–DMAHBH] complex as determined by using the Job's and molar ratio methods. The most important physico-chemical and analytical characteristics of [Cd(II)–DMAHBH] complex are summarized in Table 2.

Table 2: Physico-chemical and analytical characteristics
of [Cd(II)–DMAHBH] complex

Characteristics	Results
λ_{max} (nm)	378
Colour	yellow
pH range (optimum)	8.0–9.0
Molar absorptivity (l·mol^{-1}·cm^{-1})	$2.94 \cdot 10^4$
Sandell's sensitivity (µg·cm^{-2})	0.0036
Mole of reagent required per mole of metal ion for full colour development	10-folds
Beer's law validity range (µg/ml)	0.5035–5.0535

Optimum concentration range (µg/ml)	0.5035–5.0535
Stability constant of the complex (Jobs method)	$8.58 \cdot 10^7$
Relative standard deviation (%)	0.1
Regression coefficient	0.996
Composition of complex (M:L) obtained in Job's and mole ratio method	1 : 1

The first order derivative spectral graph was shown in Figure 5. This shows the derivative amplitudes measured at λ=430 nm. The first order was found to be proportional to the amount of Cadmium (II) respectively.
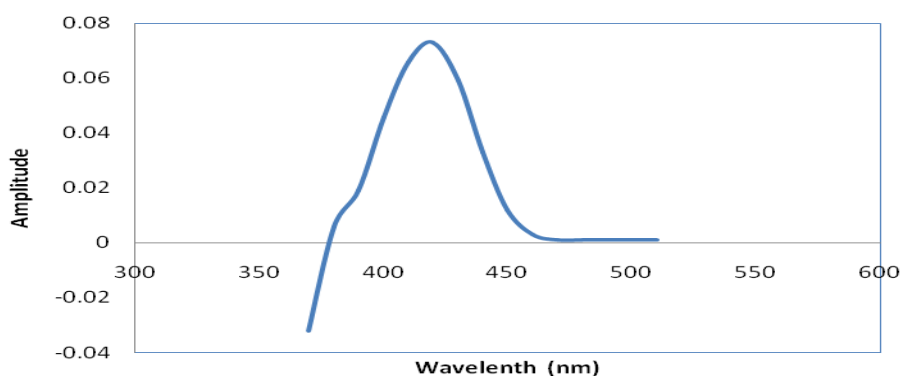

Figure 5: First derivative spectra of [Cd (II)−DMAHBH] Vs reagent

Effect of foreign ions:

Derivative spectrophotometry is a very useful technique in the sense that it decreases the interference, i.e., increases the tolerance limit value of foreign ions of metal ions having overlapping spectra. The recommended procedures have been employed for the spectrophotometric determination of Cadmium (II). The effect of various diverse ions in the determination of Cadmium (II) was studied to find out the tolerance limit of foreign ions in the present method. The tolerance limit of an foreign ion was taken as the amount of foreign ions required to cause an error of ±2% in the absorbance or amplitude. The results are presented in Table 3.

Table 3: Tolerance limit of foreign ions
in the determination of 1.5888 µg/ml of Cadmium (II)

Ion added	Tolerance limit (µg/ml)
Ascorbic acid	91
Acetate	165
Bromide	243
Phosphate	43
Chlorides	344
Citrate	654
Iodide	468
Nitrate	56
Tetra borate	136
Tartarate	523
Ba(II)	09
Co(II)	6.3
Cu(II)[a]	5.1
Hg(II)	1.9

Fe(III)[b]	1.65
Bi(III)	4.1
Ru(III)	5.1
Pd(II)	3.86
Zn(II)	6.6
Pb(II)	1.08
Ag(II)	10.4
Se(IV)	32
Sn(II)	36
V(V)	11.3
U(VI)	65
Zr(IV)	26

Notes: (a) – masked by fluoride, 132 µg/ml; (b) – masked by thiourea, 513 µg/ml

Applications

Determination of Cadmium (II) in soil samples:
Preparation of soil samples
Soil samples like agricultural soil, roadside soil and contaminated soil were taken. The soils were air dried and homogenate soil samples weighing 100 mg accurately taken and placed in a 100 ml flask. The samples were digested in the presence of an oxidizing agent. The content of the flask was filtered through No. 41 filter paper into a 25 ml volumetric flask and neutralized with a dilute NH_4OH solution. It was diluted to the mark distilled water. The calibrated results are presented in Table 4.

Table 4: Determination of Cadmium (II) in soil samples*

Sample name	Cd(II) found µg/g
Industrial sample	0.26±0.3
Agriculture soil	0.57±0.5
Road side soil	1.1±0.2

*Notes: Average of the best three determinations among five determinations

Preparation of cigarette tobacco solution
The tobacco from cigarettes was dissolved in 2 ml of AR grade concentrated sulphuric acid and heated on a hot plate for 20 min. The contents were diluted with 20 ml of water and filtered. The filtrate was collected in a 50 ml flask made up using distilled water. The amount of Cadmium (II) was determined by pre-estimated calibration plot. The calibrated results are presented in Table 5.

Table 5: Determination of Cadmium (II) in cigarette samples*

Commercial sample	Stock solution (ml)	Sample taken (ml)	Zero order
Cigarette (Tobacco) Sample-1	50	2 3 4	2.7
Cigarette (Tobacco) Sample-2	50	2 3 4	2.51

*Notes: Average of the best three determinations among five determinations

Conclusion
In basic buffer medium, the diacetylmonoxime-3-amino-4-hydroxy benzoyl hydrazone (DMAHBH) reacts with Cadmium (II) and imparts yellow coloration of the water soluble [Cd(II)–DMAHBH] complex. The color reaction between Cadmium (II) and DMAHBH is instantaneous

and the absorbance of the colored compound remains to be constant for three hours. The addition of other constituents (buffer, metal ion and reagent) has no adverse effect on the absorbance of the complex. DMAHBH has been proven a sensitive and selective chromogenic organic reagent for the determination of Cadmium (II). Molar absorptivity of the colour complex makes up $2.94 \cdot 10^4$ $l \cdot mole^{-1} \cdot cm^{-1}$. The proposed method was especially sensitive and selective with respect to metals, which commonly seriously interfere with the determination of Copper and Iron performed by literature methods. The proposed method can be successfully applied the determination of Cadmium (II) in soil and cigarette samples. This method was favorably compared with previously reported spectrophotometric methods.

Acknowledgements

References:

1. Lee S.D. *Biochemical Effects of Environmental Pollutants* – Ann Arbor, Mich.: Ann Arbor Scince Publishers Inc., (1977).

2. Salim R., Al-subu M.M., Sahrhage. E. *Sci. Health A* (1992), 27. (3), 603.

3. Cheung C.W., Porter J.F., Mckay G. *J Chem. Technol. Biotechnol.* (2000). 75, 963.

4. Hirano Y., Nakajima J., Oguna K., Terui Y. *J. Anal. Sci.* (2001), 17, 1073.

5. Clayton G.D., Clayton. F.A. (eds.). "*Patty Industrial Hygiene and Toxicology*", 3rd ed. New York: John Wiley and Sons (1981), 1563 p.

6. Hammond P.B., Robert Beliles. In: P. Klassen C.D., Amdur O.M., Doull J. (eds.). *"Metals in Casarett & Doull's Toxicology"*, 3rd ed. – New York: Macmillan (1986), 428 p.

7. Friberg L., Piscator M., Norbberg G.F., Kjellstrom T. (eds.). "*Cadmium in the Environment*", 2nd ed. – New York: CRC Press Inc., Cleveland (1974).

8. Taylor D.M., Willams D.R. *The Royal Society of Chemistry Cambridge* (1995), 22.

9. Key M.M., Hensche A.F., Butter J., Ligo R.N., Tabershaed I.R. (eds.). "*Occupational diseases - A Guide to their Recognition*" – Department of Health, Education and Welfare, Washington: US Government Printing Washington D.C., June (1977), 265 p.

10. Ghazy S.E. *Sep. Sci. Technol,* (1995), 30(6), 933.

11. Reimann C., Caritat P. "Chemical Elements in the Environment. Berlin: Springer Verlag (1998), 80 p.

12. Szczepaniak W., Juskowisk B., Ciszewska. *W. Anal. Chim. Acta* (1984), 156, 245.

13. Hsu C.G., Hu C.S., Jing J.H. *Talanta Elsevier* (1980), 27, 676.

14. Chavanne P., Gerorimi C.L., Emploi D.U. *'Cadion' en Chimie Analytique; Anal. Chem. Acta* (1958), 19, 377.

15. Kmail F., Sinha P.P., Sindhwani S.K. *J. Inst. Chem. (India)* (1982), 54, 119.

16. Roman Ceba M., Munoz Leyva, Berzas Nevado J.A. *An. Quim.* (1980) 76, 465.

17. Hoshi S., Yotsuyangi T., Amoura K. *Bunseki Kagaku* (1977), 26, 592.

18. Vajagand V., Jaredic M. *Chem. Anal. (Warsaw)* (1975), 20, 1125.

19. Baustista Rabriguez J.M., Cano Pavon J.M. *Talanta Elsevier* (1980), 27, 923.

20. DePablos Fernando, Gomez Afriza, Jose L., Pino Francisco. *Mikrochim. Acta* (1985), 411–420.

21. El-Asmy A.A., Moussa M.N.H., EI-Shafie A.A. *Bull. Soc. Chim. Fr.* (1987), 2, 247-249.

22. Casas J.S., Garcia-Tasende M.S., Sordo. J. A Structural Review. *Coord. Chem. Rev.* (2000), 2, 197.
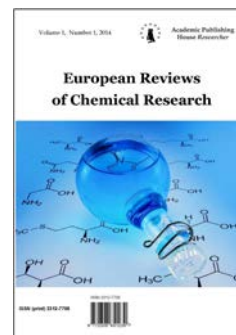
UDC 544.72.05

ZnS Films: Thermodynamic Justification of Possibility for Hydrochemical Precipitation, Synthesis, Microstructure, and Morphology

[1] Anna I. Shemyakina
[2] Ragneta Kh. Saryeva
[3] Larisa N. Maskaeva
[4] Vyacheslav F. Markov

[1] Ural Federal University named after the first President of Russia B.N. Yeltsin, Ekaterinburg, Russian Federation
620002, Ekaterinburg, Mira Street, 19
Assistant researcher
E-mail: anutan145@mail.ru
[2] Ural Federal University named after the first President of Russia B.N. Yeltsin, Ekaterinburg, Russian Federation
620002, Ekaterinburg, Mira Street, 19
Assistant researcher
E-mail: ragneta@rambler.ru
[3] Ural Federal University named after the first President of Russia B.N. Yeltsin, Ekaterinburg, Russian Federation
620002, Ekaterinburg, Mira Street, 19
D. Sc. (Chemical), Professor
E-mail: mln@ural.ru
[4] Ural Federal University named after the first President of Russia B.N. Yeltsin, Ekaterinburg, Russian Federation
620002, Ekaterinburg, Mira Street, 19
D. Sc. (Chemical), Professor, head of the department of physical and colloidal chemistry
E-mail: v.f.markov@ustu.ru

Abstract

The analysis of the thermodynamic equlibria in the «$Zn^{2+} - NH_3 - OH^-$» systems has been carried out; boundary conditions and formations area for ZnS and associated impurity phases of $Zn(OH)_2$ и $ZnCN_2$ have been determined. The nanocrystalline films of zinc sulfide with a thickness of 200-240 nm have been synthesized. The X-ray diffraction analysis and scanning electron microscopy in conjunction with energy-dispersion analysis have been applied for attestation of the structural condition for the zinc sulfide thin films. The effect of the zinc salt nature on the morphology, composition, and structure of the synthesized ZnS layers has been established.

Keywords: ion equilibrium, thermodynamic calculation, chemical precipitation, thin films, zinc sulfide, cubic structure.

Introduction

Zinc sulfide - a binary nontoxic semiconductor of $A^{II}B^{VI}$ group with fine passing capacity in the large interval of wavelengths, low coefficient of reflection, high chemical resistance and thermal stability attracts increased attention of researchers. At 300 K the hexagonal zinc sulfide has the band gap width of 3.74 eV, but the cubic one – 3.66 eV [1]. For the obtained ZnS thin films, which are met and the values of band gap are less: 3.53 eV [2], 3.51 eV [3]. But in any case the band gap width of ZnS is greater than of CdS (E_g = 2.42 eV), which allows to use zinc sulfide as the optical windows for film photocells on the base of $CuInSe_2$ (CIS), $CuIn_{1-x}Ga_xSe_2$ (CIGS) and CdTe compounds. Zinc sulfide can be recommended and both as a potential candidate for cadmium sulfide replacement of CdTe/CdS and CdS/CIGS in heterojunction solar cells. Zinc sulfide has an advantage in delivery of high-energy photons into absorbing material and decreases their intermediate loss to improve the triggering current in the solar cells. Having such properties, ZnS is widely used for the production of various optical devices and is of interest not only as individual material but as one of the components of cascade photocells [4-6].

For the creation of optoelectronic devices of different types thin films are of great interest. Effectiveness of their work is determined by the film properties depending on the way of their preparation. Zinc sulfide obtaining is carried out by the methods of thermal discrete evaporation of the powder ultrahigh vacuum equipment [7], vacuum sublimation in quasi-closed volume [8], electrodeposition [9], and deposiition from gas phase [10], aerosol pyrolysis of aqueous solutions of thiourea coordinating zinc compositions [11]. These methods require large energy expenditures to synthesize zinc sulfide at high temperature and pressures. The hydrochemical method is a perspective method for obtaining zinc sulfide thin films [12]. The method of chemical deposition of metal salts and thiourea [13-16] from aqueous solutions distinguishes from other ones by their essential advantages. It is simple from technical point of view economical and gives good replicated results, as well as allows obtaining $A^{II}B^{VI}$ compounds both as powders and as thin films. The reaction mixtures containing zinc sulfate, chloride and zinc acetate as the complex agents often use ammonia, sometimes sodium citrate are used in published materials on the chemical deposiition from aqueous conditions, thiocarbamide acts as chalcogenizator [17-20]. However scientifically based approach to the determination of optimal conditions for zinc sulfide obtaining which is perspective semiconductor material in thin-film state is absent in these papers.

Therefore the aim of the given work is the thermodynamic value of formation possibility of zinc sulfide films by hydrochemical deposiition, study of morphology, composition and structure of ZnS films.

Experimental

Hydrochemical deposition of zinc sulfide films has been carried out on previously defatted polished glass-ceramic and glass plants made of reaction mixture containing zinc sulfate ($ZnSO_4$), zinc chloride ($ZnCl_2$), thiocarbamide (CSN_2H_4) and ammonium hydroxide (NH_4OH). The film synthesis was carried out in the temperature interval of 348 − 368 K during 120 min in hermetic reactors made of molybdenum glass into which these films were put fixed in specially produced fluoroplastic holders. The reactors were put into thermostat TS − TB − 10 brand supplying accuracy of ±0,1° temperature maintaining.

The thickness of deposited layers was evaluated with interference microscope (Linnik microinterferometer) of MII-4M. Morphology of film surface was studied by scanning electron microscopy (SEM) of MIRA3LMV with increasing from 500 to 150000 times at accelerating voltage of electron beam of 10 or 20 kV. Besides this scanning electron microscope of JEOL JSM-5900 LV equipped with EDS Inca Energy 250 X-ray spectrometer − for energy-dispersive analysis (EDX) − with which surface morphology and the element composition of different parts of the film were studied at accelerating voltage of 10 kV electron beam. The accuracy of the element composition determination was ~10 rel. %.

The XRD patterns were obtained using the standard industrial diffractometer of DRON − 4 with Cu anode and a pyrolytic graphite monochromator separating the $CuK\alpha_{1,2}$ doublet from the continuous spectrum in the range of 2θ from 15 to 100°C scanned at a step of $\Delta(2\theta) = 0.02°$ and a data accumulation time of 5 s per point.

Results and discussions

The chemical reaction of obtaining zinc sulfide films by hydrochemical synthesis can be presented as following:

$$ZnL_x^{2+} + N_2H_4CS + 4OH^- = ZnS\downarrow + xL + CN_2^{2-} + 4H_2O. \tag{1}$$
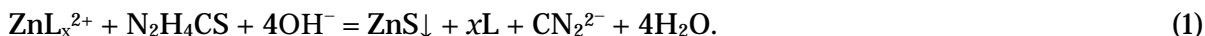
It is necessary for creation and formation of metal sulfide to slow down the process of chemical deposition of this phase by preliminary connection of the metal in the complex. Therefore complex agents different in power and concentration are introduced into reaction mixture.

We developed and tested for the number of reaction systems [12, 21-24] the methodology for determination of boundary conditions and concentration area of solid phase deposition of metal sulfide depending on the pH value and ligand concentration. It is based on the analysis of ion equilibriums in the reaction system and the reversible character of chalcogenizator decomposition [12, 25-27]. At that, the dependence of minimal metal salt composition corresponding to the beginning of the process of it transformation into sulfide on pH value of the reaction mixture is implied as boundary deposition conditions.

Boundary conditions of solid phase deposition in the diluted solutions are realized when ionic product (IP) of ZnS equals to solubility product (SP) of chalcogenide metal. Thus, it is necessary to carry out the following conditions for the formation of the slightly soluble zinc sulfide on the reaction (1):

$$IP_{ZnS} = SP_{ZnS}, \tag{2}$$

where IP_{ZnS} — an ionic product, i.e. the product of noncomplex Zn^{2+} metal form and S^{2-} sulfide ions activities, SP_{ZnS} — the solubility product of ZnS solid phase being of constant value at the given temperature.

However the initiation of some supersaturating value of ZnS appearing in IP_{ZnS}/SP_{ZnS} ratio for compensation of excess surface energy of forming of nuclei and the following growth of new phase particles is necessary for the stable formation of solid phase by homogeneous mechanism.

The value created in the system of supersaturating depends on the concentration of Zn^{2+} free ions in the volume of the reaction mixture.

The higher is supersaturation, the smaller is the Gibbs energy of nuclei formation and the less are nuclei sizes which are able to further growth. The concentration of zinc free ions in the reactor volume is determined by the nature of ligands, which are in the reactor. Deposition of ZnS films from the citrate and ammonia reactions systems containing accordingly $C_6H_5O_7^{3-}$ complexing zinc citrate ions, and NH_3 ammonia was carried out for the evaluation of role and influence of complexing zinc ammonia (NH_3).

The portion of Zn^{2+} noncomplex (active) ions in the presence of ammonia NH_3, which are able to react with sulfide ions can be evaluated according to the expression suggested in [28]:

$$\alpha_{Zn^{2+}} = \frac{[Zn^{2+}]}{C_{Zn}} = \frac{1}{1 + \dfrac{[L_1]}{k_1} + \dfrac{[L_1]^2}{k_{1,2}} + \dots \dfrac{[L_1]^n}{k_{1,2\dots n}}} \, , \tag{3}$$

where C_{Zn} — the total analytical concentration zinc ions in the solution; L — the concentration of free ligand; k_1, k_2 — instability constants of different complex metal forms.

The following values of the instability constants of complex zinc ions were used in calculations: $pk_4 = 2.18$, $pk_5 = 4.43$, $pk_6 = 6.93$, $pk_7 = 9.08$, $pk_8 = 9.46$, $pk_9 = 12.75$ for complexes with ammonia $ZnNH_3^{2+}$, $Zn(NH_3)_2^{2+}$, $Zn(NH_3)_3^{2+}$, $Zn(NH_3)_4^{2+}$, $Zn(NH_3)_5^{2+}$, $Zn(NH_3)_6^{2+}$ [29]; $pk_{10} = 6.04$, $pk_{11} = 11.1$, $pk_{12} = 13.6$, $pk_{13} = 14.6$ [29] for hydrocomplexes according to $Zn(OH)^+$, $Zn(OH)_2$, $Zn(OH)_3^-$, $Zn(OH)_4^{2-}$.

In order to determine predominating of complex forms in the solution, which influence jestingly on the rate of deposition process the analysis of ionic equilibria in the «$Zn^{2+} - NH_3 - OH^-$» system, was performed.

The distribution diagram of different complex zinc forms in the aqueous solution in the ammonia system beginning from pH value is shown in Fig. 1.
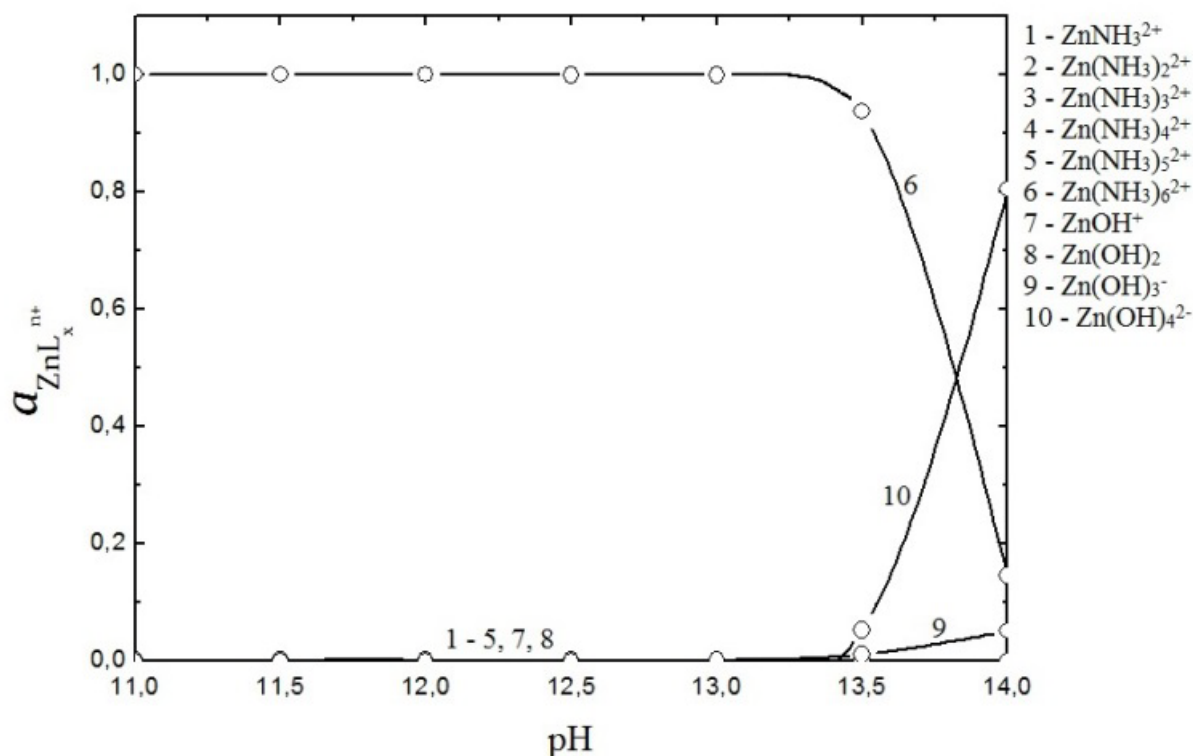

Fig. 1. The diagrams of the distribution of complex zinc forms in the «$Zn^{2+} - NH_3 - OH^-$» system. The initial concentration of zinc salt equals 0.1 mol/l.

The results of ionic equilibria calculations showed that a part of zinc hydrocomplexes in using as ammonia ligands isn`t significant: for pH < 13.0 a part is ~0.01. Let us note, that the $Zn(OH)_4^{-2}$ complex ion reaching 0.8, predominants in pH = 14 range. $Zn(NH_3)_6^{2+}$ is the predominant complex preventing the fast zinc sulfide precipitation in the system, when (pH = 10–13) thiocarbamide value is favorable for decomposition (Fig. 1).

The calculation of boundary formation conditions on the base of analysis of ionic equilibria was made, in order to determine, the concentration area of zinc sulfide existence as well as accompanying impurity phases as zinc hydroxide $Zn(OH)_2$ and zinc cyan amide $ZnNH_2$ in the studied system.

Equation [12] was used for the determination of minimally necessary concentrations of zinc salt supporting the ZnS solid phase formation in the investigated reaction system in ammonia presence:

$$pC_H = p\Pi P_{ZnS} - p\alpha_{Zn^{2+}} - \left(pk_{H_2S} - 2pH + 0.5pK_c + p[N_2H_4CS]_H + 0.5p\frac{\beta_\text{п}}{\beta_S} \right) - - \frac{0.86 \cdot \sigma \cdot V_M}{R \cdot T \cdot r_{кр}}, \quad (4)$$

where p – the index (negative logarithm); C_H – the minimal concentration of zinc salt necessary for ZnS solid phase formation; SP_{ZnS} – the solubility product of zinc sulfide; $\alpha_{Zn^{2+}}$ - part concentration of metal free ions able to enter chemical reaction; k_{H2S} – constant of hydrogen sulfide ionization which is one of thiocarbamide decomposition products (pk_{H_2S} = 19.88 [29]); K_C - constant of thiocarbamide hydrolytic decomposition (pK_c = 22.48 [12]); $[N_2H_4CS]_H$ – initial concentration of chalcogenizator (thiocarbamide) in the solution, 0.6 mol/l; σ – specific surface energy of zinc sulfide (1.0 Дж/м²); V_M – the molar volume of zinc sulfide (2.28·10⁻⁵ м³/моль); $r_{кр}$ –

radius of critical size nucleus ($3.2 \cdot 10^{-9}$ м); R – universal gas constant 8.314 Дж/(моль·К); T – process temperature (353 K).

The last component in the formula is the derivative from Thomson – Oswald relation and determines supersaturating investment in the ZnS system with the formation of critical size nuclei.

The minimal initial concentration of pC_{H} zinc salt providing the formation of zinc hydroxide and was obtained by [12]:

$$pC_{H} = p\Pi P_{Zn(OH)_2} - p\alpha_{Zn^{2+}} - 2pK_W + 2pH_H,\qquad(5)$$

where $p\Pi P_{Zn(OH)_2}$ - index of solubility product of zinc hydroxide (17.15 [29]); K_W – ionic product of water.

The equation [13] was used for calculation of the boundary conditions formation of zinc cyan amide:

$$pC_{H} = p\Pi P_{ZnCN_2} - p\alpha_{Zn^{2+}} - \left(pk^{1,2}_{H_2CN_2} - 2pH_H + 0.5pK_C + 0.5p[N_2H_4CS]_H + 0.5p\frac{\beta_S}{\beta_\Pi}\right),\qquad(6)$$

where $p\Pi P_{ZnCN_2}$ – index of solubility product of zinc cyan amide (14.1 [13]); $k^{1,2}_{H_2CN_2}$ – the total constant of zinc cyan amide decomposition by two stages ($pk^{1,2}_{H_2CN_2}$ = 21.52 [13]).

The results of calculations of the boundary conditions and the deposition area of zinc sulfide and zinc hydroxide for this reaction mixture in the form of the three-dimensional graphical dependences in the coordinates of "index of initial concentration of metal salt – concentration introduced ligand – pH values of the solution" are represented in Fig. 2. From results mentioned above is clear that the ZnS solid phase in the ammonia system (Fig. 2) can be formed in pH range from 12 to 14. The value of zinc minimal concentration necessary for proceeding of sulfide formation process grows with increasing of ligand concentration introduced in the reaction mixture.

As it is well known, the formation of films on the non activated substrate is only formation area of the thermodynamically stable metal hydroxide, i.e. the $Zn(OH)_2$ phase is performs a role of natural surface activator, but OH⁻ ions act as centers of concentration. It is seen in Fig. 2 that the hydroxide phase in presence of which influences positively the initial stage of sulfide formation is formed at pH value higher than 12.
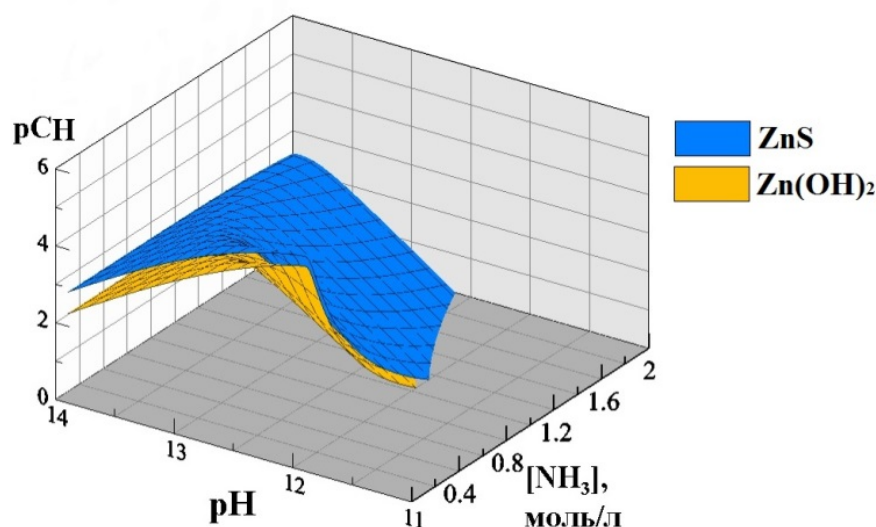

Fig. 2. The boundary conditions of zinc sulfide and hydroxide formation
in the «$Zn^{2+} - NH_3 - N_2H_4CS - OH^-$» system

Calculations have shown that the formation of zinc cyan amide phase in the reaction mixture does not create the necessary conditions.

According to the calculations most favorable for film deposition in the mixture ZnS pH range is from 12 to 14. In this case, the higher the alkalinity of the solution, the lower the required minimum concentration of zinc salt in solution. For films of zinc sulfide in the system studied was selected region pH ~ 12) at a total concentration of the reaction mixture was introduced into the zinc salt 0.1 mol / l.

In terms of the Thomson - Ostwald equation [21] the value of the critical nucleus is directly related to the degree of supersaturating. The calculated value of supersaturating generated in the reaction mixture, when used as ligands of ammonia was 9.9.104, i.e. zinc sulfide film formation should occur under conditions of sufficiently high supersaturating. Due to the large supersaturating it can be assumed that the system will produce a large number of nuclei and the crystal grains of small size.

As a result, the substrate can form a dense and homogeneous film on the structure ZnS.

The results of preliminary experiments and calculations during the two-hour chemical synthesis, conducted at a temperature of 363 K were obtained smooth shiny zinc sulfide layer uniformly covering the surface pyroceramics and glass substrates with good adhesion. Their thickness depending on the conditions of synthesis ranged from 200 to 240 nm.

The SEM images of zinc sulfide layers obtained hydrochemical deposition from a reaction mixture comprising zinc chloride and sulfate are presented in Fig. 3.

а   *б*
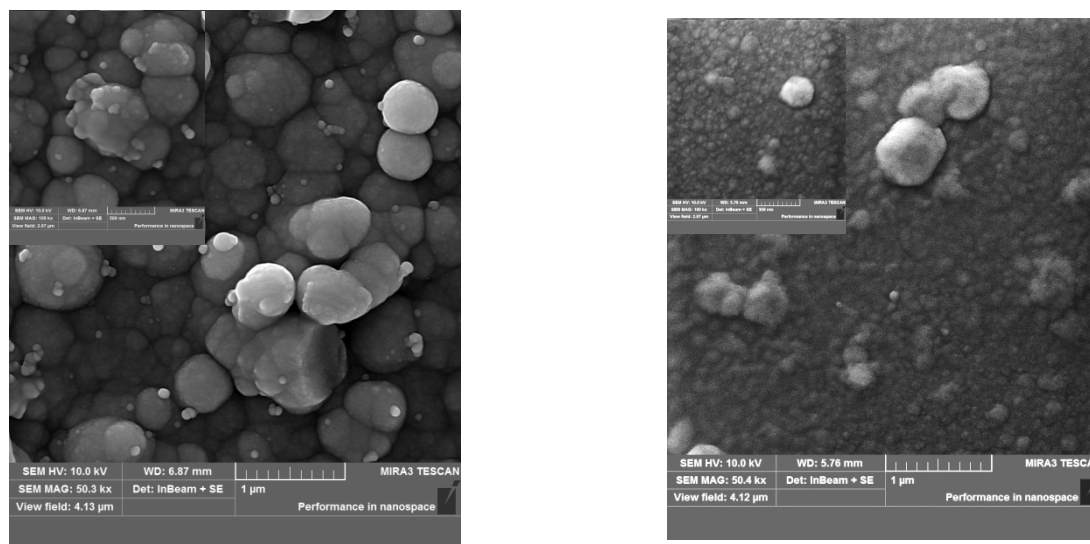
Fig. 3. The SEM images of ZnS films obtained hydrochemical deposition during 120 minutes on the pyroceramics substrates from the reaction mixture, containing zinc chloride (a) and sulfate (b). The temperature of synthesis was 368 K.

Despite their significant differences can be noted that the major structural elements of films regardless of the type of zinc salt in the reaction mixture are preferably spherical globules representing aggregate smaller particles typical spherically shaped zinc sulfide [30]. We see that in both cases a spherical shape with a primary particle size of 10-30 nm form giant clusters of globular shape. However, their diameter and morphology depending on the reaction system is noticeably different. Thus, when using zinc chloride predominant sizes of globules 400-700 nm. More dense and homogeneous film is obtained from a reaction mixture containing zinc sulfate. However, the surface can be observed a minor amount of large aggregates of 200-500 nm in size.

The proximity film of zinc sulfide to the stoichiometric composition is an important criterion for the quality of the optical material is provided that, as stated in [31], while the low-temperature synthesis. In addition, the most perfect crystal structure of the film is synthesized in highly non equilibrium conditions. It meets these requirements hydrochemical deposition used in this paper. But an important factor in the stoichiometric composition of the investigated sulfide has a zinc salt.

The obtained results allows us to conclude that for ZnS approximate to the stoichiometric composition, it is preferable to use zinc chloride, provides the relation between the Zn: S as a 49.3: 50.7 in at. 52.7% vs. 47.3 obtained when in the reactor zinc sulfate.

The XRD patterns of ZnS films (Fig. 5) indicating a preferred crystallographic grain orientation in the [111] direction in the films grown using a reaction mixture of zinc chloride and ammonia as complex agent. Observed on the XRD patterns of investigated sample the intensities of reflection indicates the preferential crystal orientation in the (111) plane. The strong reflex of cubic phase ZnS indicates that it is dominant in the test samples of the films, i.e. synthesized layers of zinc sulfide have a cubic modification of sphalerite with lattice constant $a = 0.5318$ nm. In this work [32] reported that the crystals with [111] orientation are preferable from the viewpoint of optical properties.
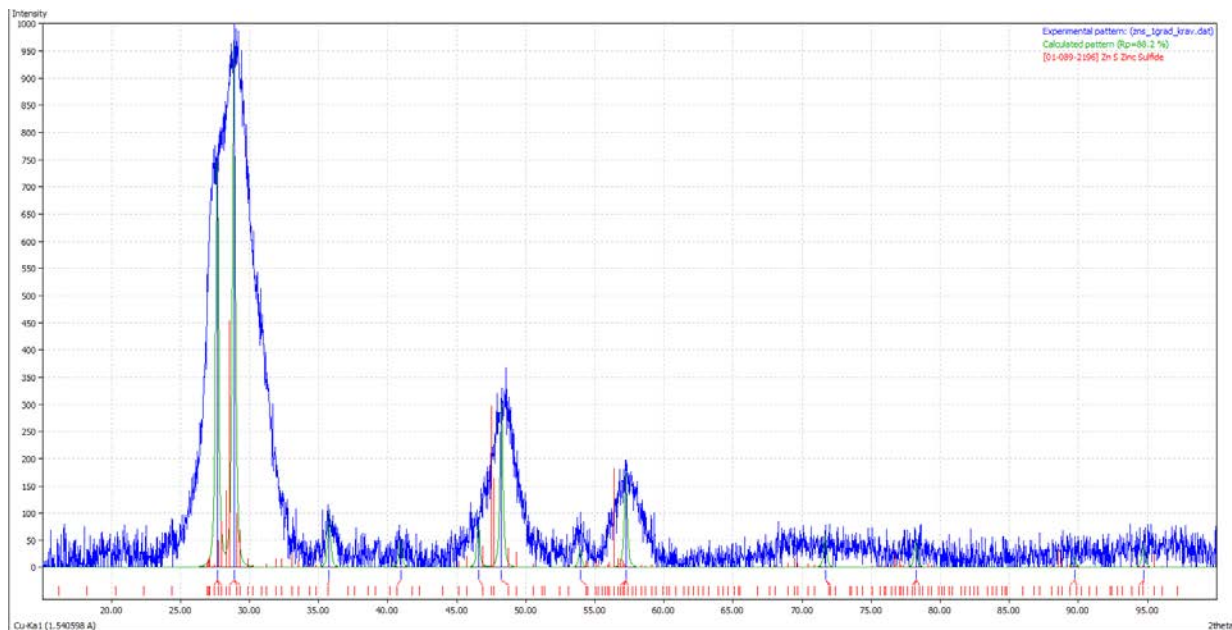

Fig. 4. The XRD pattern of ZnS film obtained by chemical deposition on during 120 minutes on the pyroceramics substrate in presence ammonia mixture, which is zinc chloride. The temperature of synthesis was 368 K.

Despite the complexity of physical and chemical process of synthesis of zinc sulfide films by chemical vapor deposition from aqueous solutions, in the present study because of thermodynamic calculations of ionic equilibria in the «Zn^{2+} - NH_3-N_2H_4CS - OH^-» layers were obtained ZnS, close to the stoichiometric composition of the cubic structure, is an important quality criterion for optical semiconductor material, particularly solar cells and the new film heterostructures.

Acknowledgments

References:

1. Georgobiani A.N., Wide-gap semiconductors $A^{II}B^{VI}$ and prospects of their application // Uspekhi Fizicheskikh Nauk. 1974. Vol. 113. № 1. P. 129–155 [in Russian].

2. Jie Cheng, Dong Bo Fan, Hao Wang, Bing Wei Liu, Yong Cai Zhang, Hui Yan. Chemical bath deposition of crystalline ZnS thin films // *Semicond. Sci. Technol.* 2003. Vol. 18. № 7. P. 676-679.

3. Liu Qi. Guobing Mao, JianpingAo. Chemical bath-deposited ZnS thin films: Preparation and characterization // Applied Surface Science. 2008. Vol. 254. Iss. 18. P. 5711–5714.

4. Chopra K.L, Das S.R. Thin film solar cells. - Plenum Press: New York, London, 1983. 283 p.

5. Dharmadasa I.M. Advances in thin film solar cells. - Pan Stanford Publishing. 2012. 225 p.

6. Kashani H. Production and evaluation of ZnS thin films by the MOCVD technique as alpha-particle detectors // Thin Solid Films. 1996. Vol. 288. Iss.1-2. P. 50-56.

7. Vetoshkin V.M., Krylov P.N., Romanov E.N. Investigation of effect of modes forion-plazma processing on roughness of supporters made of quartz, polycore, and sytall // Vacuum technics and technology. 2008. V. 18. № 2. P. 75-80.

8. Kurbatov D.I. Electrophysical properties of zinc sulfide films obtained by close-spaced vacuum sublimation technique // Semiconductors. 2013. Vol. 47 (9). P. 1175-1180 [in Russian].

9. Urazov K.A. Dergacheva M.B. Leontyeva K.A. Khussurova G.M. Yaskevich V.I. Electrochemical deposition of zinc sulfide films // Journal chemistry and chemical technology. 2014. №3. P. 36-43 [in Russian].

10. Gavrishchuk E.M., Yashina E.V. Zinc sulfide and zinc selenide optical elements for IR engineering // Journal of Optical Technology. 2004. Vol. 71. № 12. P. 24-31 [in Russian].

11. Klyeva V.G., Mayorova T.L., Fam Thi Hai M., Semenov V.N. Recombination properties of zinc sulfide films, obtained by diffusion technique // Condensed media and interphase boundaries. 2009. Vol. 9. № 2. P. 152-155 [in Russian].

12. Markov V.F., Maskaeva L.N., Ivanov P.N. Hydrochemical precipitation of sulfide metals films: modeling and experiment. - Yekaterinburg, UrO RAS. 2006. 218 p [in Russian].

13. Sorokin E., Naumov S., Sorokina I.T. Ultrabroadband infrared solid-state lasers // IEEE J Sel Top Quant Electron. 2005. Vol. 11. № 3. P. 690-712.

14. Park S., Kim H., Jin C., Lee C. Synthesis, structure, and photoluminescence properties of ZnSSe alloy nanorods // Current Appl. Phys. 2012. V. 12. Iss. 2. P. 499-503.

15. Dharmadasa I.M. Advances in thin film solar cells. - Pan Stanford Publishing. Hardback. 2012. 225 p.

16. Kashani H. Production and evaluation of ZnS thin films by the MOCVD technique as alpha-particle detectors // Thin Solid Films. 1996. V. 288. Iss. 1-2. P. 50-56.

17. Liu Qi, Guobing Mao, Jianping Ao. Chemical bath-deposited ZnS thin films: Preparation and characterization // Applied Surface Science. 2008. Vol. 254. Iss. 18. P. 5711–5714.

18. Jie Cheng, DongBoFan, Hao Wang, BingWei Liu, YongCai Zhang, Hui Yan. Chemical bath deposition of crystalline ZnS thin films // *Semicond. Sci. Technol.* 2003. Vol. 18. № 7. P. 676

19. Ben Nasr T., Kamoun N., Kanzari M., Bennaceur R. Effect of pH on the properties of ZnS thin films grown by chemical bath deposition // Thin Solid Films. 2006. Vol. 500. P. 4–8.

20. Huda Abdullah, Norhabibi Saadah and Sahbuddin Shaari Effect of Deposition Time on ZnS Thin Films Properties by Chemical Bath Deposition (CBD) Technique // World Applied Sciences Journal. 2012. Vol. 19. № 8. P. 1087-1091.

21. Mironov M.P., Loshkareva L.D., Maskaeva L.N., Markov V.F. Kynetics- thermodynamic investigation of tin precipitation (II) in trilonate system by selenourea // Butlerov communications. 2010. V. 19. № 1. P. 25-31 [in Russian].

22. Tulenin S.S., Markov V.F., Maskaeva L.N. Thermodynamic analysis of conditions for formation and chemical precipitation of solid solutions substitution in the $Cu_2S-In_2S_3$ system // Butlerov communications. 2012. Vol. 29. № 3. P. 79-85 [in Russian].

23. Fedorova E.A., Maskaeva L.N., Markov V.F. $Cu_{2-x}Se$ films: thermodynamic analysis of formation conditions, synthesis, composition, morphology // Butlerov communications. 2014. V. 38. № 6. P. 81-87 [in Russian].

24. Maskaeva L.N., Markov V.F., Voronin V.I., Gusev A.I. Hydrochemical synthesis, structure and properties of films of supersaturated substitutional $Cu_xPb_{1-x}S$ solid solutions // Thin Solid Films. 2004. V.461. P. 325–335.

25. Markov V.F., Tretyakova N.A., Maskaeva L.N., Bakanov V.M., Muhamedzyanov H.N. Hydrochemical synthesis, structure, semiconductor properties of films of substitutional $Pb_{1-x}Sn_xSe$ solid solutions // Thin Solid Films. 2012. Vol. 520. Iss. 16. P. 5227-5231.

26. Markov V.F. Maskaeva L.N. Calculating the boundary conditions of the formation of solid-phase metal sulfides and selenides by deposition with thio- and selenourea // Journal of Physical Chemistry. 2010. V. 86 №8. P. 1421-1426 [in Russian].

27. Ivanov P.N. Maskaeva L.N. Markov V.F. Voronin V.I. Investigation of Hydrochemical Deposited Films of Substitution Solid Solutions in Pb(II)-Cu(I)-S System // Journal of surface investigation. X-ray, synchrotron and neutron techniques. 2003. №8. P. 85-91 [in Russian].

28. Butler J.N. Ionic equilibrium. - Moscow: Chemistry. 1973. 448 p.

29. Lurie Yu.Yu. Handbook of Analytical Chemistry. - Moscow: Chemistry. 1989. 448 p.

30. Krasnopyorova A.P., Belikov K.N., Sofronov D.S. // Methods and objects of chemical analysis. 2013. Vol. 8. № 4. P. 194-198 [in Russian].

31. Belyaev A.P. Rubets V.P. Nuzhdin M.Yu. Kalinkin I.P. The influence of distinctly non-equilibrium conditions on the stoichiometry of the layer of cadmium telluride obtained by condensation from vapor phase // Semiconductors. 2003. Vol. 37(6). P. 641-643 [in Russian].

32. Valeev R.G. Beltukov A.N. Gilmutdinov F.Z. EXAFS spectroscopy study of the atomic structure of ZnS nanocomposite thin films // Journal of Structural Chemistry. 2011. Vol. 52 (7). P. 184-188 [in Russian].
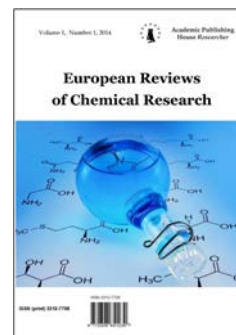
UDC 622.244.4

Investigation of Sulfur Removal from Drilling Fluid

[1*] Mostafa Mohammadi Shalmani
[2] Farshad Farahbod

[1] Islamic Azad University, Marvdasht, Fars, Iran
Department of Petroleum Engineering, Marvdasht Branch
*E-mail: Mohammadi_MSH_eng@yahoo.com
[2] Islamic Azad University, Firoozabad, Fars, Iran
Department of Chemical Engineering, Firoozabad Branch
E-mail: mf_fche@iauf.ac.ir

Abstract

The sulfur removal from drilling fluid for prevention from corrosion was studied, specially. ZnO nanoparticles are proposed as the coagulant. Turbidity of supernatant, the pH stability, settling time, the effect of auxiliary coagulants such as $FeCl_3$, $Fe_2(SO_4)_3$ and $Al_2(SO_4)_3$ on the treatment process are reported in this work. Fourier transform infrared spectroscopy (FTIR) and zeta potential is utilized to investigate the pH values related to the stable suspension. The optimum value of initial pH=8, final pH=9, amount of turbidity= 6.5 NTU is obtained after 15 days of the settling time, if the 15 g/l ZnO is used with 450 cc NaOH and Na_2CO_3 are used in coagulation process. Lowest zeta potential is 2 with using 15 g/l ZnO at the initial pH=9.5. The sulphur removal percentage is about 97% in this condition.

Keywords: Environmental pollution, nano particles, coagulation, treatment.

Introduction
1. Drilling fluid mud

Drilling fluid mud – is usually composed by water, clay, weighing material and a few chemicals [1]. Sometimes oil may be applied instead of water, or oil added to the water to give the mud certain desirable physical properties [12]. Drilling fluid is used to increase the cuttings made by the bit and lift them to the surface for disposal [3]. But equally important, it addition, provides a means of keeping underground pressures in check. The heavier or denser the mud, is the more pressure it exerts. Therefore, weighing materials – barite – are mixed to the mud to make it exert as much pressure as required to contain formation pressures [4]. The equipment in the circulating system consists of a large number of parameters. Drilling fluids are applied extensively in the upstream oil and gas industry, and are critical to ensuring a safe and productive oil or gas well. During drilling process, a large volume of drilling fluid is circulated in an open or semi enclosed system, at elevated temperatures, with agitation, preparing an important potential for chemical exposure and subsequent health effects [5]. When deciding on the type of drilling fluid system to use, operator well planners require conducting comprehensive risk assessments of drilling fluid systems, considering health aspects in addition to environmental and safety aspects, and strike a

suitable balance between their potentially conflicting requirements [6]. The results of these risk assessments require to be made available to all employers whose workers may become exposed to the drilling fluid system.

2. Functions of drilling fluid

In the early days of rotary drilling, the primary function of drilling fluids was to bring the cuttings from the bottom of the hole to the surface [7]. Today it is recognized the drilling fluid has at least ten important functions: A). assists in making hole by: A-1). removal of cuttings; A-2). cooling and lubrication of bit and drill string; A-3). power transmission to bit nozzles or turbines. B). Assists in hole preservation by: B-1). support of bore hole wall; B-2). containment of formation fluids. C). It also: C-1). supports the weight of pipe and casing; C-2). serves as a medium for formation clogging. D). It must not: D-1). corrode bit, drill string and casing and surface facilities; D-2). impair productivity of producing horizon; D-3). pollute the environment [8–10].

3. The role of drilling fluid

Undoubtedly, the drilling fluid has vital role in drilling process [11, 12]. Two basic items included; frictions and in the recycling cycle.

4. Customized solutions

Despite the excellent track record demonstrated by invert emulsion fluids, operators continue searching for a water-based system that will give comparable performance [13–15]. Increasing concern is placed on environmental impact of operations, making water-based alternatives more attractive [16–18].

"Baroid Industrial Drilling Products" has engineered high-performance water-based fluids that emulate the performance of an invert emulsion fluid. Each fluid system is customized to address specific drilling challenges [19–21].

The amount of sulfur removal from waste drilling fluid with using the ZnO nanoparticles as novel coagulant is evaluated in this paper.

Material and methods
1. Equipment

Experiments are held in two PVC series tanks equipped by adjustable agitator. The treatment process is done in two series mixing reactors. 450 cc NaOH and 600 cc Na_2CO_3 is inserted in the drilling mud feed line. First reactor is a fast mixing reactor to insert a coagulant during 5 min with 120 rpm. The second slow mixing reactor vessel (60 rpm, 20 min) is equipped with hot water jacket and also is equipped with the hot air line which is inserted into the second reactor. Feed is 4 liters watery drilling mud.

2. Operating functions for prediction of treatment performance

Some functions which are evaluated in the treatment units are listed at the below. These functions state the quality of treatment process.

3. Fourier transform infrared spectroscopy (FTIR)

This is a proper and confident technique which is used to obtain an infrared spectrum of absorption, emission, photoconductivity or Raman scattering of fluid. The FTIR spectrometer simultaneously collects spectral data in a wide spectral range. This confers a significant advantage over a dispersive spectrometer which measures intensity over a narrow range of wavelengths at a time. The used FTIR has made dispersive infrared spectrometers all but obsolete (except sometimes in the near infrared), opening up new applications of infrared spectroscopy.

Results and discussion
1. The effect of wave number on the transmittance

Usually the drilling mud is drained in the pool under the ground, so the sulfur contaminates in the mud penetrate in the soil and affect the quality of soil in view of agricultural applications. Coagulation mechanism in softening process using nano ZnO particles with mineral coagulant is investigated experimentally. The pH value, turbidity, settling time and appearance of the fluid is also considered besides the amount of sulfur.
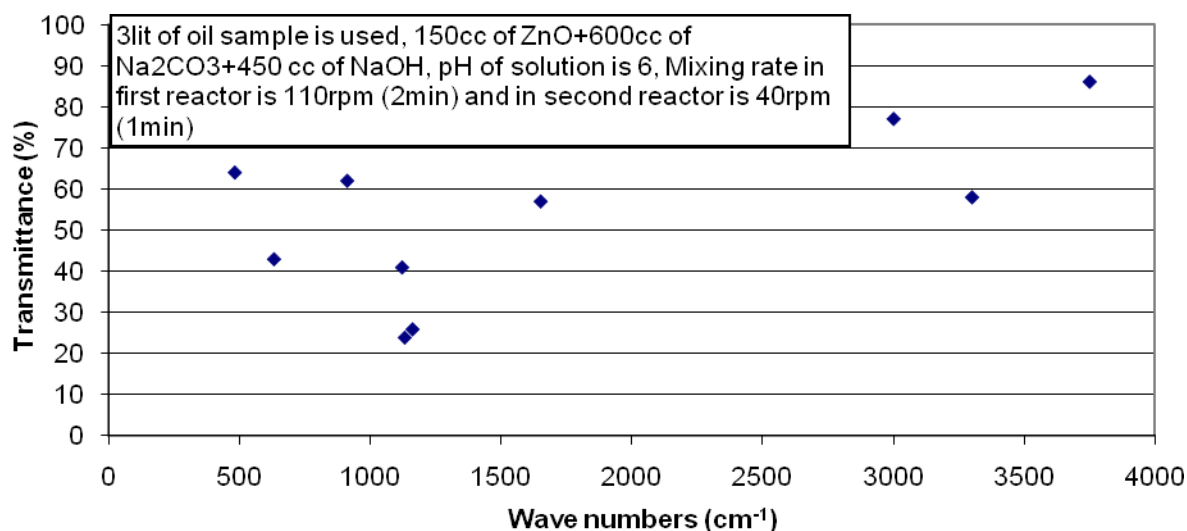

Figure 1. Transmittance versus wave number

The effect of wave number on the transmittance is shown in Figure 1. The distribution density of the transmittance is between 20% to 70% and the wave number is between 500 to 1650 cm^{-1}.

According to the Figure 1 some wave numbers illustrate the characteristic peaks at 920 cm^{-1} and 620 cm^{-1}, which are related to the bending vibration of Fe−OH−Zn bonds. The stretching vibration of Fe−O bond is overlapped up by the absorption peak caused by the bending vibration of Fe−OH−Zn bond. The peaks value at 490 cm^{-1} and 1162 cm^{-1} are assigned to the characteristic bands for Zn−O bond and Fe−O bond, respectively. The vast band of wave number indicates on the hydroxide band.

2. The effect of the nano particle concentration on the pH value

The pH value of the reaction environment affects the coagulation and flocculation process. So, Figure 2 shows the pH variation versus concentration of ZnO particles. The pH range is between 8 to 12 units during experiments. According to the results, the ZnO content in the solution is not important to obtain the specific pH value.
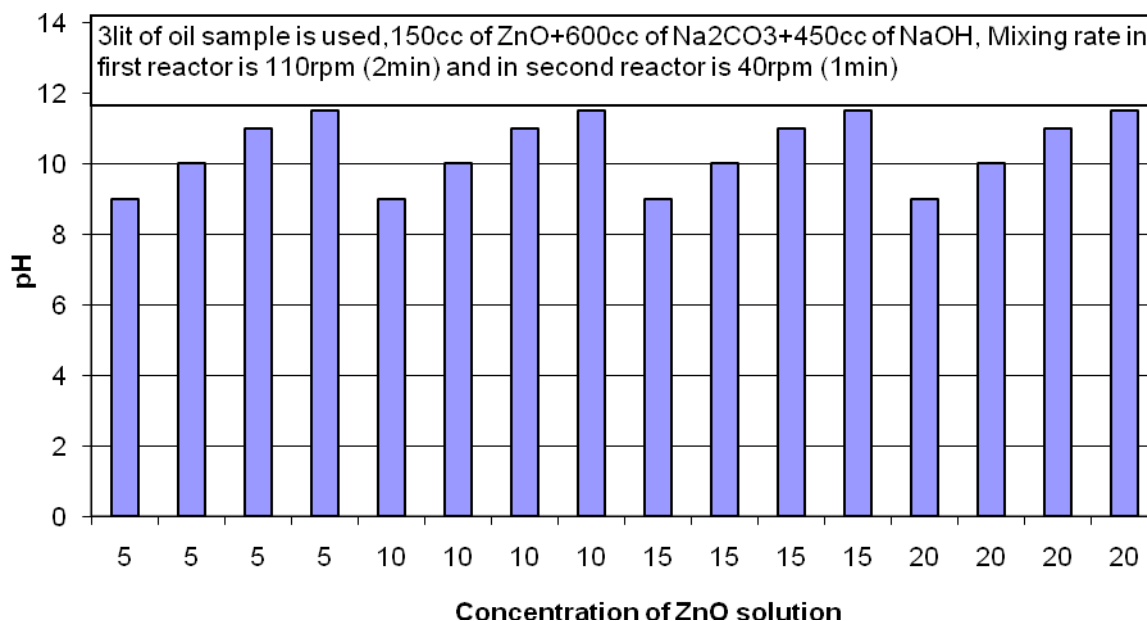
Figure 2. pH versus ZnO concentration

Conclusion

Drilling mud treatment by coagulation and flocculation applying ZnO nanoparticles is investigated, in this work. Drilling mud contains contaminants like sulphur after usage and is drained under the ground. So, surveying treatment methods to remove the contaminants from mud by nano ZnO particles is considered in this research. Two mixing reactor are used utilizing ZnO, NaOH and Na_2CO_3 as coagulants and related parameters are represented in Figures. Turbidity, pH, settling time, amount of ZnO, effect of axillary coagulants [$FeCl_3$, $Fe_2(SO_4)$, $Al_2(SO_4)_3$] are measured.

References:

1. Santosa, Sri Juari, Kunarti, Eko, Karmanto, Sri, 2013. Synthesis and utilization of Mg/Al hydrotalcite for removing dissolved humic acid, *Applied Surface Science* 254, 7612–7617.

2. W.P. Cheng, Comparison of hydrolysis/coagulation behaviour of polymeric and monomeric iron coagulants in humic acid solution, *Chemosphere* 47 (2013) 963–969.

3. Abrahamson, A.B.I., Brunstrom, B., Sundt, R.C., Jorgensen, E.H., 2008. Monitoring contaminants from oil production at sea by measuring gill EROD activity in Atlantic cod (Gadus morhua), *Environ. Pollut.* 153, 169–175.

4. Esmaeilzadeh, F., Goodarznia, I., 2005. Supercritical extraction of phenanthrene in the crossover region, *J. Chemical Engineering Data* 50, 49–51.

5. Beyer, J., Jonsson, G., Porte, C., Krahn, M.M., Ariese, F., 2010. Analytical methods for determining metabolites of polycyclic aromatic hydrocarbon (PAH) pollutants in fish bile: a review. *Environ. Toxicol. Pharmacol.* 30, 224–244.

6. Bohne-Kjersem, A., Skadsheim, A., Goksoyr, A., Grosvik, B.E., 2009. Candidate biomarker discovery in plasma of juvenile cod (Gadus morhua) exposed to crude North Sea oil, alkyl phenols and polycyclic aromatic hydrocarbons (PAHs), *Mar. Environ. Res.* 68, 268–277.

7. Duan, J., Gregory, John a, 2010. Coagulation by hydrolysing metal salts, *Advances in Colloid and Interface Science* 100, 475–502.

8. Jiang Jia-Qian, Loyd Barry, 2013. Progress in the development and use of ferrate (VI) salt as an oxidant and coagulant for water and wastewater treatment, *Water Research* 36 1397–1408.

9. Abdou, M.I., Al-Sabagh, A.M., Dardir, M.M., 2013. Evaluation of Egyptian bentonite and nano-bentonite as drilling mud, *Egyptian J. Petroleum* 25, 53–59.

10. Zouboulis A.I., Moussas P.A., Vasilakou F., 2013. Polyferric sulphate: preparation, characterization and application in coagulation experiments, *Journal of Hazardous Materials* 155 (3), 459–468.

11. Cheng, W.P., 2012. Hydrolytic characteristics of polyferric sulphate and its application in surface water treatment, *Separation Science and Technology* 36 (10), 2265–2277.

12. Fan M., Sung S., Brown R.C., Wheelock T.D., Laabs F.C., 2013. Synthesis, characterization and coagulation of polymeric ferric sulphate, *Journal of Environment Engineering* 128 (6), 483–490.

13. Leprince A., Flessinger F., Bottero J.Y., 1987. Polymerized iron chloride: an improved inorganic coagulant, *Journal of the American Water Works Association* 76, 93–97.

14. Zouboulis A.I., Moussas P.A., 2013. Polyferric silicate sulphate (PFSiS): preparation, characterization and coagulation behavior, *Desalination* 224, 307–316.

15. Gao B., Yue Q., Zhao H., Song Y., 2013. *Properties and evaluation of polyferric silicate sulfate (PFSS) coagulant as a coagulant for water treatment*, in: H.H. Hahn, E. Hofmann, H. Odegaard (Eds.), Chemical Water and Wastewater Treatment VI, Springer-Verlag, Berlin, pp. 15–22.

16. Goodarznia, I., Esmaeilzadeh, F., 2006. Treatment of oil-contaminated drill cuttings of south pars gas field in Iran using supercritical carbon dioxide, *Iranian J. Science & Technology, Transaction B, Engineering* 30, 607–611.

17. Fu, Y., Yu, S.L., 2011. Exterior shapes and coagulation performance of solid poly ferricsilicic sulfate, *Environmental Chemistry* 25 (4), 471–476.

18. Fu, Y., Yu, S.L., 2010. Characterization and coagulation performance of solid poly silicicferric (PSF) coagulant, *Journal of Non-crystalline Solid* 353, 2206–2213.

19. Ghazi M., Quaranta G., Duplay G., Hadjamor R., Khodja M., Amar H.A., Kes-saissia Z., 2011. Life-cycle impact assessment of oil drilling mud system in Algerian arid area, *Resources, Conservation and Recycling* 55, 1222–1231.

20. Issoufi, I., Rhykerd, R.L., Smiciklas, K.D., 2006. Seedling growth of agronomic crops in crude oil contaminated soil. *Journal of Agronomy and Crop Science* 192, 310–317.

21. Amuda O.S., Amoo I.A., 2013. Coagulation/flocculation process and sludge conditioning in beverage industrial wastewater treatment, *Journal of Hazardous Materials* 141, 778–783.
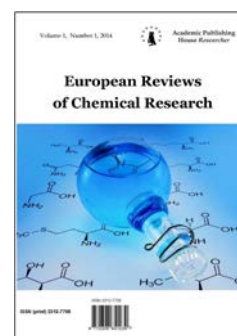
UDC 544; 547

Synthesis, Structure/Spectra Correlation and Chromism Studies of some Novel Monomethine and *bis*-Monomethine Cyanine Dyes

[1]* H.A. Shindy
[2] M.M. Goma
[3] N.A. Harb

[1-3] Aswan University, Aswan, Egypt
Department of Chemistry, Faculty of Science
*Corresponding author
E-mail: hashindy2@hotmail.com

Abstract

Novel methine cyanine dyes, covering monomethine and *bis*-monomethine cyanine dyes having the nucleus of benzo-[2,3-b;2',3'-b']-*bis*-furo-[2,3-d]-imidazoline-3,5,8,10-*tetra* were synthesized and their structure was investigated. The electronic visible absorption spectra of all the synthesized cyanine dyes were examined in 95% ethanol solution. Solvatochromism and/or halochromism for some selected dyes were investigated in pure solvents owing different polarities (water, dimethylformamide, ethanol, chloroform, carbon tetrachloride and dioxane) and/or in aqueous universal buffer solutions having varied *pH* values (1.45; 2.03; 3.72; 5.09; 7.57; 8.91; 10.20 and 12.04 units), respectively. The structural determination was carried out through the elemental analysis, visible electronic absorption spectroscopy, mass spectrometry, IR, and ^{1}H NMR spectral data.

Keywords: cyanine dyes, methine cyanine dyes, synthesis, absorption spectra, solvatochromism, halochromism.

Introduction

Cyanine dyes [1–16] were and still have been the central focus of scientists in a several fields such as chemistry, biology, physics, biotechnology, engineering, pharmacology and medicine. This is due to their multi-purpose using and applications in a diverse and a broad area. Their usage and/or applications includes photographic sensitizers, laser technology, nucleic acid and protein detection, bactericides and fungicides, intercalating dyes, data storage materials; in optical devices – as photorefractive and photovoltaic sensitive materials, fluorescent probes for bio-membrane fluidity, analytical reagents over wide *pH* values of media, indicators and/or probes for determining the solvent polarity and as inhibitors for cell growth and cell division.

Taking into consideration the above important benefits of cyanine dyes, our main goal in this research paper is the preparation of some new photosensitizers, solvatochromic and halochromic monomethine and *bis*-monomethine cyanine dyes, as new contribution for the synthesis and spectroscopic investigation in this field and/or may be used and applied in any of the wide application range of cyanine dyes, particularly as photographic sensitizers in photographic

industry, as indicators for acid/base titrations in analytical chemistry and/or as probes for determining solvent polarity in physical, physical organic and/or inorganic chemistry.

Experimental Part
1. General

All the melting points of the prepared compounds are measured using Electrothermal 15V, 45W IA9100 melting point apparatus (Electrothermal Bibby Sci. Co, UK) at Chemistry department, Faculty of Science (Aswan University), and are uncorrected. Elemental analysis was carried out at the Microanalytical Center of Cairo University by a Vario EL III Automatic Element Analyzer (Elementar Analysensysteme GmbH, Germany). Infrared spectra were measured with a JASCO FT/IR-4100 spectrometer (Jasco Analyt. Instr., Japan) at Cairo University. ^{1}H NMR spectra were accomplished using Varian Gemini-300 MHz NMR spectrometer (Gemini BV, Netherlands) (Cairo University). Mass spectra were recorded on Gas Chromatograph Mass Spectrometer GC-2010 (Shimadzu, Japan) at Cairo University. Electronic visible absorption spectra were carried out on Visible Spectrophotometer, Spectro 24RS (Labomed Inc., USA) at Chemistry department, Faculty of Science (Aswan University).

2. Synthesis:
2.1. Synthesis of benzo-[2,3-b;2',3'-b']-bis-furo-[2,3-d]-imidazoline-3,5,8,10-tetra one (3)

A mixture of unimolar ratio (0.01 mol) of p-chloranil (1) and bimolar ratio (0.02 mol) of hydantoin (2) was refluxed in ethanol (50 ml) containing pyridine (20 ml) for 8 hrs. The reaction mixture changed from a reddish colour to dark brown at the end of the refluxing. It was filtered while hot, concentrated, and precipitated by ice water. The products were collected, washed with water several times, dried and crystallized from ethanol. The results are listed in Table (1).

2.2. Synthesis of benzo-[2,3-b;2',3'-b']-bis-furo-[2,3-d]-imidazoline-5,8,10-tri-one-3[2(4)]-monomethine cyanine dyes (4a–c)

A mixture of the compound (3) (0.01 mol) and ethyl iodide quaternary salts of α-picoline, γ-picoline, quinaldine (0.01 mol) were dissolved in ethanol (50 ml) containing piperidine (3–5 drops). The reaction mixture was heated under reflux for 6–8 hrs and attained reddish colour for (4a–c) and violet colour for (4 b) at the end of refluxing. It was filtered off while hot, concentrated to half its volume and cooled. The precipitated dyes were filtered, washed with water, dried and crystallized from ethanol. The data are given in Table (1).

2.3. Synthesis of benzo-[2,3-b; 2',3'-b']-bis-furo-[2,3-d]-imidazoline-5,10–dione-3,8-[2(4)]-bis-monomethine cyanine dyes (5a–c)

Two different routes are employed to prepare these cyanine dyes:

Route (1): piperidine (3–5 drops) was added to an ethanolic solution (50 ml) of (3) (0.01 mol) and iodoethane quaternary salts of α-picoline, quinaldine and γ-picoline (0.02 mol). The mixture was heated under reflux for 6–8 hrs and attain deep red colour for (5a, c) and violet colour for (5b) at the end of refluxing. It was filtered off while hot, concentrated to half its volume and cooled. The precipitated dyes were filtered, washed with water, dried and crystallized from ethanol. The data are given in Table (1).

Route (2): the monomethine cyanine dyes (4a–c) (0.01 mol) and equimolar ratios of iodoethane quaternary salts of α-picoline, quinaldine and γ-picoline (0.01 mol) were dissolved in ethanol (50 ml), to which piperidine (3–5 drops) was added. The reaction mixture was refluxed for 3–5 hrs and attain deep red colour for (5a, c) and violet colour for (5b) at the end of refluxing. It was filtered off while hot, concentrated to half its volume and cooled. The precipitated dyes were filtered, washed with water, dried and crystallized from ethanol to give the same dyes obtained by Route (1), characterized by melting points, mixed melting points, same visible, IR and ^{1}H NMR spectral data [Table (1)].

3. Structure/Spectra Correlation

The electronic visible absorption spectra of the prepared cyanine dyes were examined in 95% ethanol solution and recorded using 1 cm Q_z cell in Visible Spectrophotometer, Spectro 24RS

(Labomed Inc., USA). A stock solution ($1 \cdot 10^{-3}$ *M*) of the dyes was prepared and diluted to a suitable volume in order to obtain the desired lower concentrations. The spectra were recorded immediately to eliminate as much as possible the effect of time.

4. Solvatochromism and Halochromism Studies

The electronic visible absorption spectra of some selected synthesized cyanine dyes were investigated in pure organic solvents of spectroscopic grade qualities [28] with different polarities and/or in aqueous universal buffer solutions of varying *pH* values, and recorded using 1 cm Q$_z$ cell in Visible Spectrophotometer, Spectro 24RS (Labomed Inc., USA). A stock solution ($1 \cdot 10^{-3}$ *M*) of the dyes was prepared and diluted to a suitable volume using the suitable solvent and/or the buffer solution to obtain the required lower concentrations. The spectra were recorded immediately to eliminate as much as possible the effect of time.

Results and discussion

1. Synthesis

1:2 molar ratios of p-chloranil (1) and hydantoin (imidazolid-2,4-dione) (2) was reacted in ethanol containing pyridine, thus achieved benzo-[2,3-b;2',3'-b']-*bis*-furo-[2,3-d]-imidazoline-3,5,8,10-*tetra* one (3) as new heterocyclic starting material [Scheme (1), Table (1)].

Equimolar reaction of (3) and iodoethane quaternary salts of α-picoline, quinaldine and/or γ-picoline in ethanol as organic solvents and piperidine as a basic catalyst gives the 3[2(4)]-monomethine cyanine dyes (4a–c) [Scheme (1), Table (1)].

Reaction of (3) and N-ethyl (α-picolinium, quinaldinium and/or γ-picolinium) iodide salts in 1:2 molar ratios in ethanol containing few milliliters of piperidine resulted in the 3,8[2(4)]-*bis*-monomethine cyanine dyes (5a–c) [Scheme (1), Route (1), Table (1)].

Chemical confirmations take place for the 3,8[2(4)]-*bis*-monomethine cyanine dyes (5a–c) *via* Route (2) by reactions of the previously prepared monomethine cyanine dyes (4a–c) with iodoethane quaternary salts of α-picoline, quinaldine and/or γ-picoline in equimolar ratios, in ethanol and the presence of piperidine to achieve the same 3,8[2(4)]-*bis*-monomethine cyanine dyes (5a–c) obtained by Route (1), were characterized by melting points, mixed melting points, the same visible, IR and ¹H NMR spectral data [Scheme (1), Route (2), Table (1)].

The structure of the prepared compounds was confirmed by the elemental analysis (Table 1), electronic visible absorption spectra (Table 1), mass spectrometry, IR [17], and ¹H NMR [18] (Table 2) spectroscopic data.

2. Structure/Spectra Correlation

The electronic visible absorption spectra of the monomethine cyanine dyes (4a–c) and *bis*-monomethine cyanine dyes (5a–c) in 95% ethanol solution disclose bands in the visible region at 370–580 nm and 370–610 nm, respectively. The positions of these bands and their molar extinction coefficients are largely influenced by the nature of the heterocyclic quaternary residue (A), their linkage positions and the number of the electronic charge transfer pathways inside the dye molecule. So, substituting A = l-ethyl pyridinium-2-yl salts in the monomethine cyanine dye (4a) and in the *bis*-monomethine cyanine dye (5a) by A = l-ethyl quinolinium-2-yl salts to get the monomethine cyanine dye (4b) and the *bis*-monomethine cyanine dye (5b) causes strong bathochromic shifts at 130 nm and 140 nm respectively, accompanied by increasing in the number and intensity of the absorption bands in the case of the *bis*-monomethine cyanine dye (5b) [Scheme (1), Table (1)]. This can be attributed to increasing π-delocalization conjugation in the latter dyes due to the presence of the quinoline ring system in correspondence to the pyridine ring system in the former dyes.

Changing the linkage positions from 2-yl salts to 4-yl salts passing from the monomethine cyanine dye (4a) and the *bis*-monomethine cyanine dye (5a) to the monomethine cyanine dye (4c) and the *bis*-monomethine cyanine dye (5c) resulted in a remarkable red shift by 10 nm accompanied by increasing the number and intensity of the absorption bands [Scheme (1), Table (1)]. This can be explained in the light of increasing the length of the π-delocalization conjugation in the latter 4-yl salts dyes (4c) and (5c) compared to the former 2-yl salts dyes (4a) and (5a).

Comparing the electronic visible absorption spectra of monomethine cyanine dyes (4a–c) with those of the *bis*-monomethine cyanine dyes (5a–c), we declared that the latter dyes have in their spectra bathochrromically shifted bands related to the former ones. This can be attributed to the presence of two electronic charge transfer pathways inside the latter dyes molecules in correspondence to one electronic charge transfer pathways inside the former dyes molecules [Scheme (2), Table (1)].

3. Solvatochromism

Solvatochromism is the reversible colour changing induced by solvents. This often derives from changes in polarity of various solvents. This affects charge transfer mechanisms in solvatochromic compounds, causing colour changes. Cyanine dyes had been useful in studies of the colour of organic compounds [19] and today there are existed several fundamental principles that correlate origin of colour to chemical structures of the solute, as well as natures of the solvents [19–22]. Besides, this class of organic heterocyclic dyes compounds are useful in various industrial fields [23].

This encouraged us and directed our attention to study the solvachromism of some selected monomethine cyanine dyes (4b) and (5b) in pure solvents having different polarities to select the best solvents when these dyes used and/or applied as photosensitizers. Also, this study evaluates the possibility of uses and/or the applications of these dyes as probes for determining solvent polarity due to their solvatochromic properties.

The electronic visible absorption spectra of the monomethine (4b) and the *bis*-monomethine (5b) cyanine dyes in pure solvents with different dielectric constants, namely water (78.54), dimethylformamide (DMF) (36.70), ethanol (24.3), chloroform (4.806), carbon tetrachloride (2.238) and dioxane (2.209) [24], were recorded. The λ_{max} and ε_{max} values of the absorption bands are shown in Table (3).

From Table (3), it is clear that the electronic visible absorption spectra of the examined dyes in the ethanolic medium are characterized by the presence of four essential absorption bands. These bands can be attributed to intermolecular charge transfer [25] associated with a lone pair of electrons from the HN-imidazoline nitrogen atom migrating towards the positively charged center of the quaternary nitrogen atom of the quinolinium salt residue [Scheme (2)].

The data given in Table (3) show, that the charge transfer band exhibits a hypsochromic shift in ethanol relative to DMF, dioxane, chloroform and carbon tetrachloride. This effect may be related to the following factors:

a) The bathochromic shift in addition to the higher molar extinction coefficients in DMF relative to ethanol is a result of the increase in solvent polarity (positive solvatochromism);

b) The hypsochromic shift occurring in ethanol in addition to the lower molar extinction coefficients relative to dioxane, chloroform and carbon tetrachloride (negative solvatochromism) is a result of the solute-solvent interaction through the intermolecular hydrogen bond formation between ethanol and the lone pair of electrons of the HN-imidazoline nitrogen atom; this minimize slightly the electron density on the HN-imidazoline nitrogen atom and consequently decreases to some extent the moving and mobility of the attached π-electrons over the conjugated pathway to the positively charged quaternary nitrogen atom of the quinolinium salt residue, and accordingly a blue shift occurs in ethanol relative to dioxane, chloroform and carbon tetrachloride [Scheme (3) (A)].

Also, from the data given in Table (3) it is observed the occurrence of unexpected hypsochromic shift, as well as decreasing the number and intensity of the absorption bands in water relative ethanol and the other solvents. This can be mainly ascribed to the possible interaction of water molecules with the lone pair of electrons of the HN-imidazoIine nitrogen atom forming the intermolecular hydrogen bond. This makes difficult the transfer of electronic charge from the HN-imidazoline nitrogen atom to the quaternary nitrogen atom of the heterocyclic salt residue in the quinolinium ring system, and consequently a hypsochromic shift occurs in water relative to ethanol and the other solvents [Scheme (3) (B)].

From the above discussed results we could conclude that the solvatochromism of the investigated cyanine dyes in pure solvents having different polarities underwent displacements to give positive solvatochromism (occurrence of a bathochromic shift with increasing solvent polarity) and/or negative solvatochromism (occurrence of a hypsochromic shift with increasing solvent polarity) depending upon the following factors:

a) Increasing and/or decreasing the polarity and/or the dielectric constant of the solvent (general solvent effect);

b) Hydrogen bond and/or molecular complex formation between the solute (dyes molecules) and the solvent used (specific solvent effect).

4. Halochromism

Halochromism means the colour change, which occurs on addition of acid or base or salt to a solution of a compound. A chemical reaction such as ion formation transforms a colourles compound into a coloured one. Halochromic compounds are compounds, which change their colour when *pH* changes occur. The term chromic is defined as a material that can change colour reversibly with the presence of a factor, and in this case the main factor is *pH*. The *pH* indicators, therefore have this property.

Solutions of the monomethine (4b) and the *bis*-monomethine (5b), cyanine dyes behave as halochromic compounds, where their ethanolic solutions gave changeable colours in acid/base media, being yellow or colourless on acidification and getting back (restore) their original permanent intense colour on basification. This encouraged us and directed our attention to study their spectral behavior in different buffer solutions having varied *pH* values to select the optimum condition and/or the suitable *pH* values for use of these dyes as photosensitizers. The other purpose of this study is to evaluate the possibility of uses and/or applications of these dyes as indicators in acid/base titrations in analytical chemistry. The acid dissociation or protonation constants of these dyes have been determined. The effect of these compounds as photosensitizers increases when they are present in the ionic form, which has higher planarity [26] and therefore more conjugation.

The electronic visible absorption spectra of the dyes (4b) and (5b) in aqueous universal buffer solutions with varying pH values (1.45; 2.03; 3.72; 5.09; 7.57; 8.91; 10.20 and 12.04) showed bathochromic shifts with intensification of their absorption bands at high *pH* values (alkaline media) and hypsochromic shifts with reduction in the intensity of the bands at low *pH* (acidic media) [Table (4)].

These phenomena can be explained and/or illustrated in the light of that that these dyes which have free lone pair of electrons on the HN-imidazoline nitrogen atom undergo protonation in acidic media. This generates positive charge on the HN-imidazoline nitrogen atom, and consequently the electronic charge transfer from the HN-imidazoline nitrogen atom to the heterocyclic quaternary nitrogen atom in the quinolinium salt residue will be greatly affected resulting in a hypsochromic shift, protonated and/or colourles structures [Scheme (4) (A)]. On increasing the *pH* value of the media, the absorption bands are intensified and bathochromicaly shifted as a result of deprotonation of the HN-imidazoline nitrogen atom, and accordingly the electronic charge transfer to the quaternary heterocyclic nitrogen atom of the quinolinium salt residue will be easier and facilitated resulting in a bathochromic shift, deprotonated and/or coloured structures [Scheme (4) (B)].

Several methods have been developed for the spectrophotometric determination of the dissociation or protonation constants of weak acids. The variation of absorbance with *pH* values can be utilized. On plotting the absorbance at fixed λ_{max} vs *pH*, S-shaped curves are obtained. On all of the S-shaped curves obtained, the horizontal portion to the left corresponds to the acidic form of the indicator, while the upper portion to the right corresponds to the basic form, since the pKa value is defined as the *pH* value for which one half of the indicator is in the basic form and the other half – in the acidic form. This point is determined by intersection of the curve with a horizontal line midway between the left and the right segments [27]. The acid dissociation or protonation constants values of the dyes (4b) and (5b) are listed in Table (5).

From this study we can conclude that the electronic visible absorption spectra of the monomethine (4b) and the *bis*-dimethine (5b) cyanine dyes in aqueous universal buffer solutions having varying *pH* values underwent displacements to give the hypsochromic shifted and lower intensity bands in the lower *pH* and/or acidic media due to the protonated and/or colourless structures of the dyes in these media. Inversely, the bands of these dyes are intensified and bathochromically shifted in high *pH* and/or alkaline media due to the deprotonated and/or coloured structures of the dyes in these media.

Table (1): Characterization of the prepared compounds (3), (4a-c) and (5a-c)

Comp. No	Nature of products			Molecular formula (M.Wt)	Analysis, %						Absorption spectra in 95% ethanol	
	Colour	Yield %	M.p. °C		Calculated			Found			λ_{axm} (nm)	ε_{max} (mol⁻¹·cm²)
					C	H	N	C	H	N		
3	Brown crystal	60	199	$C_{12}H_4N_4O_6$ (300)	48	1.33	18.67	47.99	1.31	18.65	....	....
4a	Red	75	175	$C_{20}H_{14}N_5O_5I$ (531)	45.2	2.64	13.18	45.18	2.6	13.15	430,450	710,1550
4b	Violet	79	179	$C_{24}H_{16}N_5O_5I$ (581)	49.57	2.75	12.05	49.54	2.73	12.02	410,450,480,580	6120,6900,6330,5280
4c	Red	64	177	$C_{20}H_{14}N_5O_5I$ (531)	45.2	2.64	13.18	45.17	2.61	13.15	370,440,460	7070,2670,2150
5a	Deep red	67	182	$C_{28}H_{24}N_6O_4I_2$ (762)	44.09	3.15	11.02	44.04	3.14	11.01	370,390,440,470	15660,14310,7170,5640
5b	Violet	74	190	$C_{36}H_{28}N_6O_4I_2$ (862)	50.12	3.25	9.75	50.9	3.24	9.7	440,480,580,610	9410,8140,6630,3000
5c	Deep red	68	188	$C_{28}H_{24}N_6O_4I_2$ (762)	44.09	3.15	11.02	44.03	3.13	11	390,410,460,480	21920,21530,10840,9700

Table (2): IR and ^{1}H NMR (Mass) Spectral Data
of the Prepared Compounds (3), (4b) and (5b)

Comp. No.	IR Spectrum (KBr, cm^{-1})	^{1}H NMR Spectrum (DMSO, δ); & (Mass Spectrometry data)
3	1027, 1144, 1166(C-O-C cyclic) 1605 (C=C) 1627 (C=O quinone) 1750 (C=O imidazolone) 3429 (NH)	3.5 (b, 4H, 4NH) M+1 : 301
4b	828, 880, (o-disubstituted benzene) 1077, 1154 (C-O-C cyclic) 1438, 1514 (C=N) 1605 (C=C) 1750 (C=O imidazolone) 2936, 2522 (quaternary salt) 3432 (NH)	1.5 (m, 3H, CH$_3$, N-quinolinium) 3.1 (m, 2H, CH$_2$, N-quinolinium) 5 (s, 4H, 4NH) 7.9-9.2 (m, 7H, aromatic + heterocyclic + =CH-)
5b	828, 882, (o-disubstituted benzene) 1077, 1119 (C-O-C cyclic) 1437, 1517 (C=N) 1604 (C=C) 1719 (C=O quinone) 2930, 2523 (quaternary salt) 3430 (NH)	1.5 (m, 6H, 2CH, N-quinolinium) 3.1 (m, 4H, 2CH$_2$, N-quinolinium) 5 (s, 4H, 4NH) 7.8-9.2 (m, 14H, aromatic + heterocyclic + 2 =CH-)

Table (3): Solvatochromism of the dyes (4b) and (5b) in solvents having different polarities

Dye No.	H₂O λmax (nm)	H₂O εmax (mole⁻¹cm²)	EtOH λmax (nm)	EtOH εmax (mole⁻¹cm²)	DMF λmax (nm)	DMF εmax (mole⁻¹cm²)	CHCl₃ λmax (nm)	CHCl₃ εmax (mole⁻¹cm²)	CCl₄ λmax (nm)	CCl₄ εmax (mole⁻¹cm²)	Dioxane λmax (nm)	Dioxane εmax (mole⁻¹cm²)
4b	430	5820	410	6120	425	6890	420	8440	415	6920	410	7120
	470	5330	450	6900	440	7500	450	7360	430	8320	430	8340
	570	4280	480	6330	530	4980	550	4530	460	7150	565	5600
			580	5280	570	5410	591	2000	560	5550	604	2840
					609	2950			600	3120		
5b	420	8140	440	9410	460	1000	420	8480	450	10460	430	8650
	460	8070	480	8140	484	2550	442	8900	480	9480	455	9750
	560	6230	580	6630	540	5970	480	8090	588	7800	482	8280
	593	2630	610	3000	592	7800	584	6150	620	3800	589	4640
					629	5555	617	2500			624	3300

Table (4): Halochromism of the dyes (4b) and (5b) in aqueous universal buffer solutions

| Dye No.	1.45 λmax (nm)	1.45 εmax (mol⁻¹cm²)	2.03 λmax (nm)	2.03 εmax (mol⁻¹cm²)	3.72 λmax (nm)	3.72 εmax (mol⁻¹cm²)	5.09 λmax (nm)	5.09 εmax (mol⁻¹cm²)	7.57 λmax (nm)	7.57 εmax (mol⁻¹cm²)	8.91 λmax (nm)	8.91 εmax (mol⁻¹cm²)	10.20 λmax (nm)	10.20 εmax (mol⁻¹cm²)	12.04 λmax (nm)	12.04 εmax (mol⁻¹cm²)
(4b)	410	2770	440	7360	442	4970	442	5100	443	5510	443	5380	420	5510	442	5400
	430	5100	470	6790	470	6390	470	6280	470	6710	470	6360	450	7070	472	6550
	460	2000	468	3680	570	4030	571	4620	573	5150	575	6000	470	6380	578	6700
	560	1740	......	......	......	......	......	......	......	......	......	......	577	6600	......	......
(5b)	440	7340	450	7340	450	6980	450	7440	450	7800	450	7940	450	8230	450	8390
	480	6800	480	6710	482	6440	482	6870	480	7330	480	7430	480	7630	480	7830
	580	4060	581	4500	583	4960	585	5520	587	6000	588	7000	580	8000	590	9000

Table (5): The variation of absorbance with *pH* at fixed λ for the cyanine dyes (4b); (5b) in different buffer solutions

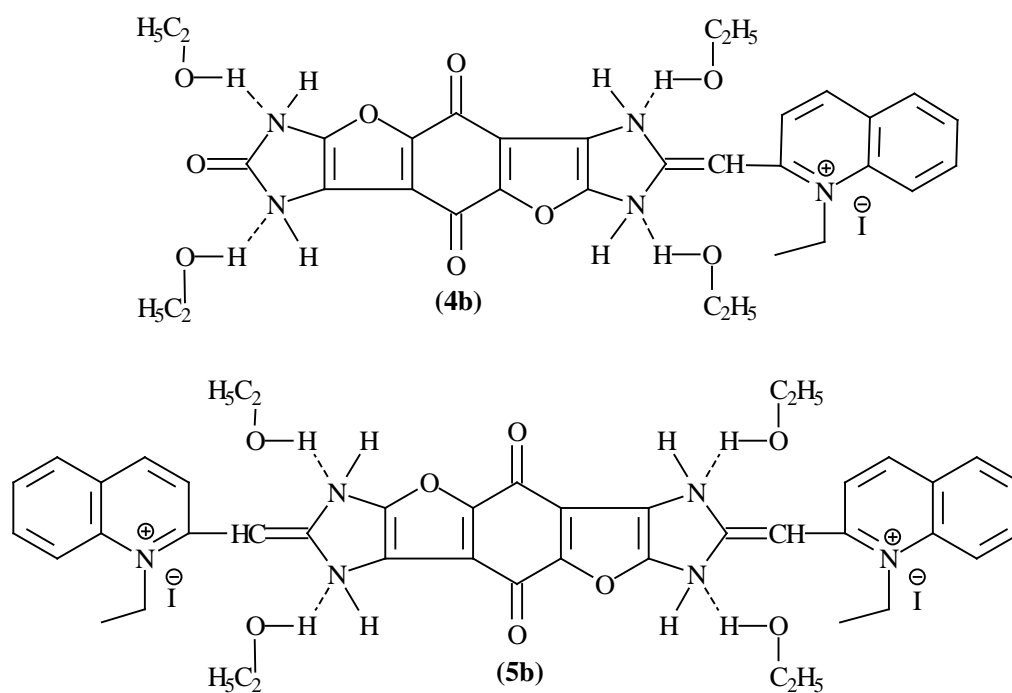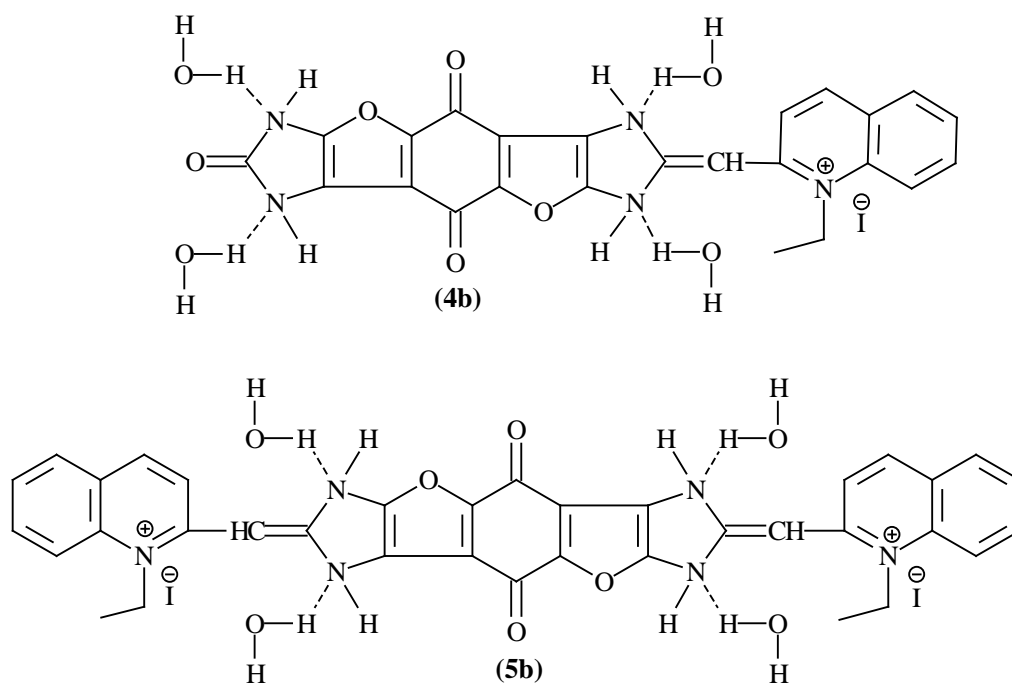| Dye		pH										pKₐ
		1.45	2.03	3.72	5.09	7.57	8.91	10.20	12.04			
Absorbance at fixed wavelength	(4b) λ 560 (nm)	0.2	0.39	0.4	0.44	0.45	0.59	0.6	0.64			4.8; 8.5
	(5b) λ 580 (nm)	0.4	0.42	0.49	0.54	0.58	0.64	0.8	0.82			9.4
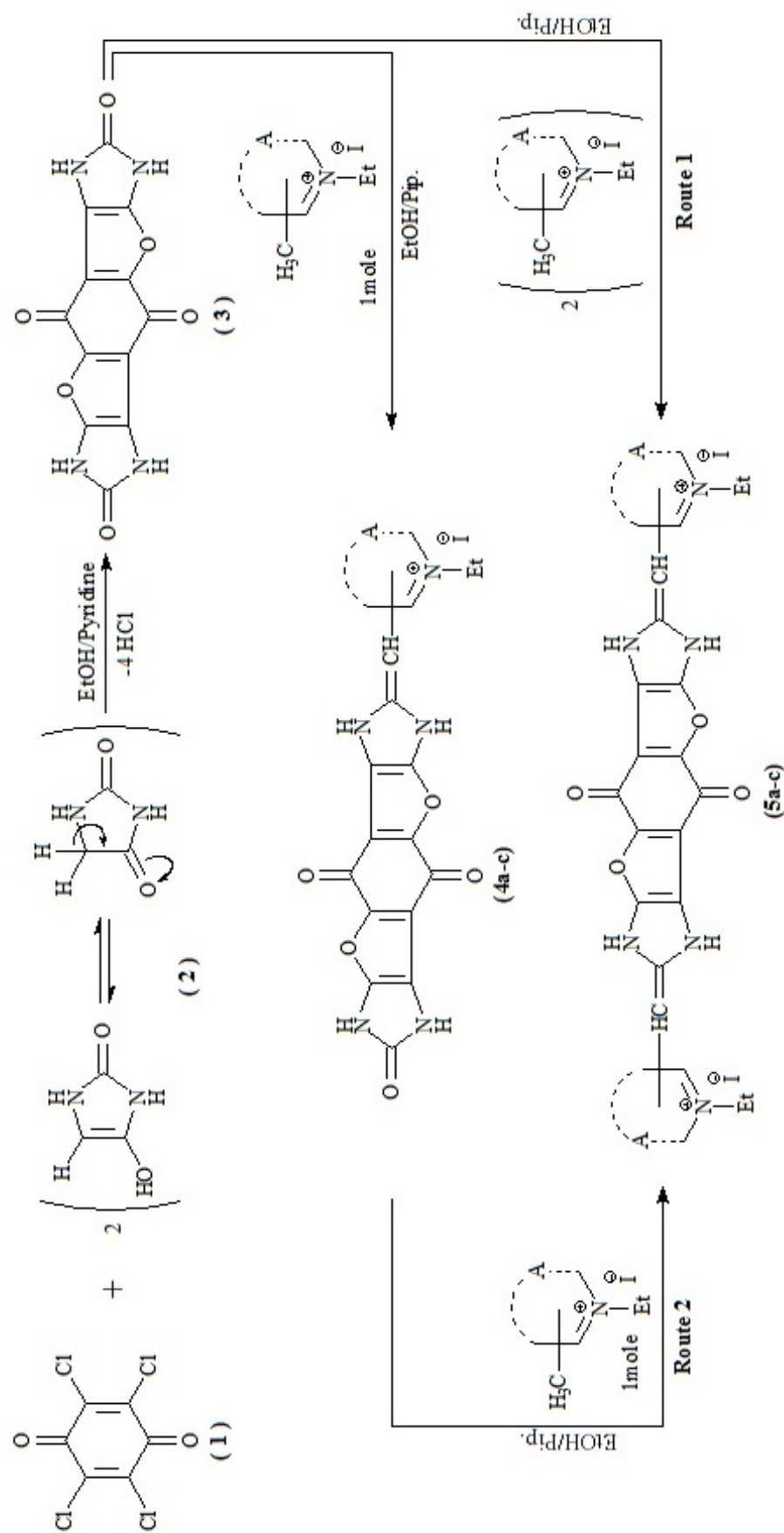
Scheme (1)

Substituents in Scheme (1):

(4a-c); (5a-c): A = 1-ethyl pyridinium-2-yl salt (a); 1-ethyl quinolinium-2-yl salt (b); 1-ethyl pyridinium-4-yl salt (c).
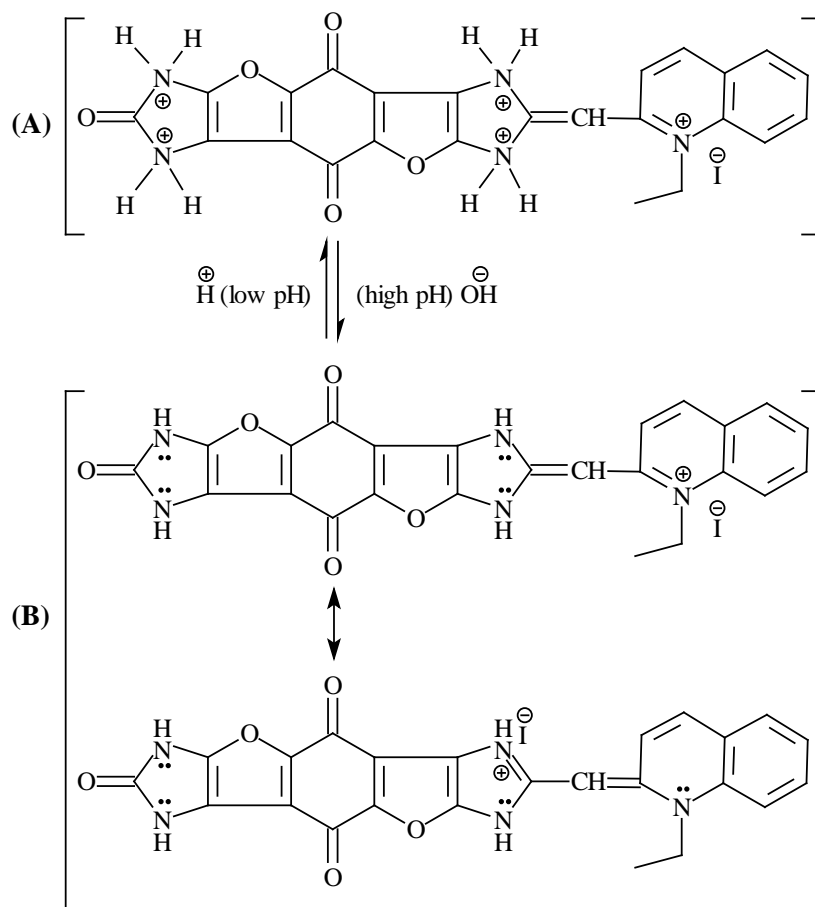
Scheme (2)

(4b)

(5b)

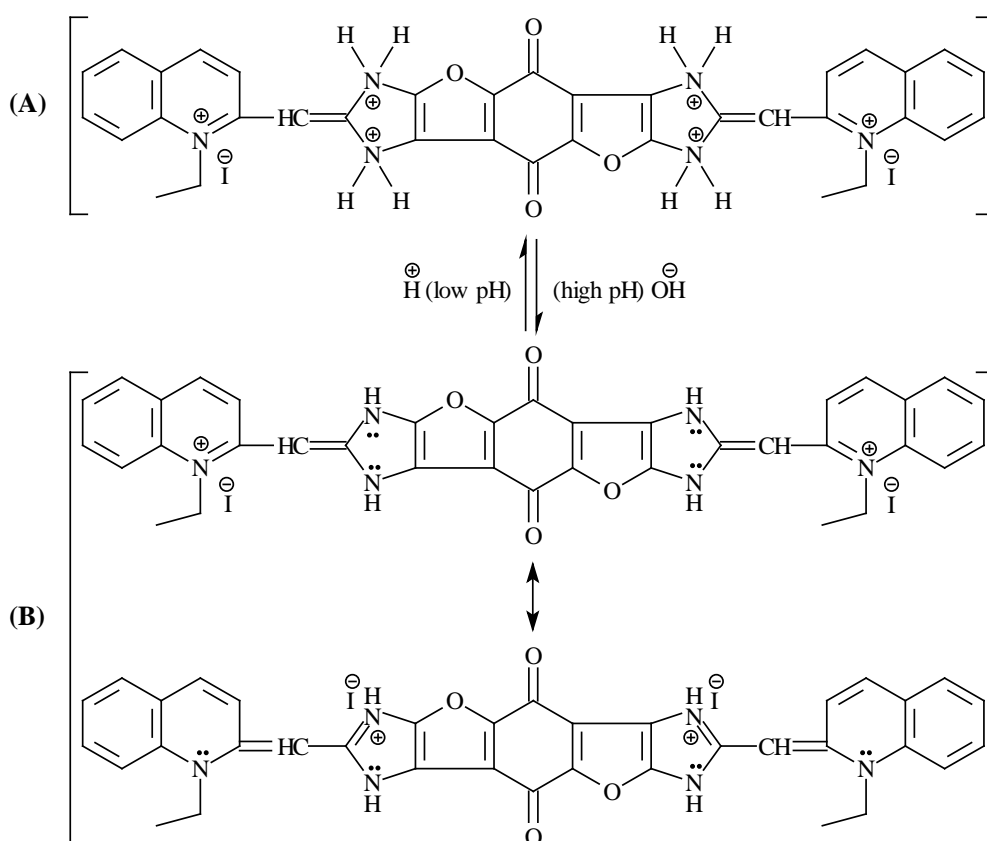**Scheme (3) (A)**

(4b)

(5b)
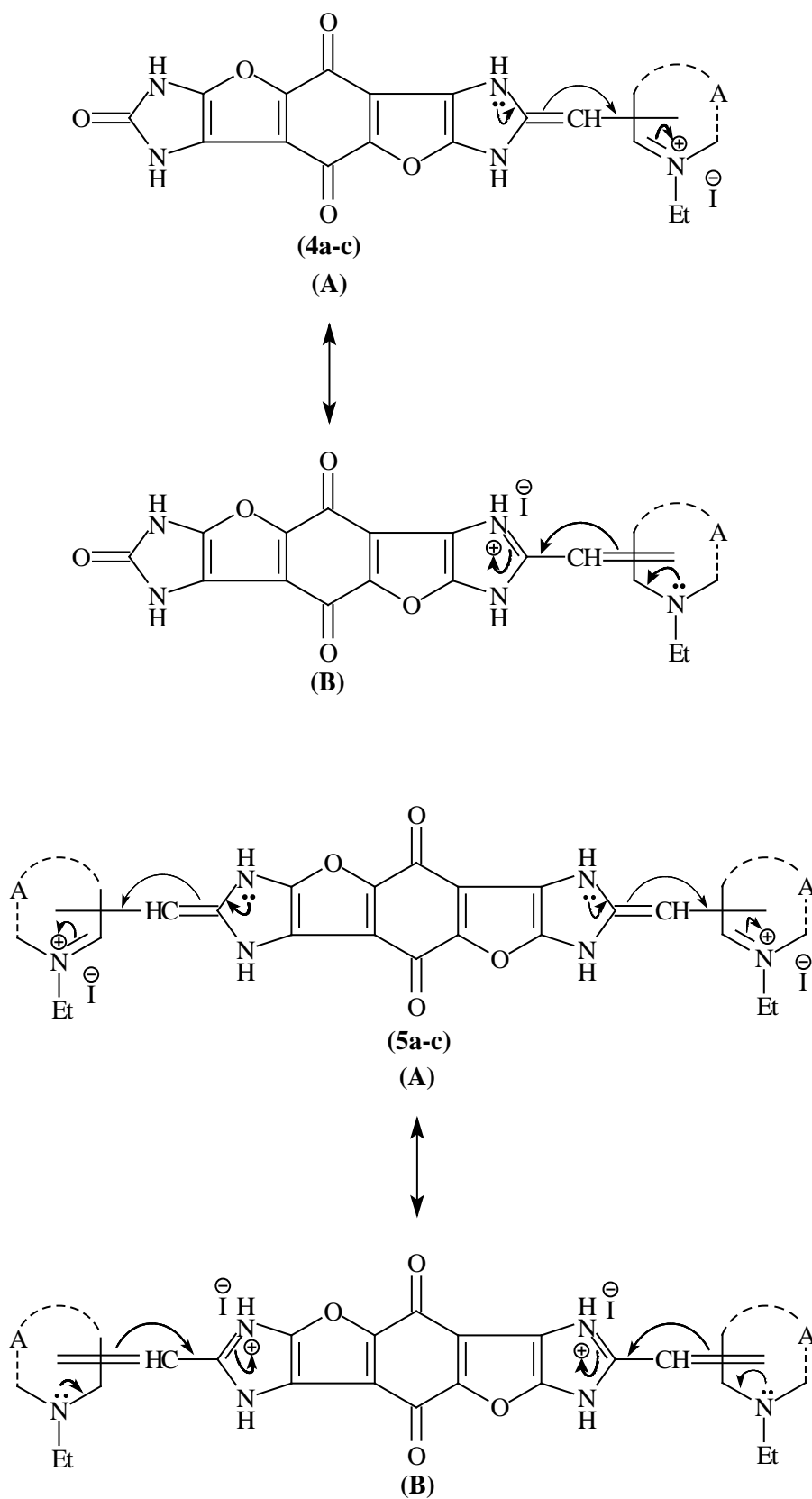
Scheme (3) (B)

Scheme (4):

Decolorization (protonation) and colorization (deprotonation)
of the dye (4b) in acid/base media, respectively

Scheme (4) continue:

Decolorization (protonation) and colorization (deprotonation)
of the dye (5b) in acid/base media, respectively

Conclusions

a) The electronic visible absorption spectra of the monomethine cyanine dyes (4a–c) and the *bis*-monomethine cyanine dyes (5a–c) underwent displacements to give bathochromic and/or hypsochromic shifts depending upon the following factors:

1) Type of the heterocyclic quaternary salt (A) in the order of: quinaldinium dyes > α-picolinium dyes;

2) Linkage positions of the heterocyclic quaternary salts in the order of: γ-picolinium dyes > α-picolinium dyes;

3) The number of the electronic charge transfer pathways inside the dyes molecules in the order of: two electronic charge transfer pathways dyes > one electronic charge transfer pathways dyes;

b) The intensity of the colour of the monomethine cyanine dyes (4a–c) and the *bis*-monomethine cyanine dyes (5a–c), can be attributed to two suggested mesomeric structures (A) and (B) producing a delocalized positive charge over the conjugated system [Scheme (2)].

Acknowledgements

References:
1. C.H. Greville Williams. *Trans. R. Soc. Edinburgh* **21**, 377 (1856).
2. L.G.S. Brooker. In: C.E.K. Mees, Ed. *The Theory of the Photographic Process.* 1st ed. – New York: Macmillan, 1942, p. 987.
3. J. Pietkiewicz, K. Zielinska, J. Saczko, J. Kulbacka, M. Majkowski, A.K. Wilk. *European Journal of Pharmaceutical Sciences* **39**, 322–335 (2010).
4. G. Ficken. *Chem. Ind.* **70**, 672–677 (1989).
5. D.M. Sturmer, A.P. Marchetti. In: J.M. Sturge, V. Walworth & A. Shepp, eds. *Imaging Processes and Materials, Neblette's*, 8th ed. – New York: Van Nostrund Reinhold, 1989, p. 96.
6. C.D. Gabbutt, L.V. Gibbons, B.M. Heron, S.B. Kolla. *Dyes and Pigments* **92**(3), 995–1004 (2012).
7. U.S. Patent 2925417 (Feb. 16, 1960), E.F. Elslager, D.F. Worth (to Parke-Davis and Co.); U.S. Pat. 2515912 (July 18, 1950), E. Van Lare, L.G.S. Brooker (to Eastman Kodak Co.).
8. U.S. Patent 2893914 (July 7, 1959), M.C. Mecowen, P.F. Wiley (to Eli Lilly and Co.).
9. R. Sun, B. Yan, J. Ge, Q. Xu, N. Li, X. Wu, Y. Song, J. Lu. *Dyes and Pigments* **96**, 189–195 (2013).
10. U.S. Patent 2895955 (July 21, 1959), D.W. Heseltine, L.G.S. Brooker (to Eastman Kodak Co.).
11. M. Lu, N.C. Seeman, N.R. Kallenbach. *Biochemistry* **29**, 3407–3412 (1990).
12. R.V. Solomon, R. Jagadeesan, S.A. Vedha, P. Venuvanalingam. *Dyes and Pigments* **100**, 261–268 (2014).
13. J. Davila, A. Harriman, K.S. Gulliya. P*hotochem. Photobiol.* **53**(1) (1991).
14. F.J. Duarte, L.W. Hillman, eds. *Dye Laser Principles with Applications.* – New York: Academic Press, 1990, 433 p.
15. O.R. Keisar, E.K. Finfer, S. Ferber, R. Finaro, D. Shabat. *Nature Protocols* **9**(1), 27–36 (2014).
16. L.G.S. Brooker. In: C.E.K. Mees, T.H. James, eds. *The Theory of the Photographic Process*, 3rd ed. – New York: Macmillan, 1966, 198 p.
17. L.G. Jr. Wade. *Organic Chemistry*, 4th ed. – New Jersy: Printice Hall, 1999, 500 p.
18. L.G. Jr. Wade. *Organic Chemistry*, 4th ed. – New Jersy: Printice Hall, 1999, 544 p.
19. G.E Ficken. In: *The Chemistry of Synthetic Dyes*, ed. K. Venkataraman. – New York: Academic Press, 1971, vol. 4, pp. 212–340.
20. W. West, A.L. Geddes. *J. Phys. Chem.* **68**(4), 837–847 (1964).
21. N.A. Derevyanko, G.G. Dyadyusha, A.A. Ishchenko, A.I. Tolmachev. *Theoret. Experim. Khim.* **19**, 169–178 (1983).
22. A.A Ishchenko, N.A. Derevyanko, V.M. Zubarovski, A.I. Tolmachev. *Theoret. Experim. Khim.* **20**, 443–451 (1984).
23. A.A. Ischchenko, V.A. Svidro, N.A. Derevyanko. *Dyes and Pigments* **10**, 85–96 (1989).
24. R.C. Weast, Ed. *CRC Handbook of Chemistry and Physics.* 61nd ed. – Florida: CRC Press, 1980–1981, p. 56.
25. M.S. Mottaleb, Z.H.Z. Khalil. *Phys. Chemie Leipzig* **260**(4), 650 (1979).
26. M.R. Mahmoud, Z.H. Khalil, R.M. Issa. *Acta Chem. Acad. Sci. Hung.* **87**(2), 121 (1975).
27. G. Ewing, Ed. *Instrumental Methods of Chemical Analysis.* – New York: Mc. Graw-Hill Book Company Inc., 1960, 22 p.
28. J.A. Reddick, W.A. Banger. In: A. Weissberger, Ed. *Techniques of Chemistry*, Vol. II, Organic Solvents, 3rd ed. – New York: Wiley, 1970; Becker, G.O. Heinz, W.B. Gunter, eds. *Organikum. Organisch-Chemisches Grundpraktikum*, 9th ed. – Berlin: DVW, 1969.